Impact of Hydroxyglutarate on Dendritic Cell Activation

DISSERTATION ZUR ERLANGUNG DES
DOKTORGRADES DER NATURWISSENSCHAFTEN (DR. RER. NAT.)
DER FAKULTÄT FÜR BIOLOGIE UND VORKLINISCHE MEDIZIN

DER UNIVERSITÄT REGENSBURG

vorgelegt von

Zugey Elizabeth Cárdenas Conejo

Aus

Lázaro Cárdenas, Michoacán

México

im Jahr 2018

The present work was carried out from November 2013 to December 2017 at the Department of Internal Medicine III at the University Hospital Regensburg.

Die vorliegende Arbeit entstand im Zeitraum von November 2013 bis December 2017 an der Klinik und Poliklinik für Innere Medizin III des Universitätsklinikums Regensburg.

Das Promotionsgesuch wurde eingereicht am:
27 March 2018

Die Arbeit wurde angeleitet von:
Prof. Dr. Marina Kreutz

Prüfungsausschuss:

Vorsitzender:	Prof. Dr. Stephan Schneuwly
Erstgutachter:	Prof. Dr. Marina Kreutz
Zweitgutachter:	Prof. Dr. Wolfgang Müller-Klieser
Drittprüfer:	Prof. Dr. Wolfram Gronwald
Ersatzprüfer:	Prof. Dr. Richard Warth

Signature

Table of Contents

List of Figures

List of Tables

List of Abreviations

Abreviations	Definition
Acetyl-CoA	Acetyl coenzyme A
Akt	Protein Kinase B
AMP	Adenosine Monophosphate
APC	Antigen-Presenting cell
APS	Ammonium persulfate
ATP	Adenosin triphosphate
BSA	Bovine Serum Albumin
CD	Cluster of differentiation
cDNA	Copy DNA
CIMP	CpG island methylator phenotype
CO_2	Carbon dioxide
COX	Cyclo oxygenase
CREB	cyclic AMP response element-binding
CSF	Colony-stimulating factor
CTLA-4	Cytotoxic T lymphocyte-associated protein 4
CXCL2	Chemokine (C-X-C motif) ligand 2
DAPI	4',6-diamidino-2-phenylindole
DCs	Dendritic cells
D-HG	D-2-Hydroxyglutarate
DMEM	Dulbecco Modified Eagle Medium
DMSO	Dimethyl sulfoxide
DNA	Deoxyribonucleic acid
dNTPs	2'-deoxyribonucleosid-5'-triphosphates
dsDNA	double-stranded DNA
DSMZ	Deutsche Sammlung von Mikroorganismen und Zellkulturen
ECL	Enhanced chemiluminescence
ECM	Extracellular matrix
EDTA	Ethylene diamine tetraacetate
EGFR	Epidermal growth factor receptor
EGTA	Ethylene glycol tetraacetic acid
ELISA	Enzyme-linked immunosorbent assay
ETC	Electron Transport Chain
ETS	Electron Transport System
F-FDG	^{18}F-fluorodeoxyglucose
FACS	Fluorescence-activated cell sorting
FCCP	Carbonyl cyanide-*p*-trifluoromethoxyphenylhydrazone
FCS	Fetal calf serum
FDH	Formate Dehydrogenase
FH	Fumarate hydratase
FITC	Fluorescein isothiocyanate
^{18}F-FLT	^{18}F-fluorothymidine

FSC	Forward scatter
GBM	Glioblastoma Multiforme
GLUT	Glucose transporter
GM-CSF	Granulocyte-macrophage colony-stimulating factor
GTP	Guanosine triphosphate
H_2O_2	Hydrogen peroxide
H_2O_{bidest}	Double-distilled water
H_2O_{USB}	Diethylpyrocarbonate treated RNAse-free water (USB Corporation)
HCl	Hydrochloric acid
HG	2-Hydroxyglutarate
HIF	Hypoxia-inducible factor
HLA	Human Leukocyte Antigen
HPLC	High-performance liquid chromatography
HRP	Horse raddish peroxidase
IDH	Isocitrate dehydrogenase
IFN	Interferon
Ig	Immunoglobulin
IGF	Insulin-like growth factor
IL	Interleukin
IRF-1	Interferon regulatory factor 1
JAK	Janus Kinase
JHDM	JmjC-domain-containing histone demethylase proteins
JNK	c-Jun N-terminal kinase
KG	Ketoglutarate
LBP	LPS-binding Protein
L-HG	L-2-Hydroxyglutarate
LOH	Loss of hererozygosity
LPS	Lipopolysaccharide
M-MLV	Murine moloney leukemia virus
MAP	mitogen- activated protein
MAPK	mitogen- activated protein kinase
MCT	Monocarboxylate transporter
MDSCs	Myeloid-derived suppressor cells
MHC	Major histocompatibility complex
miR	Micro RNA
MMP	Matrix Metalloprotease
mRNA	Messenger RNA
NAD	Nicotinamide adenine dinucleotide
NADP	Nicotinamide adenine dinucleotide phosphate
NADPH	Nicotinamide adenine dinucleotide phosphate-oxidase
NF-κB	Nuclear factor kappa-light-chain-enhancer of activated B cells
NFAT	Nuclear factor of activated T cells
NK	Natural killer
NMR	Nuclear Magnetic Resonance
NO	Nitric oxide

NOS	Nitric oxide synthase
OXPHOS	Oxidative phosphorylation
PBS	Phosphate buffered saline
PBST	Phosphate buffered saline with Tween 20
PCR	Polymerase chain reaction
PD-1	Programmed cell death 1
PD-L1	Programmed cell death ligand 1
PDGFRA	Platelet Derived Growth Factor Receptor α
PDH	Pyruvate dehydrogenase
PDK1	Pyruvate dehydrogenase kinase 1
PE	Phycoerythrin
PET	Positron emission tomography
PHDs	Prolyl hydroxylases
PI3K	Phosphoinositide 3-kinase
PTEN	Phosphatase and tensin homolog
PVDF	Polyvinylidene difluoride
qRT-PCR	Quantitative real-time PCR
RNA	Ribonucleic acid
ROCK	RhoA/Rho kinase
ROS	Reactive oxygen species
ROX	Residual Oxygen consumption
RPMI	Roswell Park Memorial Institute medium
RT	Room Temperature
SDH	Succinate dehydrogenase
SDS-PAGE	Sodium dodecylsulfate polyacrylamide gel electrophoresis
SEM	Standard error of the mean
shRNA	Short hairpin RNA
siRNA	Small interfering RNA
SSC	Side scatter
STAT3	Signal transducer and activator of transcription 3
TAMs	Tumor-associated macrophages
TBS	Tris buffered saline
TBST	TBS buffer + Tween 20
TCA	Tricarboxylic acid
TCR	T cell receptor
TEMED	N,N,N',N'-tetramethylethylenediamine
TET2	Tet oncogene family member 2
TGF	Transforming growth factor
Th	T helper
TIR	Toll/interleukin 1 receptor
TIRAP	TIR domain containing adaptor protein
TLR	Toll-like Receptor
TMZ	Temozolomide
TNF	Tumor necrosis factor
TP53	Tumor protein p53

TRAM	TRIF-related adaptor molecule
TRIF	TIR-domain-containing adapter-inducing interferon-β
VEGF	Vascular endothelial growth factor
WB	Western Blot
WHO	World Health Organization

1. Introduction

1.1 Glioma

Gliomas are brain tumors originated from glial cells[1], which are non-neuronal cells whose main functions are myelin formation, support and maintenance of neurons. Glial cells can be grouped in microglia and macroglia[2].

Microglia are specialized macrophages derived from hematopoietic precursors localized on the brain. They originate from the ectodermal layer and have a large and star-like morphology. Their principal function is to phagocytose damaged neurons and glial cells. Macroglia are subdivided into three principle types, namely astrocytes, oligodendrocytes and ependymal cells. Each of them has special functions:

- Astrocytes: the provision of nutrients, oxygen, and mechanical support; the development guidance, waste disposal and immune functions.
- Oligodendrocytes: the production of myelin sheath, a modified plasma membrane surrounding the nerve axon, enhancing the efficiency of electrical signal propagation.
- Ependymal cells: create and secrete cerebrospinal fluid (CSF) and assist in their circulation through the brain ventricles and the spinal cord [3].

Glial cells divide and multiply by asymmetric cell division. When the control of this ability is lost, the formation of gliomas takes place. Astrocytomas are tumors derived from astrocytes and constitute 75% of all gliomas[4]. Other less common types of gliomas are oligodendroglioma (9%) and ependymoma (6%), which originate from oligodendrocytes and ependymal cells, respectively [5,6]. Tumors derived from mixed cell types constitute the remaining cases. Traditionally, astrocytomas have been subdivided depending on their malignancy grade. An established histological grading created by the World Health Organization (WHO) assigned grades from I to IV, with I being the least aggressive and IV being the most aggressive[5].

The updated classification of the WHO is based on morphology, molecular and genetical factors of astrocytomas. Two of the principal changes on the updated WHO classification is the incorporation of Isocytrate Dehydrogenase (IDH) mutations, and a characteristic

translocation of the p arm of chromosome 1 with the arm of chromosome 19 (1p/19q codeletion) as important factors for the subdivision of gliomas [7,8].

Astrocytomas with IDH mutations show no 1p/19q codeletion, whereas oligodendriogliomas carries both IDH mutation and 1p/19q codeletion. Astrocytomas with no IDH mutation (IDH wild-type) show a worse prognosis in comparision with astrocytomas with IDH mutations (Figure 1.1)[7,8].

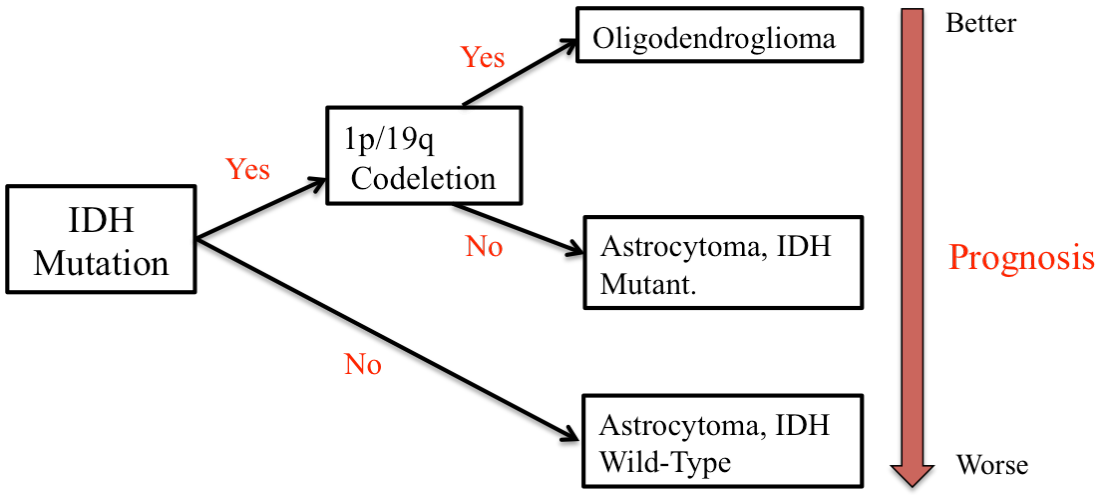

Figure 1.1 Astrocytoma classification in the updated 2016 Central Nervous System WHO classification (adapted from Johnson et al., 2016)[8].

1.2 Glioblastomas

The highest-grade astrocytoma, the glioblastoma multiforme (GBM, astrocytoma WHO grade IV) is the most common and most aggressive nervous system tumor. It can be divided in primary and secondary GBM. The "primary" (de novo) GBMs are common and display no signs of a preceding low-grade tumor. They develop predominantly in elderly patients [5,9]. In contrast, secondary GBMs develop in younger patients through progression from lower-grade diffuse astrocytoma (WHO grade II) or anaplastic astrocytoma (WHO grade III)[5,10].

The current treatment for GBM patients consists of surgery, radiotherapy and chemotherapy. Complete surgical resection is practically impossible. Radiotherapy in combination with the adjuvant temozolomide (TMZ) represents the standard treatment for newly diagnosed GBM and the overall survival after 5 years of diagnosis is less than 5% [6,11].

1.2.1 Molecular basis for the development of GBMs

Genetic alterations are commonly assumed to be the basis of tumor development. These mutational events trigger the activation of genes related to tumor formation (oncogenes) or the silencing of tumor suppressor genes[9]. Several mutations, for example TP53, PDGFRA, EGFR, and NF1, have been described in the context of GBM development [12].

Depending of the subtype of GBM, the presence of IDH1 mutations varies. IDH1 mutations are more frequent (80%) in secondary GBMs, progressed from anaplastic astrocytomas, whereas in primary GBMs the incidence of this mutation is only 5% [13,1415,16]. The small fraction of primary GBMs with IDH1 mutations is only found in younger patients [13,17].

Interestingly, a rare fraction of secondary GBMs lacks IDH1 mutations. These GBMs have progressed from grade III glioma, while the majority of secondary GBMs, that exhibit IDH1 mutations, have developed from grade II gliomas[15].

Remarkably, IDH mutations do not result in a complete loss of function as only one IDH1 gene copy is altered. This specific mutation leads to a single amino acid exchange, namely arginine 132 to histidine, in the IDH1 active site [18].

The updated WHO classification, incorporate the traditional "primary" and "secondary" glioblastomas classification into two new subtypes based on the presence of IDH mutations [7].

Table 1.1 Glioblastoma classification based on the presences of IDH mutation [8].

Glioblastoma, IDH Mutant	**Glioblastoma, IDH Wild-type**
10 % of GBMs	90% of GBMs
Younger median age	Older median age
Good Prognosis	Poor Prognosis
Secondary GBMs	Primary GBMs

1.3 Glioblastoma and metabolism

Several imaging studies used in brain tumor diagnosis have their basis in the metabolic activity of tumor cells.

Positron emission tomography (PET) is an imaging technology that is able to detect and characterize tumors based on their molecular and biochemical properties, as it is the case of glucose uptake, nucleoside or amino acid metabolism. During a PET scan a small amount of e.g. radioactive glucose is injected, which is uptaken by the tumor cells depending on malignancy[19,20]. Studies with fluoro-2-deoxyglucose (^{18}F-FDG) have demonstrated differences in ^{18}F-FDG uptaking between brain tumor subtypes, being higher in GBM than in meningioma or surrounding gray matter [21,22].

Analogical, studies with amino acid tracers focus principally on ^{11}C-methionine [23] and the thymidine analog 3´-^{18}F-fluorothymidine (^{18}F-FLT) to track the proliferation of brain tumors *in vivo* [24]. Amino acid imaging is based on the observation that amino acid transport is generally increased in cells undergoing malignant transformation [25].

1.3.1 Warburg Effect

Otto Warburg observed that cancer cells present an altered glucose metabolism compared with non-cancerous cells[26]. Warburg demonstrated that cancer cells displayed an increase in their glycolytic activity, taking up glucose and producing higher levels of lactic acid even in the presence of sufficient levels of oxygen, which would allow energy production via oxidative phosphorylation (OXPHOS)[27].

Glycolysis is a sequence of chemical reactions where one molecule of glucose is converted into two molecules of pyruvate; these reactions occur in the cytosol of the cell. The overall energy release from this process is two ATP and two NADH molecules per molecule of glucose [28]. Pyruvate is further metabolized into acetyl-CoA, which enters the mitochondrial matrix where the tricarboxic acid cycle (TCA) takes place. In contrast, in cancer cells high amounts of glucose are taken up and metabolized to pyruvate, but instead of entering into the TCA, most of the pyruvate is converted to lactate, which later is secreted from the cell [29]. It has been reported that “aerobic” glycolysis supports tumor growth and proliferation due to fast generation of ATP and biomolecules [30,31].

Warburg considered that the functions of mitochondria were impaired in cancer cells; nevertheless several studies observed that in many cancer types, mitochondrial oxidative phosphorylation is intact [32–35].

The Warburg effect has been associated with several oncogenic factors, which include HIF-1, MYC, GTP-binding proteins, RAS, tyrosine kinase pathway, p53 and IDH mutations [30,36].

1.3.2. Isocitrate dehydrogenase (IDH) and tumor cell metabolism

IDH is an important enzyme of the TCA. Three isozymes of IDH are known in humans: IDH1, IDH2 and IDH3. These isozymes are encoded by five genes: *IDH1*, *IDH2*, *IDH3A*, *IDH3B* and *IDH3G*[37]. All isozymes are metabolic enzymes that catalyze the interconversion of isocitrate into alpha-ketoglutarate (α-KG). IDH1 is located in the cell cytoplasm and peroxisomes, whereas IDH2 and IDH3 are found in the mitochondrial matrix[37].

α-KG is a ketone, which can be generated via glutaric acid from glutamine, and is involved in nitrogen transportation, oxidation reactions, and amino acid formation[37]. Mutated IDH gains the new ability to convert α-KG into D-2-hydroxyglutarate (D-HG) [38,39]. IDH mutations have not only been described in glioblastoma but also in other tumor entities such as acute myeloid leukemia [40]. D-HG can be detected in culture supernatants of mutant cells and acute myeloid leukemia patient sera[41]. It has been reported that the serum HG levels did not differ between *IDH1/2* allelic variants. In addition to this, high HG levels were also detected in some patients without IDH mutations in acute myeloid leukemia and thyroid carcinoma[41]. Importantly, high concentrations of HG predicted shorter overall survival in patients with acute myeloid leukemia [42]. In contrast, patients with malignant gliomas and anaplastic astrocytomas that harbor IDH mutations show improved survival in comparison with patients whose tumors lack these mutations [43,44].

The presence of HG in cell lines that lack IDH mutations raises the question what mechanism leads to HG production in these cells. In conditions of hypoxia, mitochondrial glutamate levels are high, favoring the reverse TCA reaction, a process replenished through glutaminolysis. In this case glutamine is converted into glutamate, which subsequently is metabolized into α-KG by glutamate dehydrogenase (GDH). Then IDH converts α-KG into isocitrate using NADP+ as an electron acceptor leading to the production of NADPH. Isocitrate is further metabolized to acetyl-CoA for lipid

metabolism [45]. This inverse catalytic reaction by IDH has been reported in a SF188 glioblastoma cell line under hypoxic conditions, along with an increase in HG levels[46].

In line with these results, high levels of cellular HG have been reported to drive the hydroxylation of HIF-1α, leading to decreased HIF expression and increased glioma transformation. Additionally, HG has been reported to competitively inhibit α-KG binding to several histone demethylases, including JmjC-domain-containing histone demethylase proteins (JHDM) leading to a widely aberrant histone methylation profile. Furthermore, HG is an inhibitor of hydroxymethylases TET methylcytosine dioxygenases (TET) 1 and 2, enzymes that catalyze the conversion of methylcytosine to 5-hydroxymethylcytosine, inducing DNA demethylation. The epigenetic dysregulation caused by altered levels of HG and α-KG in IDH1 and IDH2 mutant cells may contribute to aberrant regulation of gene expression in cancer[47] (See Figure 1.2).

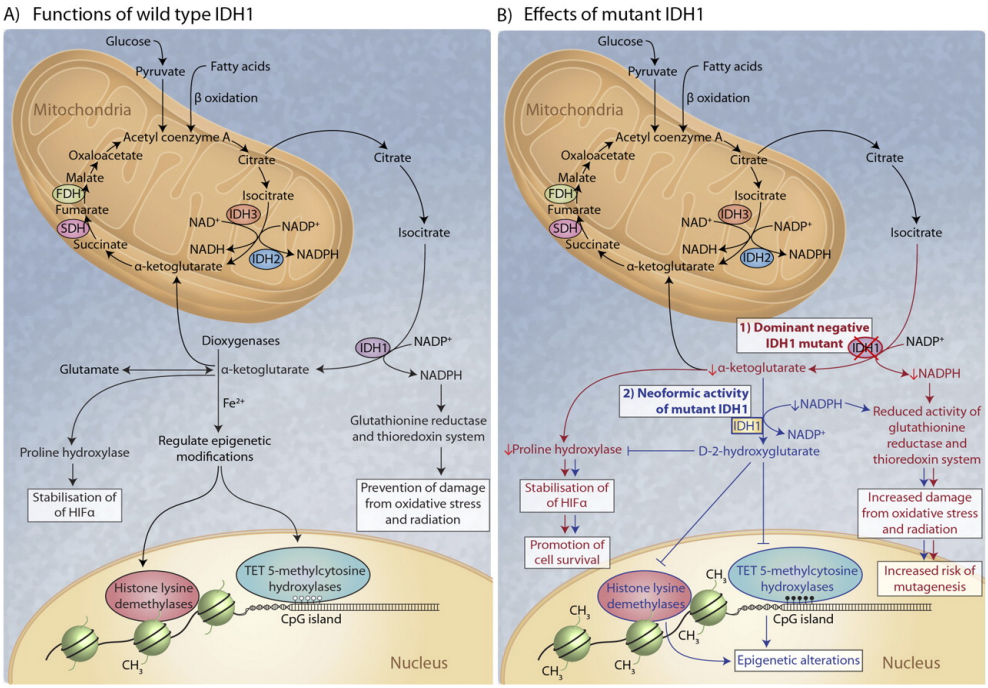

Figure 1.2. The role of IDH in metabolism of gliomas. The figure shows schematically that mutated IDH1 enzyme gains the ability to produce HG from α-ketoglutarate; this could lead to HIF stabilization through impairment of PHD activity. The stabilization of HIF promotes cell survival. In addition, the buildup of HG in IDH1- and IDH2-mutated cells has been linked to epigenetic changes through the inhibition of TET and JHDMs [48]. Abbreviations: isocitrate dehydrogenase (IDH), hypoxia inducible factor (HIF), formate dehydrogenase (FDH), ten-eleven translocation (TET), prolyl hydroxylase domain (PHD), succinate dehydrogenase (SDH). Adapted from Gupta et al., 2011[48].

1.4 The role of tumor stroma in malignant gliomas

T cells have been reported to infiltrate gliomas, and could be linked with an survival improval in patients with malignant gliomas [49,50]. Genome microarray analysis supported the theory that host immunity can control tumor growth of high-grade gliomas. T cell-associated genes were shown to be enriched in high-grade astrocytoma from long-term versus short-term survivors[51].

High intratumoral numbers of $CD4^+$ and $CD8^+$ T cells have been related with prolonged survival in other tumor entities. In melanoma, $CD4^+$ T cells has been proved to control tumor invasion and metastasis [52], whereas in hepatic metastases of colorectal cancer high intra-tumoral $CD8^+$ T cell infiltration predict better response to chemotherapy and prolonged survival [53]. Interestingly, in renal cell carcinoma as well as in head and neck cancers T cell infiltration seems to be controlled by the metabolic phenotype of the tumor, as an accelerated glucose metabolism was shown to be associated with a low CD8 effector T cell infiltration [54].

Fibroblasts are an heterogenous population of stromal cells, with multiple functionalities, as wound-healing regulation, immune modulators production (growth factors, cytokines, chemokines) and play an important role in chronic inflammation [55]. Numerous reports have identified stromal fibroblasts as important players in the induction of angiogenesis and metastasis in brain tumors [56,57], and tumor-associated macrophages are involved in fibroblast recruitment [58,59]. The interaction of these stromal cells with brain tumor cells induced the production and activation of matrix metalloproteinase leading to glioma progression [60–64]. Microglia cells/ macrophages play also an important role in the production of cytokines, particularly IL-10 [65]. The expression levels of IL-10 can significantly be related with tumor cell proliferation, migration and the promotion of metastasis in gliomas [66,67]. The expression of proinflammatory cytokines in glioblastomas is associated with typical immune signaling cascades as is the case of p38 MAPK; an inhibition on p38 MAPK cascade results in the incapacity of glioma cells to metastasize [68].

1.5 Immune biology

The immune system is a complex interactive network of cells, humoral factors and cytokines. The principal function is the host's protection from harmful environmental agents [69].

The immune response is divided into two types of responses, determined by the speed and specificity of the reaction. These responses are innate and adaptive immunity [70].

1.5.1 Innate Immunity

The innate immunity is the faster reaction against infectious agents. The main components of this type of response are: 1) physical, chemical, and microbiological barriers, 2) phagocytes (neutrophils, monocytes, macrophages and dendritic cells (DCs)), 3) acute phase proteins, 4) complement factors, and 5) natural killer cells [69,70].
This type of immunity occurs in the same magnitude all the time regardless of repeated encounters with the infectious agent [71].

The primary function of mononuclear phagocytes, like monocytes, macrophages and DCs, is phagocytosis. Phagocytosis is defined as the engulfment of antigens, a process in which a remodelling of actin is necessary, leading to the formation of the so-called phagosome. Phagocytic macrophages manage the defense against bacteria via surface receptors, which are able to recognize and bind several components of bacterial surfaces. The binding of bacterial molecules to the surface receptors of phagocytic macrophages induces the absorption of the bacterium and the secretion of biological active molecules, such as cytokines. This leads to a cell to-cell communication during the immune responses and promotes the migration of cells towards sites of inflammation, infection and trauma [72–74].
In the central nervous system, monocyte-derived macrophages are called microglial cells [70]. Several studies investigated monocytes as an important component of the glioblastoma microenvironment. GBM cells attract circulating monocytes to the tumor parenchyma, where these monocytes adopt immunosuppressive properties [75–78].

1.5.2 Adaptive Immunity

The adaptive immunity is composed of different types of lymphocytes, namely B cells and T cells, which are capable of reacting highly specific to foreign antigens. In addition, the adaptive immunity is able to “remember” infectious agents due to the induction of so-called “memory” cells. This leads to a faster response upon secondary exposure of the infectious agent [70].
B cells are capable of producing antibodies. They recognize extracellular antigens and differentiate into antibody-secreting plasma cells. T lymphocytes recognize antigens presented on MHC molecules via their specific T cell receptor (TCR). There are different types of T lymphocytes: $CD4^+$ helper T cells, $CD8^+$ cytotoxic T cells (CTLs) and

regulatory T cells. The $CD4^+$ helper T cells secrete cytokines in response to an antigenic stimulation and thereby activate macrophages, DCs or other T cells. Cytotoxic $CD8^+$ T cells are responsible for the killing of virus-infected cells and can also destroy tumor cells. In contrast, regulatory T cells represent "the brake" of the immune system and can inhibit activated $CD4^+$ T cells [70], $CD8^+$ T cells and B cells, thereby limiting the immune response [79].

1.5.3 Antigen Presenting Cells (APCs)

Antigen presenting cells (APCs) are a heterogeneous group of immune cells that mediate the cellular immune response by taking up, processing and presenting antigens to T lymphocytes. The principal APCs in the immune system are dendritic cells (DCs), macrophages, and B cells.

APCs capture infectious antigens through several mechanisms:

- receptor-mediated endocytosis
- pinocytosis
- phagocytosis

As previously mentioned, phagocytosis is based in the remodelling of actin and the formation of a phagosome. Recent studies have shown that phagosome maturation is regulated by signals originating from pattern recognition receptors discriminating between self and non-self antigens [80].

1.5.3.1 Dendritic cells

Dendritic cells (DCs) are the most potent APCs of the immune system and act as link between innate and adaptive immunity [81]. To become potent T cell stimulators, DCs have to mature. This process is accompanied by functional and phenotypic changes.

DCs are competent inducers of B and T cell responses [82,83]. TCRs recognize peptides attached to molecules of the major histocompatibility complex (MHC) on the surface of APCs. There are two types of MHC: MHC class I and MHC class II, which stimulate CTLs and helper T cells, respectively [82].

DCs capture and process antigens, and display large amounts of MHC-peptide complexes at their surface. In contrast, the amounts of antigen-MHC complexes and costimulatory molecules on tumours are often small.

Immature DCs (iDCs) are unable to stimulate T cells due to the absence of costimulatory signals such as CD40, CD54 and CD86 that are needed for proper T cell activation. Nevertheless, iDCs are able of capturing and processing antigens to form MHC peptide complexes. iDCs show large amounts of MHC class II-rich compartments (MIICs), which are endosomal structures, that include HLA-DM or H-2M, which enhance and rearrange peptide binding to MHC class II molecules[83–87].

iDCs reside in peripheral tissues until they are exposed to inflammatory stimuli and take up antigen. After being stimulated, iDCs migrate to the peripheral lymph nodes where they mature and express additional molecules that induce T cell stimulation [83]. Mature DCs (mDCs) produce high levels of IL-12 [88–90], a cytokine that enhances both innate and adaptive immunity. During the maturation process the expression of co-stimulatory molecules such as CD83, CD80 and CD86 is upregulated [91]. Maturation can be influenced by diverse factors: bacteria, microbial cell wall components like lipopolysaccharide (LPS)[84], and cytokines like IL-1, GM-CSF, and TNF-α. In contrast, IL-10 inhibits the maturation process [92].

To generate anti-tumoral immune responses, APCs have to present peptides bound to MHC molecules. Mature and functional active DCs seem to be absent in many tumour types, resulting in a failure in the generation of a tumor-specific T cell response; a possible underlying mechanism is the accumulation of immunosuppressive factors such as IL-10, TGF-ß and vascular endothelial growth factor in the tumor environment, that reduce DC development and function [83,93].

1.5.4 Cytokines

Cytokines are a group of proteins involved in the regulation of the innate and adaptive immunity. Their synthesis is induced by cellular activation, differentiation and proliferation signals of immune cells [70].

Mononuclear phagocytes are mainly stimulated by bacterial compounds and secrete inflammatory cytokines like tumor necrosis factor alpha (TNF-α), IL-6 and IL-1. As a feedback regulation mononuclear phagocytes can also produce anti-inflammatory cytokines like IL-10, which suppress the immune response; for example the production of TNF-α is inhibited by IL-10 [94].

IL-6 is secreted by macrophages and T cells and is able to cross the blood brain barrier [95]. It mediates pro-inflammatory and anti-inflammatory responses [96].

After stimulation, DCs produce IL-12. IL-12 is a prerequisite for the initiation of a $CD4^+$ T helper 1 (T_H1) response, which consequently activates CTLs. IL-10 counteracts the effects of IL-12 [70]. A reduction in the production of IL-12 and IFN-γ has been related with the inhibition of tumor- infiltrating T cells in ovarian cancer [97].

1.5.4.1 IL-12 regulations

iDCs become activated through the stimulation of their pattern-recognition receptors (PRRs). In this context, toll like receptors (TLR) play a crucial role in the activation of DCs. Ten functional TLRs have been identified in humans [98]. Each TLR detects specific molecular structures of pathogens as their ligand (pathogen-associated molecular patterns (PAMPs)) [72]. After the ligand binds to its typical TLR, pro-inflammatory activities take place [99]. All TLRs but TLR3, bind to the adaptor protein myeloid differentiation primary-response protein (MyD88) [100].

TLR4 is localized on the cell surface and is generally stimulated by LPS, the cell wall component of Gram-negative bacteria. In the serum, LPS is connected to LPS-binding Protein (LBP) which interacts with a receptor complex of TLR4, CD14 and associated proteins [101]. After stimulation, signalling cascades (see figure 1.3), mediated by TLR4, modulate gene expression and subsequently the production of several pro-inflammatory cytokines such as IL-6, TNF-α and IL-12. IL-12 production is modulated mainly under 3 different pathways, each one with their own kinetics.

Pathway 1 "Canonical Pathway"

This pathway consists in a series of phosphorylations of IκB proteins by a multiple IκB kinases complex (IKK complex), which consists of two catalytic components (IKKα and IKKβ) and a regulatory component (IKKγ)[102]. After the phosphorylation of IκB proteins, IκB is degradated through an ubiquitin system by the 26S proteasome. The free unbound Nuclear Factor κB (NF-κB) can then translocate to the nucleus and activate the transcription of specific target genes [103] .

Pathway 2 "PI3K induced-signalling pathway"

IL-12 production has been also linked to mitogen-activated protein (MAP) kinases pathway. Three subgroups of MAP kinases have been identified: extracellular signaling regulated kinases ERKs, c-Jun N-terminal kinase (JNK) and the p38 MAPK [104]. After stimulation of TLR4 by LPS, phosphoinositide-3 kinases (PI3Ks) pathway is activated

leading to a downstream phosphorylation of serine/threonine kinase Akt and extracellular signal-regulated protein kinases 1/2 (ERK1/2) [105]. Akt activation modulates the activation of p38 MAPK and JNK. The production of IL-12 is regulated by PI3K in a negatively manner while p38 MAPK and JNK are positively regulated [106].

Pathway 3 "G proteins and cAMP"

Heterotrimeric G proteins participate in the activation of MAPK and Akt signaling pathways. G $_{i/o}$-mediated activation of the MAPK is independent of the canonical signaling cascade. Heterotrimeric G proteins inhibit adenylate cyclase activity and the cAMP accumulation in human monocytes. High cAMP levels are able to hamper IL-12 production. It has been reported that $G\alpha_i$-protein suppresses IL-12 production via Akt signaling (JNK, and ERK 1/2 pathway, but not p38) independently of PI3 kinase (see figure 1.3) [107,108].

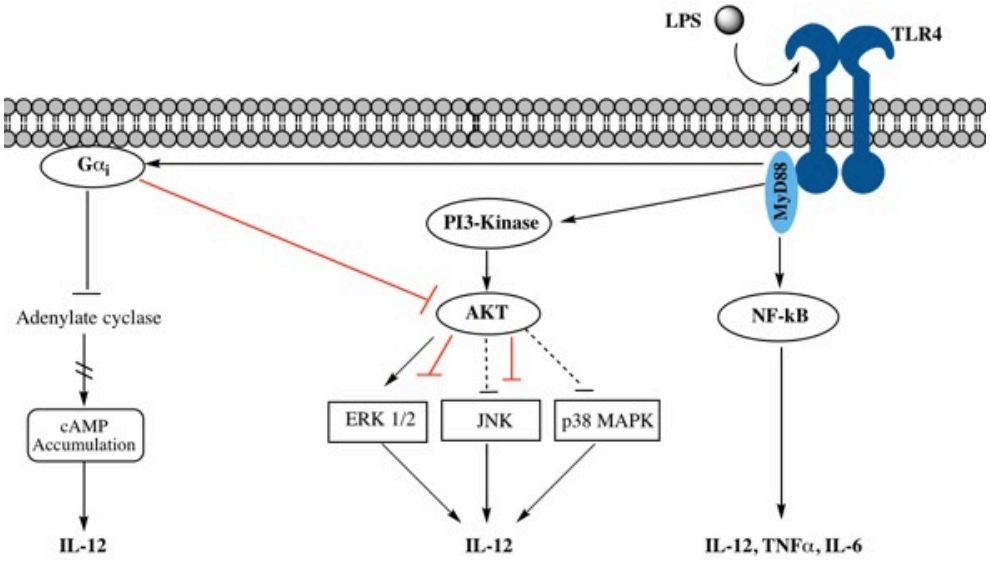

Figure 1.3 LPS-stimulated pathways associated with IL-12 regulation. LPS stimulates the TLR4-mediated activation of the NFκB-pathway and thereby the production of TNF-α, IL-6 and IL-12p40. $G\alpha_i$-mediated inhibition of adenylate cyclase and cAMP accumulation, Gβγ-mediated activation of Akt pathway but not p38. Adapted from Hildebrand et al.,[109].

1.6 Aim

During my Masters thesis we found that IL-12 production was strongly decreased in dendritic cells after incubation with D-HG whereas IL-10 production was increased. As these two cytokines are important players in the regulation of an anti-tumour response, D-HG could be involved in the immunosuppression in the tumour environment.

The aim of this thesis was to further characterize the effects of HG on immune cells and tumor cells (differentiation, effects on metabolism) and to evaluate possible mechanisms which are involved in the suppression of IL-12 production in dendritic cells (regulation of transcription factors and signalling pathways).

2. Material

2.1 Equipment

2.1.1 Cell Culture

Equipment	Company
AMG Microscope Evos xl	Fischer Scientific, Darmstadt Germany
CASY Cell Counter and Analyzer System Model TT	Roche Innovatis AG, Reutlingen Germany
Centrifuge Biofuge fresco	Heraeus, Osterode, Germany
Centrifuge Megafuge 3,0 R	Heraeus, Osterode, Germany
Hemocytometer	Marienfeld, Lauda-Königshofen, Germany
Incubator BBD 6220	Heraeus, Osterode, Germany
Laminar Flow Air HA 2472	Heraeus, Osterode, Germany
pH-Meter	Hanna Instruments, Kehl am Rhein, Germany
Vortex	Scientific Industries, New York, USA
Wellwash™ Microplate Washer	Thermo Electron Corporation, Darmstadt Germany

2.1.2 Elutration

Equipment	Company
Centrifuge Avanti J-20XP; Rotor JE 5.0	Beckmann, München, Germany
Elutriator Avanti J-20XP	Beckmann Coulter, Krefeld, Germany
Waterbath	Julabo, Seelstadt, Germany

2.1.3 Lysate, Isolation and PCR

Equipment	Company
Heat sealer	Eppendorf, Hamburg, Germany
Multipipette Multipette plus	Eppendorf, Hamburg, Germany
Multipipettor Multipette plus	Eppendorf, Hamburg, Germany
NanoDrop ND1000	Thermo Fisher Scientific, Schwerte, Germany
PCR-Thermocycler Modell PTC-200	MJ-Research/Biometra, Göttingen, Germany
Realplex Mastercycler epGradient S	Eppendorf, Hamburg, Germany
Rotilabo® mini centrifuge	Carl Roth, Karlsruhe, Germany
Welding machine for PCR plates Fermant 400	Josten & Kettenbaum, Bensberg, Germany

2.1.4 Western Blot

Equipment	Company
Electrophoresis Device	Biometra,Göttingen, Germany
Forceps	Aesculap, Tuttlingen, Germany
ImageQuant LAS4000	GE Healthcare, Freiburg, Germany
Pipetboy	Integra Biosciences, Fernwald, Germany
Power supplies	Biometra, Göttingen, Germany
Pulsed field electrophoresis	GE Healthcare, Chalfont St Giles, UK
Pulsed field gel electrophoresis equipment	Biostep, Jahnsdorf, Germany
Test tube shaker IKA®	Sigma-Aldrich, St. Louis, MO, USA
Thermomixer	Eppendorf, Hamburg, Germany
Water purification system	Millipore, Eschborn, Germany
Western-Blot-camera	Biometra, Göttingen, Germany

2.1.5 Flow Cytometry

Equipment	Company
FACS Calibur flow cytometer	BD Biosciences, Franklin Lakes, NJ, USA

2.1.6 Respirometry

Equipment	Company
Gastight 1700 Syringes (10,25,50µl)	Hamilton, Bonaduz, Switzerland
Hot-Air Disinfectable Gassed Incubator BBD 6220	Termo Fisher, Langenselbold, Germany
OxoDish®	PreSens, Regensburg, Germany
Oxygraph-2k	Oroborus Instruments, Innsbruck, Austria
SDR SensorDish® Reader	PreSens, Regensburg, Germany

2.2 Consumables

2.2.1 Cell Culture

Material	Company
Cell Culture Flask	Costar, Cambridge, USA
Cell culture plates	BD, Franklin Lakes, NJ, USA
Cryo tubes	Corning, Corning, NY, USA
Microtiter plates (6, 12, 96 wells)	Falcon, Heidelberg, Germany
Pipette Tips	Eppendorf, Hamburg, Germany
Pipettes (2, 5, 10, 25, 50ml)	Costar, Cambridge, USA
Plate for ELISA	Costar, Cambridge, USA
Polystyrene test tubes	Falcon, Heidelberg, Germany
Polystyrene test tubes with cell strainer cap	Corning, Corning, NY, USA
Sterile Filter	Millipore, Eschborn, Germany

2.2.2 Lysate, Isolation and PCR

Material	Company
Cell scrapers	Sarstedt, Nümbrecht, Germany
Cell strainer (70µm, 100µm)	Falcon, Heidelberg, Germany
Combitips for Eppendorf multipette	Eppendorf, Hamburg, Germany
Heat sealing film	Eppendorf, Hamburg, Germany
Micro test tubes (0.5ml, 1.5ml, 2ml)	Eppendorf, Hamburg, Germany
Micropore filters	Sartorius, Göttingen, Germany
PCR plate Twin.tec 96 well	Eppendorf, Hamburg, Germany
Syringe Filters, sterile	Sartorius, Göttingen, Germany
Syringes and needles	Becton Dickinson, Heidelberg, Germany
Twin Technology PCR plates (96 wells)	Eppendorf, Hamburg, Germany

2.2.3 Western Blot

Material	Company
Filter paper 3MM	Whatman, Dassel, Germany
Fotofilm Hyperfilm™ ECL	Amersham, Braunschweig, Germany
Hyperfilm™ ECL	GE Healthcare, Chalfont St Giles, UK
Immobilon-P PVDF membrane	Millipore, Schwalbach, Germany

2.3 Reagents

2.3.1 Cell Culture

Reagent	Company
Bovine serum albumine	Sigma-Aldrich, St. Louis, MO, USA
CasyTON	Roche, Basel, Switzerland
Dimethyl Sulfoxide (DMSO)	Sigma-Aldrich, SHDB7695v, St. Louis, MO, USA
Dulbecco´s Modified Eagle Medium (DMEM) High Glucose	GIBCO, 21969-035 Paisley, UK
Dulbecco´s Modified Eagle Medium (DMEM) Low Glucose	GIBCO, 31885 023, Paisley, UK
Fetal Calf Serum, FCS	PAA, A11102, Freiburg, Germany
Granulocyte-macrophage colony-stimulating factor, GM-CSF	Peprotech, 300 03, Hamburg, Germany
Interleukin- 4 (IL-4)	Peprotech, 200 04, Hamburg, Germany
L-Alanyl-L-Glutamine	Biochrom, K0302, Berlin, Germany
Lipopolysaccharides, LPS	ENZO, ALX-581-009, Lörrach,

	Germany
Penicillin/Streptomycin (Pen/Strep)	GIBCO, 15140122, Paisley, UK
Phosphate Buffered Saline (PBS)	Sigma, D8537, St. Louis, MO, USA
RPMI Medium 1640 (1X)	GIBCO, Paisley, UK
Trypsin/EDTA	PAN Biotech, P10 024100, Aidenbach, Germany

2.3.2 Elutration

Reagent	Company
Aqua	B.Braun, Melsungen, Germany
Bovine serum albumine	Sigma-Aldrich, St. Louis, MO, USA
CasyTON	Roche, Basel, Switzerland
H2O2	Merck, Darmstadt, Germany
Hanks' Balanced Salt Solution	Sigma-Aldrich, St. Louis, MO, USA
HCl	Carl Roth, Karlsruhe, Germany
Isopropanol	Braun, Melsungen, Germany
PBS	Sigma-Aldrich, St. Louis, MO, USA

2.3.3 Lysate, Isolation and PCR

Reagent	Company
2-Mercaptoethanol	Gibco/Life Technologies, Carlsbad, CA, USA
Nuclease-free water	Gibco/Life Technologies, Carlsbad, CA, USA

2.3.4 Western Blot

Reagent	Company
Acrylamide	Carl Roth, Karlsruhe, Germany
APS	Merck Millipore, Billerica, MA, USA
TEMED	Sigma-Aldrich, St. Louis, MO, USA
Triton X100	Sigma-Aldrich, St. Louis, MO, USA
Tween 20	Sigma-Aldrich, St. Louis, MO, USA

2.3.5 Flow Cytometry

Reagent	Company
FACS clean	BD Biosciences, Franklin Lakes, NJ, USA
FACS flow	BD Biosciences, Franklin Lakes, NJ, USA
FACS rinse	BD Biosciences, Franklin Lakes, NJ, USA

2.3.6 Respirometry

Reagent	Company
2-Propanol	Braun, Melsungen, Germany
Methanol	Thermo Fisher Scientific, Waltham, MA, USA

2.3.7 Inhibitors and Metabolites

Inhibitor / Metabolite	Concentration	Catalogue #	Company
Cyclosporin A (Sandimmune)	32pM		Novartis, Basel, Switzerland
D- α -Hydroxyglutaric acid disodium salt (D-HG)	10mM	H-8378	Sigma-Aldrich, St. Louis, MO, USA
Rotenon	0.1 µM	R8875	Sigma-Aldrich, St. Louis, MO, USA
L- α -Hydroxyglutaric acid disodium salt (L-HG)	10mM	90790	Sigma-Aldrich, St. Louis, MO, USA
Nicotinic acid	100µM	72309	Sigma-Aldrich, St. Louis, MO, USA
Oligomycin	0.5µM	1404199	Sigma-Aldrich, Taufkirchen, Germany
cAMP	100µM	1337	Tocris, Wiesbaden, Germany
α-Ketoglutarate (Di-Keto)	10mM	K-1875	Sigma-Aldrich, St. Louis, MO, USA
Forskolin	10µM	3828S	Cell Signaling, Germany

2.3.8 Antibodies for Western Blot

Antibody	Species	Dilution	Company
Anti-AKT	Polyclonal Rabbit	1:1000	Cell signaling, 9272S
Anti –IgG Rabbit (HRP-conjugated)	Polyclonal Goat	1:2500	Dako, P0448
Anti-Actin (human)	Rabbit (IgG)	1:2000	Sigma, A 2066
Anti-IgG Goat HRP	Polyclonal Rabbit	1:2500	Dako, P0449
Goat-Anti-Mouse	Goat	1:2500	Dako, HRP P0447
Anti-HIF	Rabbit (IgG)	1:1000	Santa Cruz, SC10790

Anti-IκB-α	Monoclonal Mouse	1:1000	Cell signaling, 4814S
Anti Oxphos	Rodent	1:5000	Abcam, ab110413
Anti P-p38	Polyclonal Rabbit	1:1.000	Cell signaling, 9211S
Anti p38	Polyclonal Rabbit	1:1000	Cell signaling, 9212S
Anti P-Akt	Polyclonal Rabbit	1:2000	Cell signaling, 9271S
Anti Tubulin	Monoclonal Mouse	1:5000	MECK, 05-829

2.3.9 Molecular Kits

2.3.9.1 Lysate, Isolation and PCR

Kits	Company
dNTPs	Roche diagnostics, Mannheim, Germany
QuantiFast SYBR-Green	Qiagen, Hilden, Germany
Random-Decamer-Primer	Ambion, Darmstadt, Germany
Reverse Transcriptase M-MLV	Promega, Mannheim, Germany
RNA Spike-in-Kit	Agilent Technologies, Böblingen, Germany
RNA*later*™	Qiagen, Hilden, Germany
RNase-free DNase Set	Qiagen, Hilden, Germany
RNeasy Midi- and Mini-Kit	Qiagen, Hilden, Germany
RNeasy Mini Kit	Qiagen, Hilden, Germany

2.3.9.2 Western Blot

Kits	Company
Amersham™ ECL™ Prime Western Blotting	GE Healthcare, Chalfont St. Giles, UK
ECL-Detection-Kit	GE Healthcare, Chalfont St. Giles, UK
ReBlot Plus Mild	Milipore, Darmstadt, Germany
SDS	Sigma-Aldrich, St. Louis, MO, USA

2.3.9.3 ELISA

Kits	Company
DuoSet ELISA IL-10, IL-12,	R&D Systems, Wiesbaden, Germany
Cyclic AMP XP Assay Kit #4339	Cell signaling, Germany

2.3.10 Molecular weight standard proteins

Western Blot Standard	Company
Kaleidoscope Pre-stained Standard	BioRad, München
Spectra Multicolor Broad Range Protein Ladder	Thermo scientific, Lithuania #26634
Rat heart Mitochondria	MitoSciences, Oregon, USA Lot. MS812/H2631
Rat heart Mitochondria	Abcam, Cambridge, UK MS812 Lot. L0163

2.3.11 Primers for qRT-PCR

Genes	Primer sequence
GPR109 Forward	5’ GCG-TTG-GGA-CTG-GAA-GTT-TG 3’
GPR109 Reverse	5’ GCG-GTT-CAT-AGC-CAA-CAT-GA 3’

2.3.12 Antibodies for Flow cytometry

Specificity	Isotype	Fluorochrome	Clone	Manufacturer
CD1a	Mouse IgG1	PE	SFCI19Thy1A8	Beckman Coulter, CA, USA
CD80	Mouse IgG1	APC	2D10	Biolegend, CA, USA
CD83	Mouse IgG1	PE-Cy7	HB15e	eBioscience, CA, USA
CD86	Mouse IgG1	FITC	2331(FUN-1)	BD, Franklin Lakes, NJ, USA
HLA-DR	Mouse IgG2a	FITC	B8.12.2	Beckman Coulter, CA, USA

2.4 Cell Lines

U87-MG: Human glioblastoma cell line was kindly provided by Prof. Dr. med. Peter Hau, Department of Neurology, University of Regensburg, Regensburg, Germany; source (American Type Culture collection).

TP365-MG: Human glioblastoma cell line was provided by Prof. Dr. med. Markus J. Riemenschneider, Department of Neuropathology, University of Regensburg, Medical School, Regensburg, Germany.
(http://www.ncbi.nlm.nih.gov/geo/query/acc.cgi?acc=GSM371063)

2.5 Software

2.5.1 Software for qRT-PCR

Software	Company
CellQuestPro	BD, Heidelberg
GraphPad Prism 6	GraphPad Software, La Jolla, USA
PubMed	www.ncbi.nlm.nih.gov/entrez
DatLab4	PreSens, Regensburg
Microsoft Office 2011	Microsoft Redmond, USA
Gene runner version 3.05	http://www.generunner.com
PerlPrimer version 1.1.14	http://perlprimer.sourceforge.net/
UCSC Genome browser	http://www.genome.ucsc.edu
FlowJo v9.5.3	FlowJo,LLC, Ashland, OR, USA
ImageLab v4.0	Bio-Rad, Munich, Germany
Enrichr	Amp.pharm.mssm.edu/Enrichr/

Unmodified, HPLC-purified oligonucleotides were designed using UCSC genome browser and PerlPrimer software followed by the analysis under Gene RunnerPrimer. Sequences were purchased from Eurofins MWG Operon (Ebersberg, Germany).

3. Methods

3.1 Standard Cell Culture Procedures

3.1.1 Freezing and Thawing

Cell aliquots were quickly thawed and immediately transferred in 10 ml of cell culture medium to avoid any toxic effects of dimethyl-sulfoxide (DMSO, Sigma). After centrifugation (300xg, 7 minutes) the supernatant was discarded and cells were resuspended in fresh medium and plated.
For cell storage, cells were transferred to RPMI with 40% Fetal Calf Serum (FCS, PAA) and 10 % DMSO and frozen in liquid nitrogen.

3.1.2 Splitting of adherent cells

To split cells, culture medium was removed and cells were washed with Phosphate Buffered Saline (PBS, Sigma); Trypsin/EDTA (PAN) was added, and cells were incubated for 5 minutes in the incubator and subsequently neutralized with fresh medium. The suspension was centrifuged at 300xg for 7 minutes, the supernatant was discarded and the pellet was resuspended in fresh medium. The amount of trypsin was adapted to the size of the culture flask, for a 162cm^2 Corning Flask 3ml of trypsin were used, for a 75cm^2 Corning Flask 1 ml and for a 25cm^2 Corning Flask 350µl were used.

3.2 Cell types and culture conditions

3.2.1 Cancer cell lines U87, TP365

Both cell lines were cultured in DMEM supplemented with 0.5% Pen/Strep, 1% glutamine and 10% FCS in a humified atmosphere of 95% air, 10% CO_2 at 37°C. The splitting of the cells was performed after 3 days, or after 75% of confluence was reached.
Depending on the experimental setting different cell densities were employed.
For RNA isolation and protein measurement, 2.5x10^6 cells were plated in 6-well plates with a final volume of 4ml. Every experimental setting was performed in parallel in DMEM High glucose (4.5g/L) and Low Glucose (1g/L) plus supplements.
For respirometry with the Presens technology, densities of 100 000, 200 000, 300 000 cells per ml were plated in an OxoDish® for 1 hour to achieve adherence, followed by the

addition of metabolites and measurement with SDR SensorDish® Reader for 24 hrs. For respirometry with the oxygraph technology, $1x10^6$/ml was added into each chamber with an end volume of 2ml during 2-3 hours.

3.2.2 Immune Cells

3.2.2.1 Monocyte isolation

Peripheral blood mononuclear cells (PB-MNCs) were separated by leukapheresis of healthy donors, followed by density gradient centrifugation over Ficol/Hypaque. Monocytes were then isolated by counter current centrifugal elutriation as described previously [110].

Elutriation was performed in a J6M-E centrifuge equipped with a JE 5.0 elutriation rotor and a 50ml flow chamber (Beckman, Munich, Germany). The chamber was sterilized with 6% H_2O_2 for 20 min and washed with PBS. Afterwards the calibration was performed at 2500 rpm and 4°C with Hanks Buffer. Mononuclear cells (MNCs) were loaded into the chamber and fractions were collected. Monocytes are the largest cells within MNCs hence are mainly obtained in the last fraction. The purity of monocytes was at least 85% as determined by the expression of CD14, a monocyte-specific antigen.

Table 3.1: Elutriation parameter and cell types

Fraction	Volume (ml)	Main cells isolated
Ia	1000	Platelets
Ib	1000	B- and T- lymphocytes. NK cells
IIa	1000	
IIb	500	
IIc	400	
IId	400	
III	800	Monocytes

3.2.2.2 Generation of dendritic cells

For the generation of dendritic cells, isolated monocytes were cultured in culture flasks at a concentration of $1x10^6$ cells/ 1.5ml for 7 days in RPMI 1640. The medium was supplemented with 10% FCS, 2mM glutamine, 50U/ml of penicillin and 50 mg/ml of streptomycin (0.5%), 225U/ml granulocyte macrophage colony stimulating factor (GMCSF, Peprotech) and recombinant IL-4 (144 U/ml, Peprotech) [111]. After 7 days the cells were harvested, immature dendritic cells (iDCs) were seeded at different densities depending on the experimental test.

- For supernatant experiments 200 000 iDCs were plated per well in a 24-well plate with 1ml of supplemented RPMI 1640. DC maturation was induced by addition of 100ng/ml lipopolysaccharide (LPS). For some samples the metabolites D-HG (D- α- Hydroxyglutaric acid disodium salt) and L-HG (L- α- Hydroxyglutaric acid disodium salt) were added during the culture. Supernatants were harvested after 24h, frozen at -20°C and used for cytokines determination.
- For experimental settings such as RNA isolation, Protein isolation or HG uptake measurements, $2.5x10^6$ iDCs/well were seeded in a 6-well plate. In a final volume of 4ml, which include RPMI + supplement, 100ng/ml LPS and metabolites.
- For experimental settings, such as determination of mitochondrial respiration, cells were plated (in 24-well OxoDish® for PreSens technology) or added (per chamber for Oxygraph technology) at a $1x10^6$ cells/ml concentration, plus LPS and metabolites addition.

3.3 Measurement of cytokines and Lactate

3.3.1 Enzyme Linked Immunosorbent Assay (ELISA)

Interleukins were determined in the culture supernatants using commercially available enzyme-linked immunosorbent assay (ELISA) kits (Duoset ELISA, R&D Systems, Minneapolis, MN) according to manufacturer's protocols.

96 well plates were coated with 10µL/well capture antibody for each cytokine. Plates were incubated at room temperature (RT) overnight. The next day, plates were washed three times with 400µL of Elisa wash buffer (0.05% Tween in PBS) per well. Plates were blocked for 1 hour by adding 300µL/well Reagent Diluent (1% BSA in PBS). Meanwhile samples were thawed at RT; a seven point standard was prepared according to manufacturer's recommendation. Plates were washed three times to eliminate excess of blocking solution. Prepared standards and the samples were pipetted, 100µL per well. Samples were incubated for 2 hours at RT. Plates were washed three times, the detection antibody was added, and incubated for 2 hours at RT. Plates were aspirated/washed, the working dilution of 100µL/well Streptavidin-HRP was added, and incubated at RT avoiding light exposure for 20 minutes. Plates were washed; 100uL of substrate solution (equal volume of hydrogen peroxide and tetramehtylbenzidine) was added to plate wells

for 20 minutes, stored at RT in the dark. Without washing, 50µL of stop solution was added. Plates were tapped gently to ensure thorough mixing. The optical density of each well was immediately determined with a microplate reader which was set according to the interleukin recommended wavelength.

To measure cAMP levels on iDCs, $1x10^6$ cells were placed on FACS tubes, centrifuge at 1400rpm during 7min and the supernatant discarded. Cells were then resuspended with 1mL cold PBS, and this procedure was repeated 2 times. Cells were then Lysated adding 200µl 1x lysisbuffer (diluted in H2O, stored in -20°C), incubated on ice for 10 mins, centrifuged at 1600rpm during 4 min, followed by the supernatant collection and storage at -80°C. Supernatant was then use to performed cAMP XP Assay according to manufacter protocol.

3.3.2 Enzymatic determination of lactate

To determine lactate concentrations, supernatants were harvested and frozen at -20°C until analysis. Lactate concentration was determined enzymatically using an ADVIA 1650 instrument (Bayer, Tarrytown, NY) and specific reagents (Roche, Mannheim, Germany). All values were corrected for lactate concentration of the culture medium. Lactate measurement was performed at the Department of Clinical Chemistry (University Hospital Regensburg, Germany).

3.4 Cell counting with a cell analyzer (CASY system)

The cell number was determined by using a cell analyzer, the CASY system. An aliquot of 50µl from the cell suspension was taken and placed in 10ml of Casy-ton solution. The mean of three cycles, (400µl each) was calculated by the Casy® software. In addition to cell number, cell diameter and volume were determined. Appropriate cursor settings based on cell size for determining cell number and viability were established for each cell type.

3.5 RNA /Protein lysates

3.5.1 RNA

After trypsinazing and counting the cells, the samples were centrifuged at 300xg for 7 minutes. Supernatant was discarded, and the pellet was resuspended in 350µl Lysis Buffer

(10µl of ß-mercaptoethanol per 1ml of Lysis Buffer (Qiagen,Germany)) and stored at -80ºC.

3.5.1.1 RNA Sequenciation

RNA was isolated using the Qiagen RNeasy kit. RNA-seq libraries were generated using the ScriptSeq^{TM} Complete Kit from Illumina according to the manufacturer's instructions (Experimental setting performed by Prof.Dr. Michael Rehli's research group). Libraries were sequenced paired-end (2 x 75bp) on a HiSeq 3000 at the Biomedical Sequencing Facility (BSF) in Vienna, Austria.

3.5.2 Protein

3.5.2.1 Ripa Buffer

After trypsinaizing and cell counting, cells were centrifuged at 300xg for 7 minutes, supernatant was discarded and pellet washed 2 times with PBS, after the second wash the pellet was resuspended with 100µl (per 5x10^6 of cells) of Ripa Buffer. Aadherent cells were detached with cell scrapers and thereafter vortexed thoroughly for 1 minute, frozen for 5 minutes at -20ºC, vortexed again and placed in liquid nitrogen followed by the final storage at -80ºC.

3.5.2.2 Phosphorylate Buffer

For subsequent analyzes of the phosphorylated form of proteins, cells were lysed after different incubation times (30 minutes, 1hr or 24hrs). After incubation times, well plates were placed on ice and the supernatant was transferred into 15ml centrifuge tube and centrifuged. Subsequently, both the cells adherent in the culture plate and the centrifuged cells were washed twice with ice-cold PBS, the centrifuged cells were then transferred into 1.5ml tube. In the next step, the cells in the 1.5ml tube were resuspended in 500µl of Buffer B and recentrifuged again. During the centrifugation time, the adherent cells were also treated with 500µl of Buffer B. Cells treated with Buffer B, which mainly contains protease and phosphatase inhibitors, was used to prepare the cells for subsequent lysis with Buffer C. After Buffer B had been removed from both cell populations, 150µl of Buffer C was pipetted onto the adherent cells. Then adherent cells were detached with cell scrapers, combined with the centrifuged cell fraction and placed on ice for 10 minutes.

Then 150µl of sodium dodecyl sulfate (sodium dodecyl sulfate, SDS) sample buffer (2x) was added, following heated at 95°C for 10 minutes and stored at -80°C until further use.

Buffer A

10mM	(1ml)	Tris/HCl (pH 7.9) (1M)
60mM	(447mg)	KCl
1mM	(37mg)	EDTA
100ml		H2O

Buffer B

1.5mM	(3µl)	EDTA (pH 8.0) (500mM)
1mM	(10µl)	Dithiotreitol (100mM)
1mM	(5µl)	EGTA (200mM)
50mM	(50µl)	β-Glycerophosphat (1M)
50mM	(50µl)	Sodium Flouride (1M)
25mM	(100µl)	Sodium Pyrophosphat (250mM)
1mM	(5µl)	Sodium Orthovanadate (200mM)
2µg/ml	(2µl)	Leupeptin (1mg/ml) (Roche, Mannheim)
2µg/ml	(2µl)	Pepstatin A (1mg/ml) (Roche, Mannheim)
2µg/ml	(1µl)	Aprotinine (2mg/ml) (Roche, Mannheim)
1ml		Buffer A

Buffer C (Lysate buffer)

0.4%	(40µl)	Nonidet P40 (10%) (Boehringer, Ingelheim)
100µg/ml	(5µl)	Chymostatin (20mg/ml) (Roche, Mannheim)
10µg/ml	(2µl)	Bestatin (5mg/ml) (Roche, Mannheim)
3µg/ml	(1µl)	E64 (3mg/ml) (Roche, Mannheim)
1mM	(1µl)	1,10-Phenantrolin (0.1mg/ml)
1ml		Buffer B

SDS (2x) Buffer

20%	(10ml)	Glycerin
125mM	(5ml)	Tris/HCl (pH 6.8) (1.25 M)
4%	(2g)	SDS
10%	(5ml)	2-Mercaptoethnol
0.02%	(10mg)	Bromophenol Blue
50ml		H2O

3.6 Western Blot Analysis

3.6. 1 Preparation of Sodium Dodecyl Sulfate (SDS) Gel

Protein samples were separated using a discontinuous gel system, which is composed of stacking and separating gel layers that differ in salt and acrylamide (AA) concentration.

3.6.1.1 Material

SDS-PAGE stock solutions

- 70% Isopropanol
- 12% separating gel,
- Stock solution (Tris/HCL; SDS; Acrylamid)
- Tetramethyllethylenediamine (TEMED)
- 10% ammonium persulfate (APS)
- 5% Stacking gel (Tris/HCL; SDS; Acrylamid)
- Running Buffer: 5X Laemmli-Electrode Buffer.
- Distillate Water
- 2x SDS- Sample Buffer
- Protein Sample
- Standard: Kaleidoscope Prestained Standard (BioRad)

3.6.1.2 Required buffers and solutions:

- Separating gel buffer: 90.83g (1.5M) Tris/HCl, pH 8.8, in 1L ddH2O
- Stacking gel buffer: 30g (0.5M) Tris/HCl, pH 8.8, in 1L ddH2O
- SDS: 10g (10%) SDS, in 1L ddH2O
- Ammonium persulfate: 10g APS, in 1L ddH2O
- Running Buffer (5X): 15g (40mM) Tris, 21g (0.95M) Glycine, 15g (0.5%) SDS
- Running Buffer (10X) for Oxphos: Tris- Base 30g, Glycin 144g, SDS 10g and 1L distilled water.
- Running Buffer (1X) for Oxphos: 10X Running Buffer for Oxphos 100ml, ddH2O 900ml.

The separating gel was prepared a day prior to the electrophoresis and overlaid with isopropanol; 15 minutes of incubation at room temperature were necessary to finalize polymerization. Isopropanol was exchanged by the stacking gel, and the comb was inserted. After polymerization, the gel was stored overnight at 4°C.

The following day, gel was mounted in the electrophoresis tank, previously filled with 1x running buffer. For the majority of the antibodies, with the exception of samples analyzed for OXPHOS antibody, protein samples were loaded and the gel ran with 80 volts (V) until the bands reached the surface of the stacking gel (20min). Next, the voltage was

increased to 100V, after 15 minutes the voltage was increased to 120V and the gel ran for 2hrs.

For samples where mitochondrial proteins were analyzed, 5µl of sample and marker were loaded in a 10% gel, the gel initially ran in 1X Running Buffer for Oxphos with 90V during 30 min, and afterwards the voltage was increased to 120V for 1.5hrs.

Depending on the size of the desired proteins the gel concentration can vary:

Protein size	Separating Gel
< 30 kDa	14%
25 – 70 kDa	12 %
> 70 kDa	10%

For the presented experiments, with the exception of the experiment set up for samples where mitochondrial proteins were analyzed, a 12% separating gel was used.

3.6.2 Western Blot

3.6.2.1 Required Solutions and Material:

- 70 % Isopropanol
- Anode- Buffer A: 36.3g (0.3M) Tris, pH 10.4, 20% Methanol, in 1L dd H_2O
- Anode-Buffer B: 3.03g (25mM) Tris, pH 10.4, 20% Methanol, in 1L dd H_2O
- Cathode-Buffer C: 5.2g (4mM) ε -amino-n-caproic acid, pH 7.6, 20% Methanol, in 1L dd H_2O
- Blot Buffer 10X for Oxphos: 30.28g Tris-Base, 144g Glycin in 1L Distilled Water.
- Blot Buffer 1X for Oxphos: 100ml Blot Buffer 10X for Oxphos, 700ml Distilled Water, 200ml Methanol 100%
- PVDF-Membran (Millipore)
- Paper Filter (Whatman)

After separation by SDS-PAGE, with the exception of samples analyzed for mitochondrial proteins, proteins were electro-blotted into a PVDF membrane (Immobilon-P, Millipore) using a three-buffer semi-dry system and visualized by immunostaining using specific antibodies and ECL detection kit.

Three Whatman 3MM filter papers soaked with buffer A were placed on the anode, and three Whatman 3MM filter papers soaked with buffer B, followed by the membrane, previously cut smaller than the gel size and soaked first with isopropanol and after 2 minutes with buffer B.

The gel was placed on top of the membrane. Three Whatman 3MM filter papers soaked with buffer C were placed on top of the gel followed by the cathode. Air bubbles in-between the layers had to be avoided. Protein transfer was conducted for 1hr at 11V.

In case of the samples analyzed for mitochondrial proteins, 4 whatman filter papers, one membrane and the gel were placed in a bowl with 1X blot buffer for Oxphos. Following to this, 2 filter papers were separated and placed in the chamber blot, followed by the membrane placing, and then with the help of a spatula the gel was positioned on the top of the membrane, being careful not to leave bubbles in between the gel and the membrane, next the gel was covered with the other 2 soaked filter papers, and homogeneously pressed against it with a 5ml pipette, in order to eliminate the exceeding buffer. Protein transfer was conducted for 1.5hrs at 15V.

3.6.3 Immunodetection

3.6.3.1 Required buffers and materials:

- 10x Tris buffered saline (TBS)
- Distilled water
- TWEEN 20
- Milk powder/BSA
- Primary antibody
- Secondary antibody/HRP-conjugated
- ECL Solution
- 30% Hydrogen Peroxide
- ReBlot- Stripping- Solution
- Wash buffer: 1x TBS with 0.1% TWEEN 20
- Wash Buffer for Oxphos 10X: 20mM Tris (24.2g), 150mM NaCl (80g), <1000ml (ca.970ml) pH=7.6
- Wash Buffer 1X TBS-T for Oxphos: 10X Wash Buffer for OXPHOS 100ml, distilledwater 900ml, Tween 20 1ml.

- Blocking buffer: Wash Buffer with 5% Milk
- Blocking buffer for OXPHOS: BSA 5%

With the exception of the samples used to analyze mitochondrial proteins, the blotted membrane was blocked with 5% milk powder in PBST overnight at 4ºC according to the antibody specifications.
Next, the membrane was incubated with the first antibody at RT for 1hr (concentration according to the antibody).
After 3 washing steps were performed, each one for 10min with the appropriate washing buffer, the membrane was incubated for 1hr at RT with a horseradish-peroxidase (HRP)-coupled secondary antibody, detecting the isotype of the first antibody.
Three washing steps were followed by 2 minutes of incubation with ECL solution. Blots were exposed to an autoradiography film (HyperfilmTM ECL, Amersham) for 10 seconds to 20min depending on the signal intensity.
The immunodetection procedure for samples analyzed for mitochondrial proteins differs from the standard WB procedure.
After the membrane was cleaned from the Ponceau staining, it was placed in a 50ml falcon tube with 5ml 5% BSA to get blocked, during 1h in a horizontal shaker. After the incubation time the membrane was incubated overnight with the first antibody OXPHOS anti-Mouse (1:5000 dilution = 2µl in 10ml), in the shaker.
After 1st Ab incubation time, 3 washing steps were performed (5ml at 5, 10, 15min), then the membrane was incubated for 1hr at RT with Goat anti-mouse Secondary Ab. Three washing steps were followed by 2 minutes of incubation with ECL Solution. Chemiluminescence imaging was performed on ImageQuant LAS400 GE HealthCare equipment.
Western Blot procedure for the antibody ERK was performed by Dr. med. Sven Lang in the department of “Klinik und Poliklinik für Chirurgie” institute, in the University Hospital Regensburg.

3.6.4 Loading control

3.6.4.1 General protocol for loading control

After developing the membrane two washing steps were performed followed by 15 minutes of incubation with ReBlot Solution, ending the incubation time, the membrane

was washed 3 times, and blocked for 1hr, proceeding with an overnight incubation of loading control antibody. The following day, the blot was incubated with the secondary antibody. Protein detection was determined after incubation with ECL solution and autoradiography.

3.6.4.2 Ponceau Staining

After the protein transfer, the membrane was placed in a box with 10ml Red Ponceau and left for 5 minutes in the shaker. After 5 minutes, the membrane was submerged one time in 1X Washing buffer for mitochondrial proteins and placed in a plastic folder and posteriorly scanned. After the scanning, the membrane was washed for 5 minutes with 1X Washing Buffer for mitochondrial proteins, until the membrane get free of Ponceau.

3.7 RNA Isolation and determination

3.7.1 Preparation of RNA lysate

After trypsinaization and counting the cells, the samples were centrifuged at 300xg for 7 minutes, the supernatant was eliminated, the pellet was resuspended in 350µl lysis buffer (10µl of ß-mercaptoethanol per 1ml of lysis buffer (Qiagen, Germany)) and stored at -80ºC.

For RNA extraction, 350µl of 70% ethanol was added to the homogenized lysate and mixed by pipetting; 700µl of the sample was poured into a Spin Column with 2ml collection tube (Qiagen Kit). The sample was centrifuged for 15 seconds at 6708xg and the flow-through discarded, followed by the addition of 350µl wash buffer to the column, posteriorly the column was centrifuged and the flow through was discarded.

DNAse (10µl) and RNase Free DNase buffer (70µl) was added into the column and incubated at room temperature for 15 minutes. Another wash step was performed and the flow-through was discarded.
The next step was the addition of 500µl concentrated wash buffer, followed by a centrifugation step, and flow was discarded. Posteriorly 500µl of 80% ethanol were added into the column and centrifuged for 2 minutes at 6708xg in order to dry the silica-gel membrane; the flow-through and collection tube were removed. Another centrifugation step was performed.

For elution of the RNA present in the membrane of the column, 30µl of RNase-free H_2O were pipetted, followed by 1 min of centrifugation at 6708xg.
The isolated RNA was quantified with a photometer Nanodrop and stored at -80ºC.

3.8 Real-Time quantitative PCR (RT-qPCR)

3.8.1 Reverse Transcription PCR (RT-qPCR)

Total RNA was reverse transcribed into complementary DNA (cDNA) using Moloney murine leukemia virus reverse transcriptase (M-MLV RT) enzyme. Random decamers were used to prime cDNA synthesis. The volume of 1µg of total RNA was adjusted to 13µl with nuclease-free ddH2O and mixed with 1µl Random Decamers (Promega) and 1µl dNTPs (10mM) on ice. Secondary structures of RNA were dissolved by 5min incubation in Thermocycler at 65°C followed by immediate incubation on ice for 1 min. After mixing with 4µl M-MLV Buffer (5x;Promega), samples were incubated at 42°C for 2min. Reverse transcription started upon addition of 1µl RT enzyme (50min, 42°C) and was stopped by heat inactivation of the enzyme (15min, 70°C).
The RNA solution was placed In the PCR-Thermocycler for another 2 minutes at 42ºC; at the end of the 2 minutes incubation 1µl of Reverse Transcriptase was added and ran the following program.

Temperature	**Time**	
65ºC	5 min	Denaturalization
42ºC	2 min	Incubation
42ºC	50 min	
70ºC	15 min	Inactivation of MMLV RT
10ºC	For ever	

Data shown the PCR program used for the transcription of RNA into cDNA. The temperatures and duration per cycle are mentioned.

The cDNA was stored at -20ºC.

3.8.2 Quantitative Real-Time PCR (qPCR)

Reverse transcribed cDNA products were analyzed on a Mastercycler Ep Realplex using the QuantiFast SYBR Green PCR Kit. Primer sequences were purchased from Eurofins MWG Operon, Ebersberg, Germany except when other companies are mentioned. 18S

rRNA was used as a reference gene for all genes of interest. PCR reaction was carried out in a 96 well plate format adapted to the Eppendorf Realplex Mastercycler EpGradient S system. The amount of amplified DNA relative to reference gene 18S rRNA was measured through the emission of light by SYBR green dye after each extension step. Melting curve was monitored to determine the specificity of amplification product.
The reaction component and cycling protocol for RT-qPCR are listed below:

Table 3.2: RT-qPCR reaction composition

Components	Concentration	Volume
SYBR Green mix (2x)		5 µL
Nuclease-free ddH2O		3 µL
Template DNA	1000 ng	1 µL
Primer_sense	10 µM	0.5 µL
Primer_antisense	10 µM	0.5 µL
Final Volume		10 µL

Table 3.3: Cycling protocol for RT-qPCR

Cycle step	Temperature	Time consumed	Number of cycles
Initial denaturation	95°C	5 min	1x
Denaturation	95°C	8 sec	45x
Anneling and Extension	58°C	20 sec	
Final denaturation	95°C	15 sec	1x
Final extension	60°C	15 sec	
Melting Curve	60-95°C	10 min	1x
Cooling	4°C	Hold	

3.9 Respirometry

Mitochondrial respiratory activity was determined under cell culture conditions using the PRESENS technology (PreSens Precision Sensing GmbH, Regensburg, Germany) and in detail by high-resolution respirometry using the oxygraph O2-k (Oroboros Instruments, Innsbruck, Austria). For both applications $1x10^6$ cells/ml were analyzed. The SDR SensorDish® Reader is a 24-channel oxygen and pH meter. The optical oxygen (OxoDish®) sensor is integrated at the bottom of each well of a 24-well multidish. The sensors are luminescent dyes embedded in an analyte-sensitive polymer. The sensors are read out non-invasively through the bottom of the multidish by the SensorDish® Reader and cells do not have to be fixed to the bottom of the plate. The resulting signal is

converted automatically to the respective parameter using calibration parameters stored in the software.

For high-resolution respirometry cells centrifuged and resuspended in fresh respective culture medium and respiration of suspended cells was measured at 37 °C with chamber volumes set at 2ml. Data acquisition and analysis was performed with the DatLab4 software (OROBOROS, Innsbruck, Austria) including calculation of the time derivative of oxygen concentration, signal deconvolution dependent on the response time of the oxygen sensor, and correction for instrumental background oxygen flux[112]. Data points were recorded at 1s time intervals. Before closing the oxygraph chamber, 50µl samples were taken for determining cell number in each chamber. ROUTINE respiration was measured in the first 20min, afterwards D-HG or medium was added. When determining the effect of D-HG on dendritic cells LPS was added after 10min of D-HG incubation. ROUTINE respiration was measured for one hour, LEAK respiration was determined after addition of oligomycin (2µg/10^6 cells), capacity of complex I to IV (ETS) after a stepwise titration of FCCP (final concentration of approximately 3µM, 1µM by step), residual oxygen consumption (ROX) not related to the respiratory system was measured after addition of rotenone (0,5µM) and myxothiazol (2,5µM). All respiratory parameters were corrected for (ROX), mitochondrial oxygen consumption related to ATP production was calculated as the difference between ROUTINE and LEAK respiration. In the case of the glioma cell lines, respiration could not be normalized to cell number as the cells formed clusters, therefore, respective respiratory control ratios were calculated.

3.10 Fluorescence Activated Cell Sorting

Fluorescence activated cell sorting (FACS) is a flow cytometry based method that detect both intra- and extracellular protein of interest in/on the cells. Different proteins on the same cell can be marked with antibodies conjugated to different fluorochromes.

Single cells suspended in a medium are injected into a stable stream that forces cells to travel one by one in a laminar flow fashion. Cells pass through the beam of laser light. Scattered light and fluorescence emission provide information about the particle's properties. Light scattered in forward direction provides information about size of cells and side scatter measures granularity of cells.

Based on the excitation and emission wavelength of fluorochrome conjugated to cells, varying protein expression by cells can be measured. Also, using this fluorochrome labelled antibodies; different populations of cells can be sorted and collected.

3.10.1 Extracellular Staining

To access the protein expression, monocyte derived DCs were plated under 3 settings, 1st D-HG was added at day 0, 2th D-HG was added at day 5 and 3th D-HG was added at day 7, followed by the collection of the cells two washing steps with 1 ml FACS buffer were performed. Cells under the 3 different culture settings were then stained with surface markers: CD1a, CD80, CD83, CD86 and HLA-DR along with the respective isotype control. Cells were incubated at 4 ^{o}C for 30 minutes. Cells were washed thrice with FACS buffer and resuspended in 300µL FACS buffer. Flow cytometric measurement was performed on a BD FACS Calibur.

3.10.2 Intracellular staining.

Monocytes obtained from volunteer blood donors via elutriation were cultured in RPMI medium supplemented with IL-4, GM-CSF in T25 flasks. After 7 days of culture cells were treated with LPS (100ng/ml), D-HG 10mM and Protein Transport Inhibitor (containing Monensin) for 16hrs. After incubation time, monocytes-derived iDCs and supernatants were recollected. 1.5x10^{6} cells were placed in FACS tubes and centrifuge 4 minutes at 1600 RPM, resuspended with PBS, washed and permeabialized with BD perm/wash solution 2 times, follow by staining with P40 FITC, P35 APC and IgG 2b FITC, IgG1 APC isotypes. Cells were fixed with 4% PFA, and analyzed on FACS Calibur.

Composition of:

- FACS buffer: 5ml of 60mg/ml Immunoglobulin + 5ml of 10% sodium azide + 500ml PBS
- Fixation/Permeabilization solution: 1 part of Fix/Perm concentrate + 3 part of Fix/Perm diluent. (BD #554714)
- Permeabilization buffer: 1 part of 10X buffer + 9 parts of distilled water (BD #558050).

4. Results

Isocitrate Dehydrogenase (IDH) is an important enzyme that catalyzes the conversion of isocitrate to α-ketoglutarate (α-KG). Point mutations in IDH 1 and 2 are frequently found in neoplasia including acute myeloid leukemia and glioma. Mutated IDH gains the ability to convert α-KG into 2-hydroxyglutarate (HG). HG is referred in the course of this thesis as the general structure that includes both enantiomers, D-2-hydroxyglutarate, abbreviated as D-HG and L-2- hydroxyglutarate abbreviated as L-HG. IDH mutations suppress hematopoietic differentiation in leukemia models [113]. However, it is still unclear whether HG affects the activation and differentiation of non-malignant hematopoietic cells and its impact on immune cell function.

4.1 Impact of HG on Dendritic Cells

4.1.1 Effect of HG on cytokines production.

Based on the findings that HG affects proliferation and differentiation of tumor cells (AML and Glioma cells) we hypothesized that HG also has effects on non-tumoral hematopoetic cells. Dendritic cells (DCs) are the most important antigen presenting cells (APC) of the immune system, acting as a link between innate and adaptive immune response. In response to stimulation, DCs undergo maturation and produce IL-12. IL-12 production induces the differentiation of naive CD4+ T cells into T helper cells (predominantly Th1 helper cells). DCs are also capable to produce immunosuppressive cytokines like IL-10, which induces the differentiation of naive CD4+ T cells into Th2 helper cells.

During my master thesis I was able to show a suppressive effect of HG on IL-12 production of DCs. To gain further insight we analyzed the expression of the two IL-12 subunits p35 and p40 by flow cytometry. DCs were generated from monocytes isolated from the blood of healthy donors and cultured in RPMI medium supplemented with IL-4 and GM-CSF for seven days. This protocol was used throughout the whole study. After 7 days of culture IL-12 secretion was measured in supernatants of DCs treated either with LPS (100ng/ml) alone or in combination with 10mM D-HG and a protein transport inhibitor (monensin) for 16hrs. After the incubation time DCs were stained for the expression of IL-12 subunits.

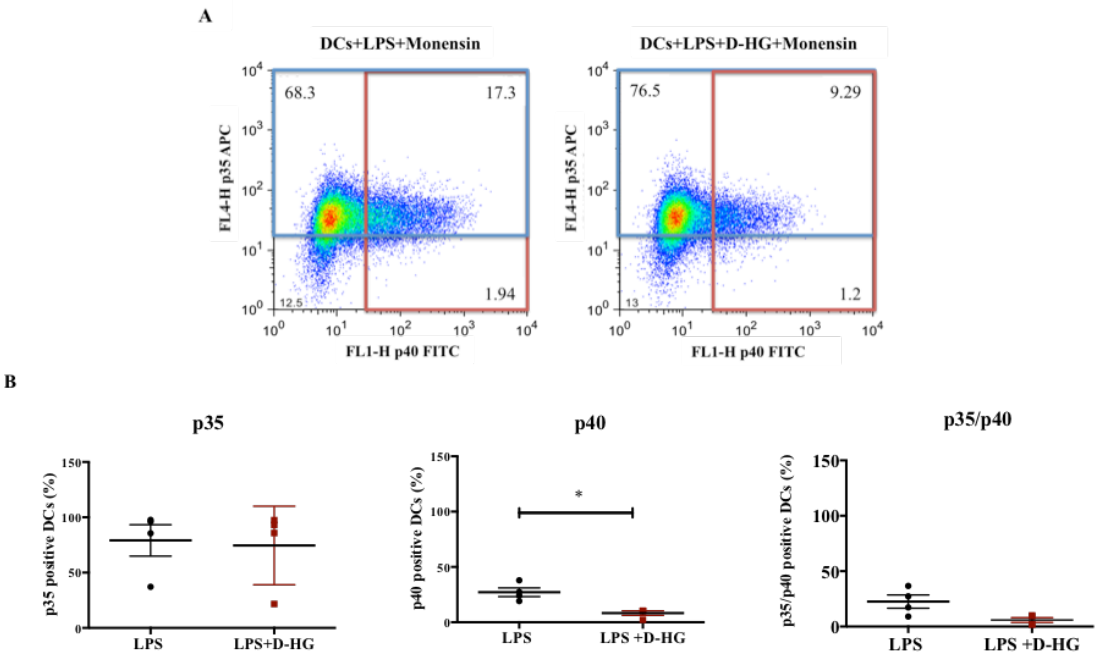

Figure 4.1. Effects of D-HG on IL-12 subunits. Human iDCs were differentiated from monocytes during 7 days and then stimulated either with 100ng/ml LPS alone or in combination with 10mM D-HG for 16hrs. A protein transport inhibitor was added (monensin) during stimulation. Cells were fixed with 4% of PFA per each 1 million cell and analyzed by flow cytometry. A) Representative staining of IL-12 subunits. B) Summarized data of the D-HG effect on IL-12 subunits p35 and p40. 3 independent experiments are presented. Statistical analysis was tested with Mann-Whitney U test (* $p \leq 0.05$, ns not significant).

D-HG did not affect the expression of the p35 subunit of IL-12 (Figure 4.1A; 85.6% positive cells after addition of LPS, 85.78% of positive cells when treated with D-HG and LPS); whereas p40 subunit expression was clearly reduced in the presence of 10mM D-HG (19.24% positive cells without D-HG and 10.49% positive cells with D-HG). This observation was statistically confirmed by analyzing at least three different donors (Figure 4.1B). These results demonstrate that D-HG mediated IL-12 reduction observed during previous studies is directly related with the specific suppression of the p40 subunit expression.

Next we investigated whether the suppression of IL-12 secretion is solely induced by the oncometabolite D-HG or also by its enantiomer L-HG. This was done by measuring IL-12 levels as well as IL-10 levels in the supernatant of D-HG and/or L-HG treated DCs.

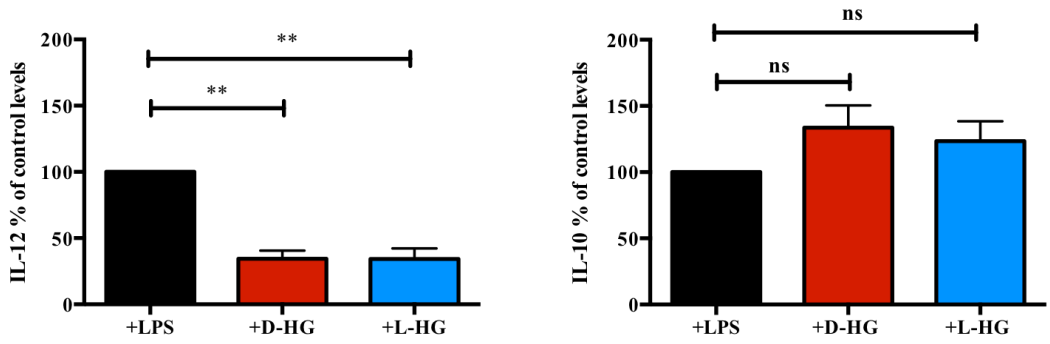

Figure 4.2 Impact of D-HG and L-HG on IL-12 and IL-10 secretion of dendritic cells. $0.2x10^6$ monocyte-derived DCs were plated in 24 well plates, iDCs were activated with 100ng/ml LPS, and in parallel exposed to 10mM of D-HG/L-HG for 24hrs. Supernatants were collected and measured for IL-12 and IL-10. The measurement was performed by commercially available ELISA. Data represent the mean +/- standard error (SEM) of 14 independent experiments (IL-12) and 10 independent experiments (IL-10). Statistical analysis was tested using the Friedman test, and Dunn multiple comparison test (** $p \leq 0.01$).

The data clearly show that L-HG suppresses the secretion of IL-12 as efficient as D-HG, strongly indicating a general suppressive activity of HG (Figure 4.2). Although not significant, it was interesting to observe the trend of upregelation of IL-10 under the influence of both isoform of HG pointing towards immunoregulatory impact of HG at least in human DCs (Figure 4.2). In the following analyses we mainly used D-2-hydroxyglutarate, abbreviated as D-HG, unless indicated otherwise.

4.1.2 Uptake of D-HG by Dendritic Cells.

In order to gain further insight, how D-HG affects dendritic cells, we measured cellular uptake of D-HG. Immature dendritic cells (iDCs) were stimulated with 100ng/ml LPS and treated with D-HG at a concentration of 10mM for 24hrs. Following stimulation, intracellular levels of D-HG were analyzed by mass spectrometry (analyses performed by Dr. Katja Dettmer-Wilde and Prof.Peter Oefner, Institute of Functional Genomics, Regensburg).

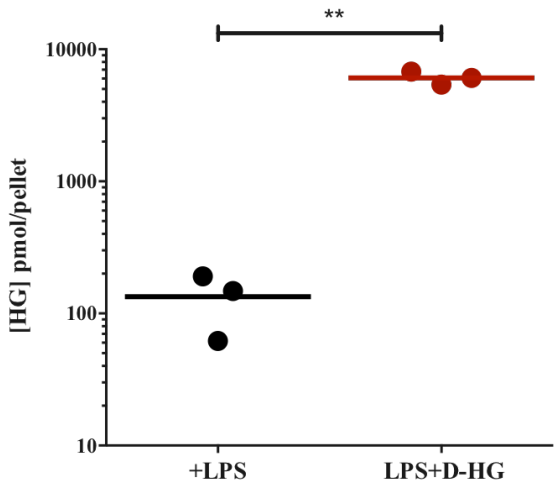

Figure 4.3. Uptake of D-HG by DCs. Human iDCs were differentiated from elutration-separated monocytes and were stimulated with 100ng/ml LPS in the presence or absence of 10mM D-HG for 24hrs. Cells were washed with PBS and intracellular levels of D-HG were analyzed by mass spectrometry (analyses performed by the Institute of Functional Genomics, Regensburg). Data represent the mean +/- SEM of 3 independent experiments. Statistical analysis was tested with the Wilcoxon-Test ** $p \leq 0.01$, ns not significant).

The measurements showed the presence of endogenous D-HG in DCs and that the addition of 10mM D-HG showed a 100 fold increase in intracellular levels (Figure 4.3). This result demonstrated the capacity of DCs to take up D-HG.

4.1.3 The role of D-HG in TLR signaling pathway

Due to IL-12 production being affected by D-HG we decided to investigate LPS/TLR4 signaling, a pathway associated with IL-12 production and modulation.

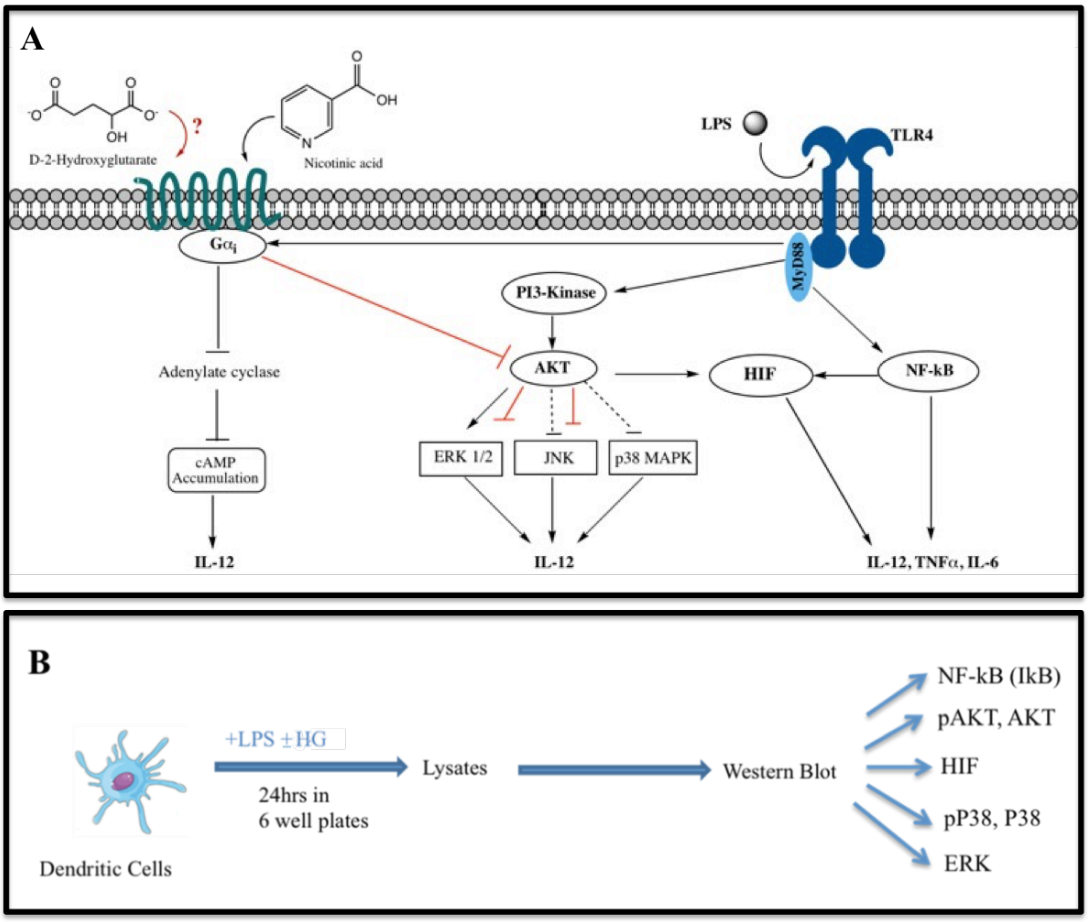

Figure 4.4 Schematical representation of TLR signaling pathways and their relation with IL-12 production by DCs. A) LPS/TLR4 pathway associated with IL-12 modulation (Modified from Hildebrand et al. 2012)[114]. B) Experimental set-up to evaluate the HG effect on LPS/TLR4 signaling pathway of DCs.

We performed western blot analyses of monocyte-derived iDCs, seeded in 6 well plates ($2.5x10^6$ cells in 4 ml medium) and stimulated with LPS or LPS plus D-HG. NF-κB, P-Akt, P-p38, ERK or HIF protein expression was analyzed in protein lysates by western blot analyses.

4.1.3.1 IκB Expression in Dendritic Cells

I κ B- α is a regulatory protein that binds NF- κ B and traps it in the cytoplasm, inhibiting NF- κ B activity. I κ B activity is controlled by sequential serine-phosphorylation, ubiquitination and degradation. It is well known that LPS reduces the expression of IκB, thereby promoting NF- κ B activity but until now the effect of HG on the NF- κ B pathway has not been studied.

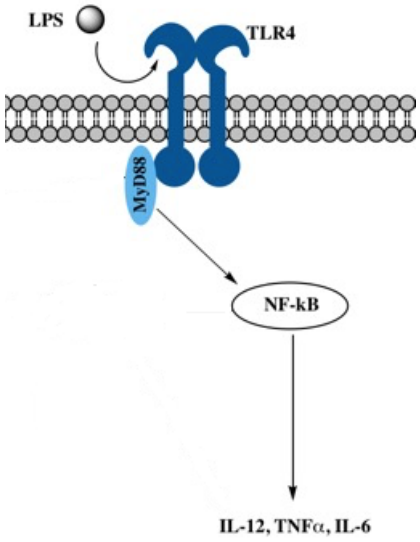

Figure 4.5. NF-κB stimulates IL-12 production in DCs. TLR4 recognizes bacterial LPS and utilizes 4 adaptors (which include MyD88) to activate the NF-κB pathway, which is strongly related with cytokine production (IL-12, TNF and IL-6).

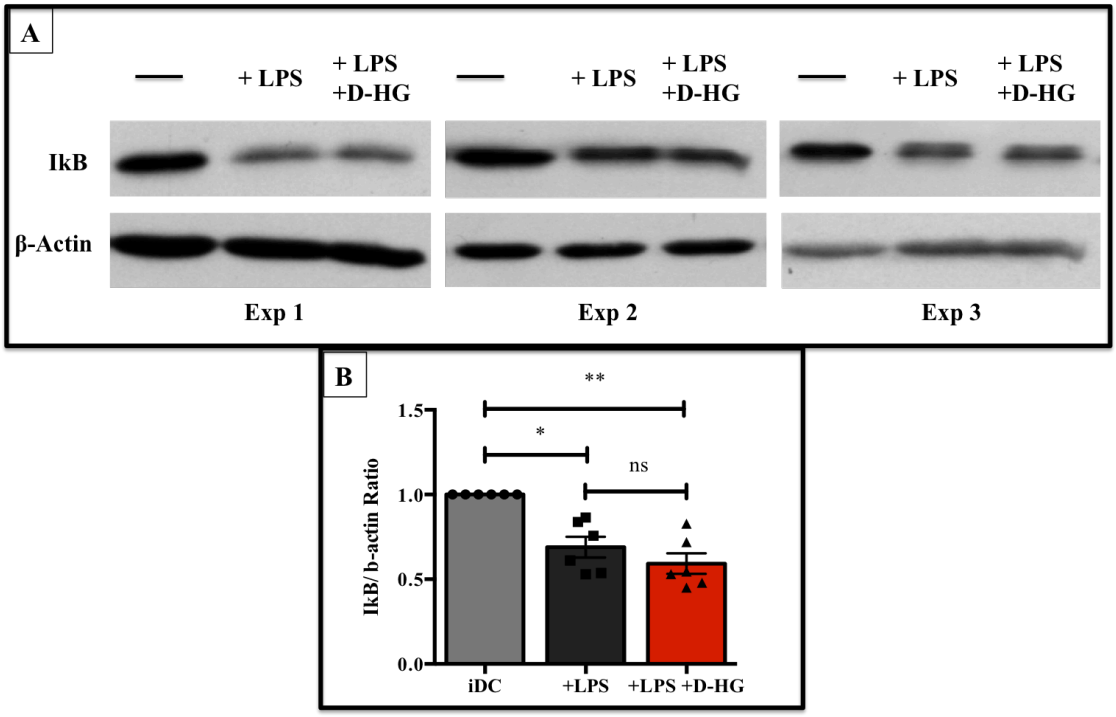

Figure 4.6. Expression of IκB protein in DCs. iDCs were stimulated with LPS (100ng/ml) and treated with or without 10mM D-HG. After 1 hr of treatment cell pellets were lysed and analyzed by Western Blotting. A) Original blots of IκB expression of 3 independent experiments. B) Quantification of IκB expression in DCs treated with LPS alone or combined with D-HG. Data represent the mean +/- SEM of 6 independent experiments. Statistical analysis was tested with the Kruskal-Wallis Test (*p≤0.05, ** p≤0.01, ns not significant).

Treatment with D-HG showed no significant effect on IκB expression (Figure 4.6 B). This result suggests that IL-12 suppression is not related to direct alterations in the NF-κB signaling pathway. Therefore, we investigated other signaling molecules related to NF-κB activity.

4.1.3.2 HIF Expression

Another signaling molecule associated with the regulation of IL-12 production by DCs is the hypoxia inducible factor (HIF). Hypoxia-inducible factors (HIFs) are regulators of hypoxic adaptation, regulating gene expression associated with glycolysis, erythropoiesis, angiogenesis, proliferation and stem cell function under low oxygen concentration. Additionally HIF-1α modulates dendritic cell maturation, activation and antigen-presenting functions in combination with LPS [115]. Degradation of HIF is regulated via prolyl-hydroxylases which have been reported to be modulated by HG [47].

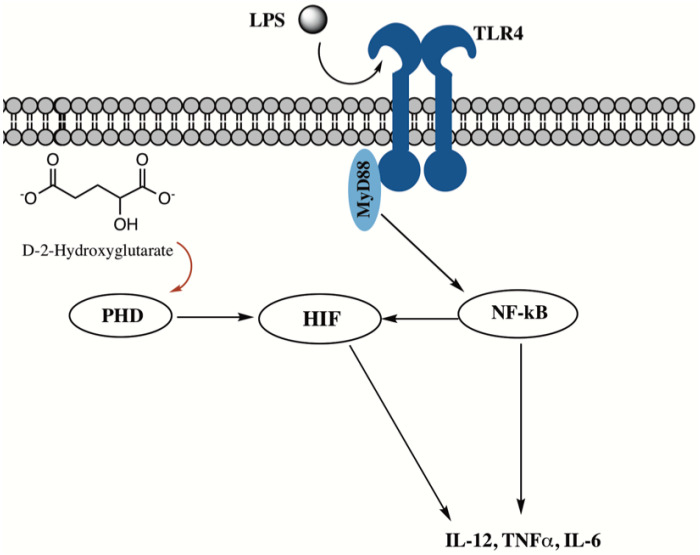

Figure 4.7. HIF involvement in IL-12 production by DCs. TLR4 pathway is activated by LPS. The activation of TLR4 induces the activity of Nuclear factor-κB (NF-κB), which leads to HIF-α accumulation, and consequently modulates the production of cytokines like IL-12, TNF and IL-6 modified from Willam et al., 2014 [116]. HIF could be targeted by HG via prolyl-hydroxylase (PHD) [47].

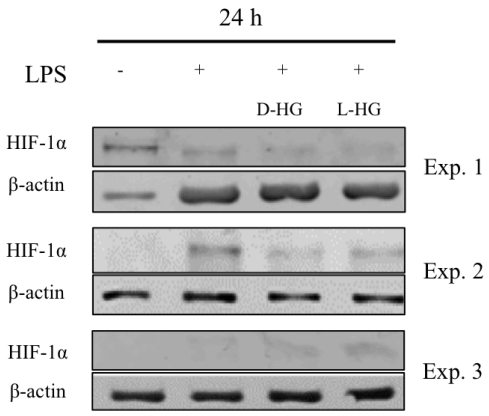

Figure 4.8. Expression of HIF-1α in DCs. iDCs were stimulated with LPS (100ng/ml) and treated with or without 10mM D-HG. After 24hrs of treatment cell pellets were lysed in RIPA buffer and analyzed by Western Blotting (n=3). Blots of 3 independent experiments are shown.

HIF-1α expression was determined after 24hrs because basal HIF levels are stabilized after this period of time in LPS stimulated cells [117] in contrast to IκB-α where degradation occurs after 2 hours [118] in resting cells.

The effect of LPS on HIF-1α was not consistent. Only in experiment 2 HIF-1α expression was induced after LPS stimulation, while in experiment 1 LPS stimulation even reduced HIF levels. No effect of LPS was determined in experiment 3. Moreover, incubation with HG (with both isoforms D/L-HG) also showed no reproducible effects (Figure 4.8).

4.1.3.3 P-Akt and Akt Expression

Akt is a serine/threonine-specific protein kinase that plays a key role in multiple cellular processes such as glucose metabolism, apoptosis, cell proliferation, transcription and cell migration. Once correctly positioned at the membrane via binding of Phosphatidylinositol (3,4,5)-trisphosphate (PIP3), Akt can then be phosphorylated by its activating kinases. In turn Akt activates or deactivates other kinases as ERK or JNK. Downstream signaling pathways of Akt can directly regulate IL-12 production.

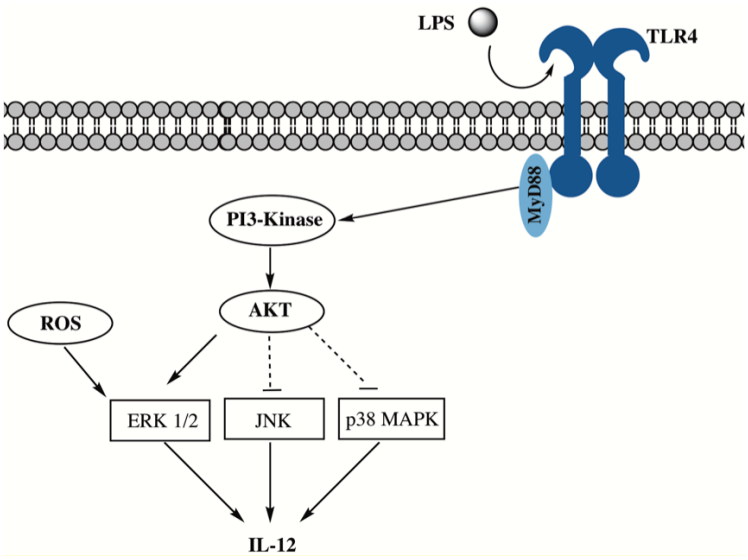

Figure 4.9. PI3-Kinase pathway and IL-12 production by DCs. PI3-kinase signaling pathway is activated by LPS binding to the TLR4 receptor which is coupled to the MyD88 complex, activation of PI3-Kinase leads to a signaling cascade of phosphorylation, resulting in the production of IL-12. Alternatively the MAPkinases can be activated via reactive oxygen species [119]

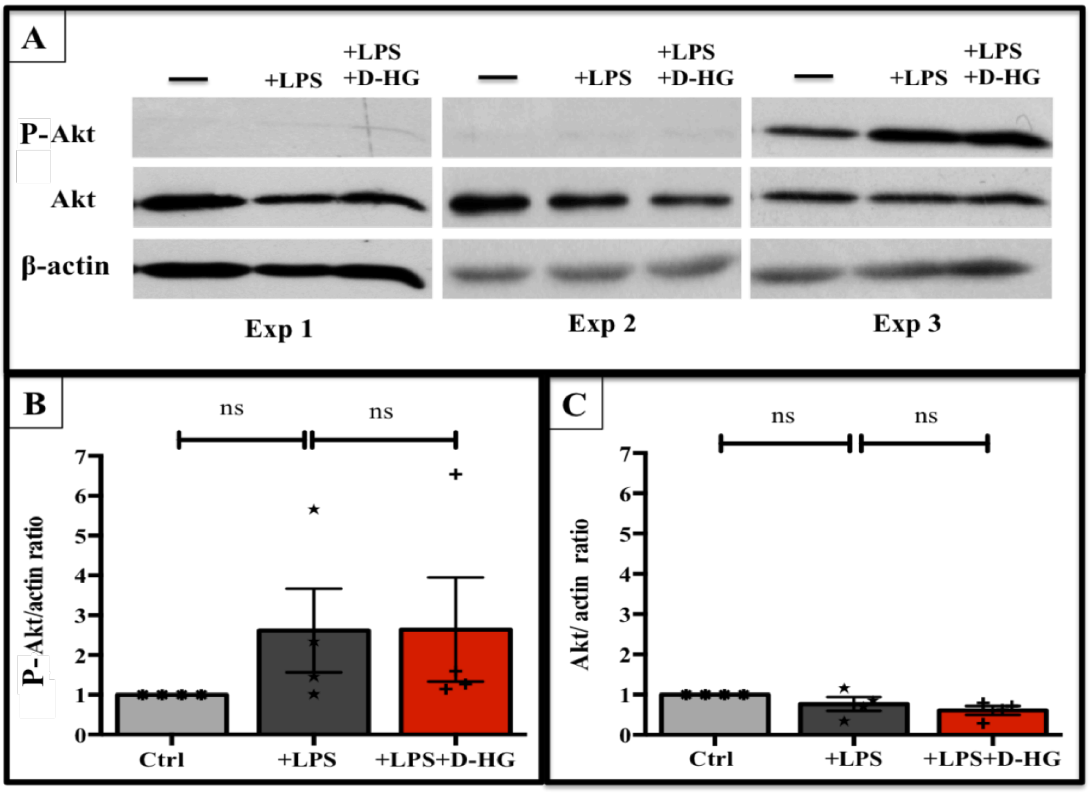

Figure 4.10. Expression of P-Akt and Akt in DCs. iDCs were stimulated with LPS (100ng/ml) with or without 10mM D-HG. After 24hrs of treatment phospholysates from cell pellets were prepared and protein expression analyzed by Western Blotting (n=4). A) Blots of three independent experiments are shown. B) Quantitative analysis of D-HG effect on P-Akt protein expression. C) Quantitative representation of D-HG effect on Akt protein expression. Statistical analysis was tested by Kruskal-Wallis test (*p≤0.05, ns not significant).

LPS-induced maturation, increased the amount of p-Akt and reduced the Akt content at the same time, although statistical signficance was not reached. D-HG had no impact on these alterations. (Figure 4.10).

This result suggests that IL-12 suppression triggered by D-HG is also not related to an impairment of the PI3/Akt signaling pathway. Next we analyzed the D-HG effect on the p38 signaling pathway.

4.1.3.4 P-p38 and p38 Expression

Because we were not able to observe any effect of D-HG on PI3/Akt signaling pathway, we proceeded to analyze whether the MAPK signaling pathway it is affected by D-HG treatment. p38 MAP kinases (α, β, γ, and δ) are members of the MAP kinase family that are activated by a variety of environmental stresses as inflammatory cytokines, lipopolysaccharides (LPS) and ROS [119]. Dual specificity mitogen-activated protein kinase kinase 3 (MKK3) activates p38 MAPK by phosphorylation at threonine (Thr)[180]/tyrosine (Tyr)[182] residues. Activated p38 MAPK phosphorylates and activates a signaling pathway involving a cascade of other kinases related to cytokine production [104].

Immature DCs were cultured as previously described and stimulated with LPS in the presence or absence of 10mM D-HG for 24hrs.

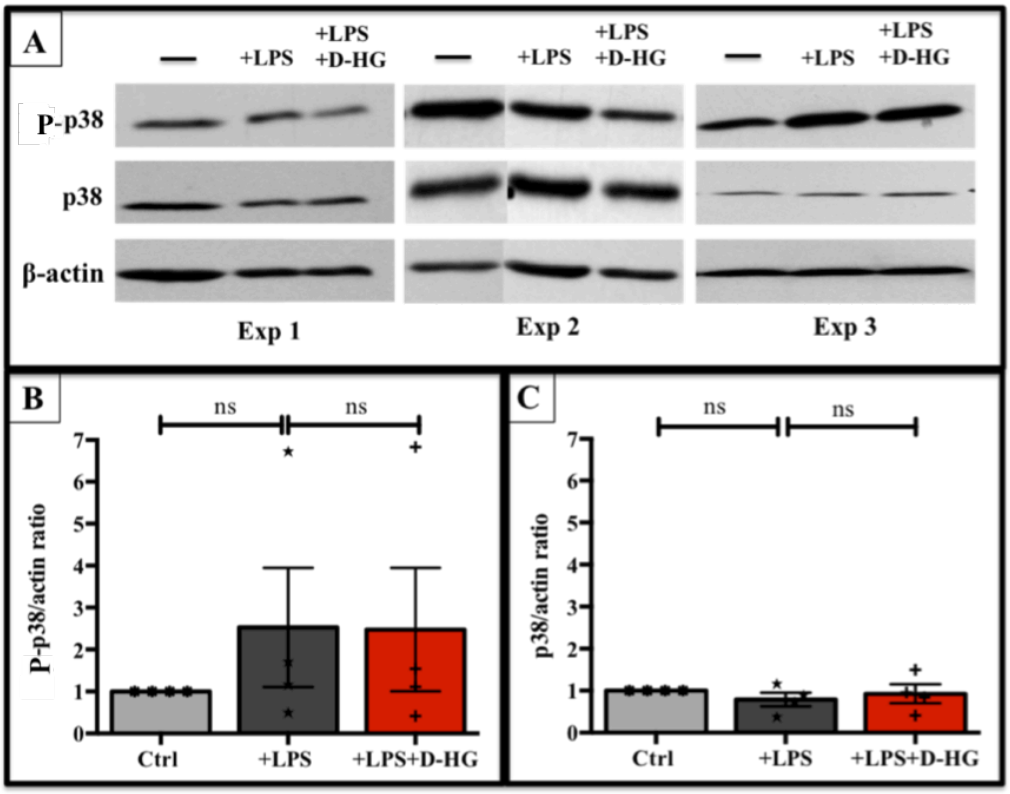

Figure 4.11. Expression of p38 protein in DCs. iDCs were stimulated with LPS (100ng/ml) with or without 10mM D-HG. After 24hrs phospholysates from cell pellets were prepared and protein expression analyzed by Western Blotting (n=4). A) Qualitative representation of P-p38 expression on DCs, 3 independent experiments of 4 are shown. B and C) Quantitative determination of P-p38 and p38 expression in DCs respectively, data represent the mean +/- SEM of 4 independent experiments. Statistical significance was performed with Kruskal Wallis Test (*p≤0.05, ns not significant).

LPS had no significant impact on the expression of the phosphorylated form of p38 protein, as well as the treatment with 10mM D-HG did not show a significant effect (Figure 4.11 A and B).

Neither LPS treatment displayed a significant effect on p38 expression, nor addition of 10mM D-HG exerted any additional impact (Figure 4.11 A and C).

Taken together, LPS induced maturation had no effect on p38 expression or phosphorylation, thus this pathway seems to be of minor importance for DC maturation. Another signaling regulated kinase related with IL-12 production is ERK, hence we proceded to analyze whether the D-HG induced reduction in IL-12 secretion is related to an impairment of this signaling pathway.

4.1.3.5 P-ERK Expression

Extracellular-signal-regulated kinases (ERKs) are involved in a variety of processes including the regulation of meiosis, mitosis, and postmitotic functions in differentiated cells. ERKs are known to activate many transcription factors, and some downstream protein kinases. Disruption of the ERK pathway is a common phenomenon in cancer. Phosphorylation of ERKs leads to the activation of their kinase activity.

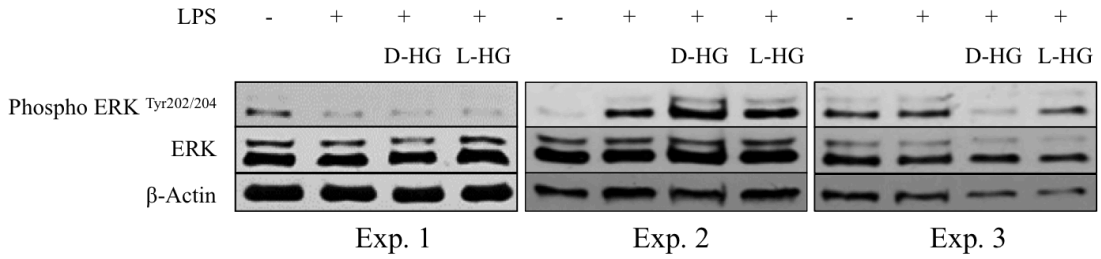

Figure 4.12. Expression of ERK protein in DCs. iDCs were stimulated with LPS (100ng/ml) with or without D-HG. After 24hrs phospholysates from cell pellets were prepared and protein expression analyzed by Western Blotting (n=3).

ERK expression itself showed no consistent alterations upon LPS treatment. Interestingly, the expression of p-ERK seems to be affected by the treatment of LPS +D-HG in three of 5 experiments. However the effect was not consistent as experiment 1 showed no impact on D-HG addition, experiments 2 showed an increased expression of p-ERK by D-HG, while experiment 3 showed a decrease although non-phosphorylated ERK expression was maintained independent of the treatment in all sets of experiment (Figure 4.12).
These results suggest, ERK signaling pathway is also not involved in the observed IL-12 suppression by the D-HG. Taken together, we did not detect any pronounced and consistent altertations in different kinase pathways related to IL-12 secretion. Therefore, other candidates were considered. We elucidated GPR related cAMP signaling, which is also important for IL-12 expression.

4.1.3.6 GPR109a Expression

G proteins are known to be expressed on DCs and regulate intracellular cAMP accumulation. Some of these proteins are: GPR81 (lactate receptor), GPR109 (butyrate and niacin receptor), GPR91 (succinate receptor) and GPR80/99 (ketoglutarate receptor). GPR109A, GPR109B and GPR81 receptors are activated by hydroxy-carboxylic acid

ligands. GPR109A has been reported to be expressed in immune cells such as monocytes, macrophages and dendritic cells [120]. As GPR109A is activated by hydroxyl carboxylic acids and HG (D-2/L-HG) contains two carboxylic acid groups, we questioned ourselves whether GPR109A could be a possible receptor for HG on dendritic cells.

With this in mind we decided to address the mRNA expression of GPR109a in iDCs in the presence or absence of HG and performed the same analysis in DCs stimulated with LPS in the presence or absence of HG. RNA from all treatment groups was isolated, and the expression of GPR109 was determined by real time PCR.

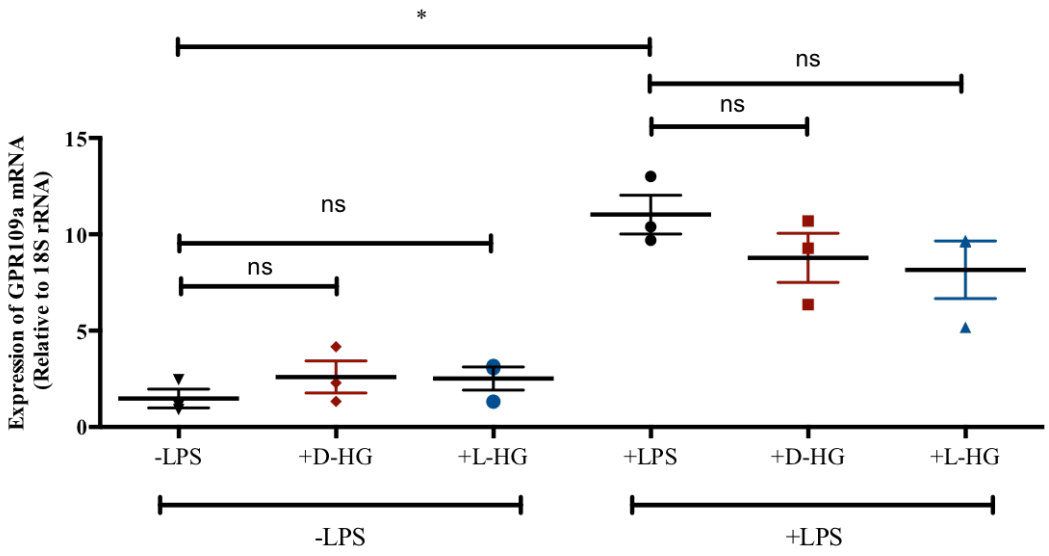

Figure 4.13. Effect of HG on GPR109a expression. RNA expression was analyzed in iDCs treated with or without 10mM D/L-HG for 24hrs and in DCs stimulated for 24hrs with LPS in the presence or absence of 10mM D/L-HG. RNA was isolated and transcribed to cDNA for further *GPR109A* expression analysis by real time PCR. Data represent the mean +/- SEM of 3 independent experiments, statistical analyses was performed with Kruskal Wallis Test (ns not significant).

Immature dendritic cells showed low levels of GPR109A expression, which was not affected by the addition of D-HG. However, LPS significantly increased GPR109A expression, which was also observed in the presence of D-HG (Fig. 4.13). Nevertheless a clear trend towards a reduced expression in the presence of D-HG was detected. Therefore, we also analyzed the impact of L-HG and got the same results. As a changed expression of GPR109A could strongly affect IL-12 secretion, we investigated this pathway in more detail. For this set of experiments we used both enantiomers D-HG and L-HG.

4.1.3.6.1 Impact of GPR109A modulators

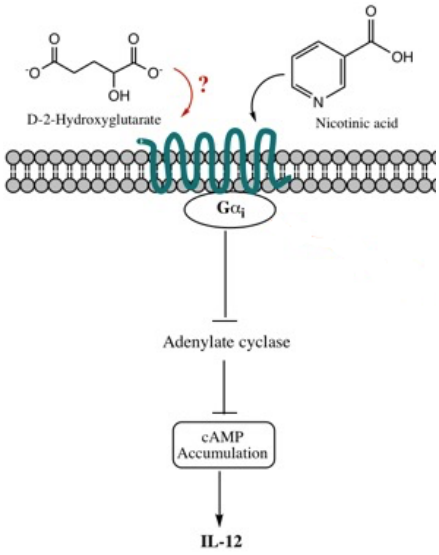

Figure 4.14. Effect of nicotinic acid on IL-12 production by DCs. GPR109A signaling pathway is activated by Niacin, but effect of D-HG on GPR109A signalling is unclear.

GPR109A has been reported to be expressed on DCs and related to cAMP levels which are directly associated with IL-12 levels. To demonstrate this relation we took a ligand for this receptor (niacin) and determined whether or not this has the same effect on IL-12 secretion as HG.

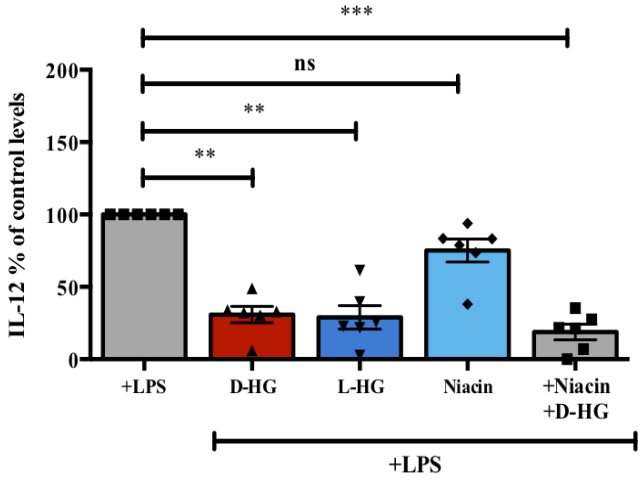

Figure 4.15. IL-12 production by DCs under HG and nicotinic acid treatment. iDCs were stimulated with LPS (100ng/ml), 10mM D-HG with and without 100µM nicotinic acid, 10mM L-HG and nicotinic acid alone. After 24hrs supernatants were collected and analyzed by ELISA. Data represent the mean +/- SEM of 6 independent experiments. Statistical analysis was tested with Kruskal Wallis -Test (** $p \leq 0.01$, **** $p \leq 0.0001$, ns not significant).

We observed no effect on IL-12 production (Figure 4.15) by niacin, suggesting that GPR 109A signaling is not responsible for IL-12 down regulation. Nevertheless, this does not rule out a possible involvement of cAMP in the D-HG induced restriction in IL-12 secretion.

4.1.3.7 Impact of cAMP modulating drugs on DCs

During the evaluation of IL-12 modulatory signaling pathways we found no relationship between the pathways analyzed and the treatment with D-HG. Several reports suggest a relation between cyclic adenosine monophosphate (cAMP) levels and dendritic cell function. A variety of studies stipulated that cAMP-inducing factors (as Forskolin) inhibit IL-12 production from DCs [121,122]. Forskolin is a rapid activator of adenylyl cyclase and has been used to increase intracellular cAMP levels.

Taking this into consideration we differentiated dendritic cells and treated them with 10mM D-HG, 100µM of cAMP analog and/or 10µM Forskolin.

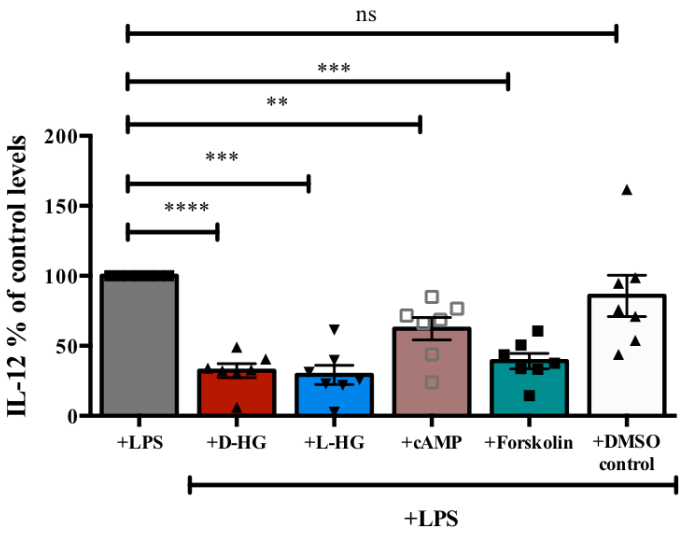

Figure 4.16. Effect of cAMP and cAMP modulators on IL-12 production by dendritic cells. Monocyte-derived iDCs were plated on 24 well plates ($0.2x10^6$ in 1ml), cells were treated with 100ng/ml LPS, 10mM D-HG/L-HG, 10µM Forskolin, 100µM cAMP-Rp and DMSO to control for carrier effects. Data represent the mean +/- SEM of 6 independent experiments. Statistical analysis was tested with Kruskal Wallis Test. (*p≤0.05, ** p≤0.01, ns not significant).

In line with published data we observed a significant reduction in IL-12 production by Forskolin and cAMP analog (cAMP-Rp) addition (Figure 4.16), which was not attributed to DMSO related effects. Forskolin restricted IL-12 level was comparable to HG treatment. These results suggest that the effect of D-HG on IL-12 production could be associated with increased cAMP levels. As a consequence, intracellular cAMP concentrations were measured upon LPS treatment in the presence or absence of D-HG.

4.1.3.7.1 cAMP Expression in Dendritic Cells

In dendritic cells cAMP mediated signaling exerts a suppressive function on the immune response. High levels of intracellular cAMP downregulate IL-12 p40 mRNA expression and IL-12 p70 production in murine myeloid cells [121].

In order to elucidate whether IL-12 downregulation by HG is related to cAMP levels in DCs, we treated iDCs with LPS 100ng/ml and 10µM Forskolin for 1 hour and measured cAMP levels.

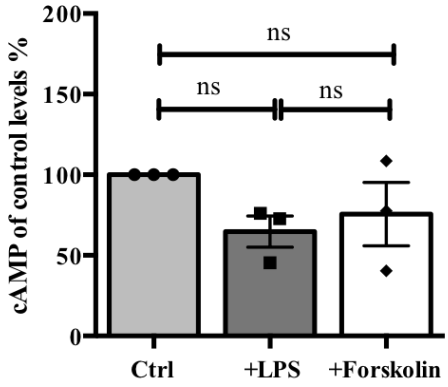

Figure 4.17. Effect of D-HG on cAMP levels. Monocytes- derived iDCs (5 x10^6/ml) were placed in FACS tubes and cells were treated with 100ng/ml LPS and/ or 10µM Forskolin. The cells were lysed and cAMP measurement was performed. Data represent the mean +/- SEM of 3 independent experiments. Statistical significance was tested with Kruskal Wallis Test. (*p≤0.05, ns not significant).

Compared to unstimulated DCs cAMP levels were reduced when LPS was present, the addition of Forskolin did not increase cAMP levels in contrast to what was expected (Figure 4.17), indicating that the methodological approach was not appropriate.

4.1.4 The impact of HG on Mitochondrial Respiration

During the last years it became more and more evident that metabolism is directly linked to immune cell function. Increased glucose metabolism but decreased mitochondrial respiration has been related to myeloid cell activation. Furthermore, increased cAMP, probably related to the inhibition of IL-12 can also activate the PKA signaling pathway which in turn increases mitochondrial respiration. Therefore, we analyzed whether D-HG induced IL-12 blockade might be associated with altered mitochondrial respiration in DCs.

4.1.4.1 Impact of D-HG on Mitochondrial Respiration

To elucidate if D-HG induces changes in mitochondrial respiration of DCs, we measured oxygen consumption of iDCs and DCs stimulated with LPS in the presence or absence of 10mM D-HG.

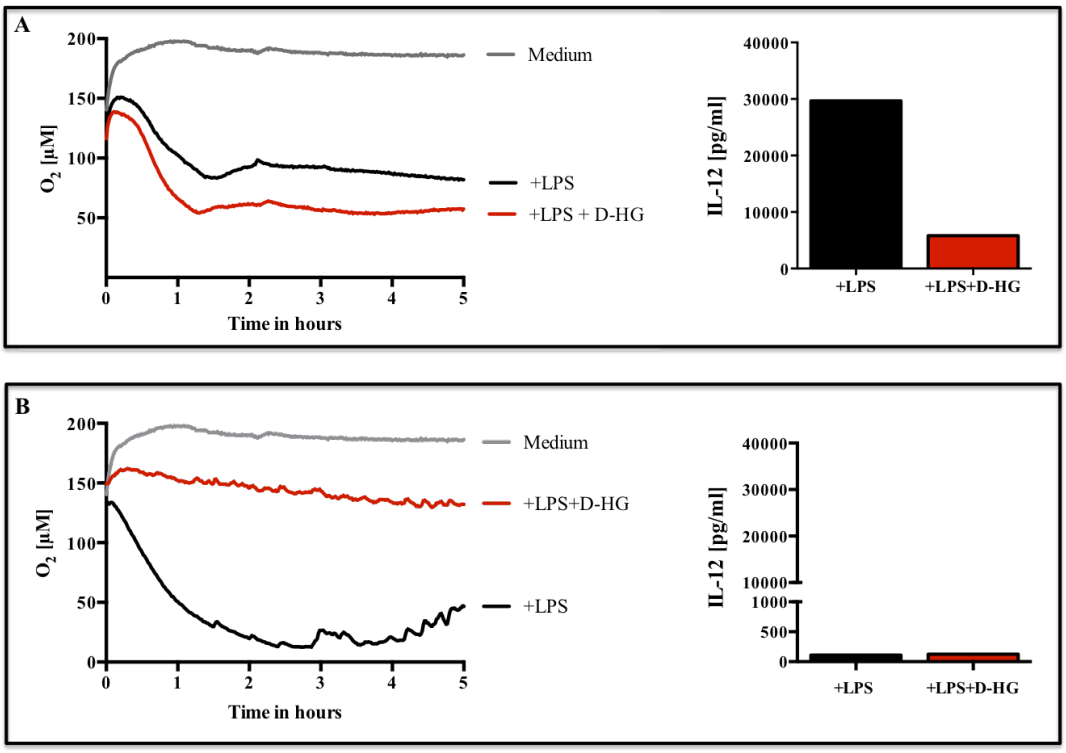

Figure 4.18. Oxygen consumption of DCs in the presence of D-HG. Monocyte-derived iDCs were seeded on a 24 well plate OxoDish® (PreSens Precision Sensing GmbH, Regensburg, Germany), activated with 100ng/ml LPS and treated with 10mM D-HG for 24hrs. Shown is the oxygen decline as a measure of oxygen consumption of 2 independent experiments as well as the respective IL-12 levels determined by ELISA.

In experiment 1 (Figure 4.18 Athe exposure to D-HG lowered oxygen levels compared to LPS treatment alone (more O2 consumption). Analyzing IL-12 levels in the supernatants revealed a high basal level of IL-12 and a strong reduction under D-HG treatment.
Nevertheless, in the second experiment (Figure 4.18 B) D-HG treated DCs showed a lower oxygen consumption. However, IL-12 levels in the supernatant were very low and D-HG exerted no clear effect. For further clarification we decided to analyze mitochondrial respiration by a technology providing absolute values of oxygen consumption.

4.1.4.2 The effect of D-HG on Mitochondrial Respiration analyzed by high resolution respirometry

In order to evaluate the effect of D-HG on mitochondrial respiration in detail we used the classical respirometry, a technology that allows to measure the rate of respiration in a closed system thereby increasing the sensitivity.

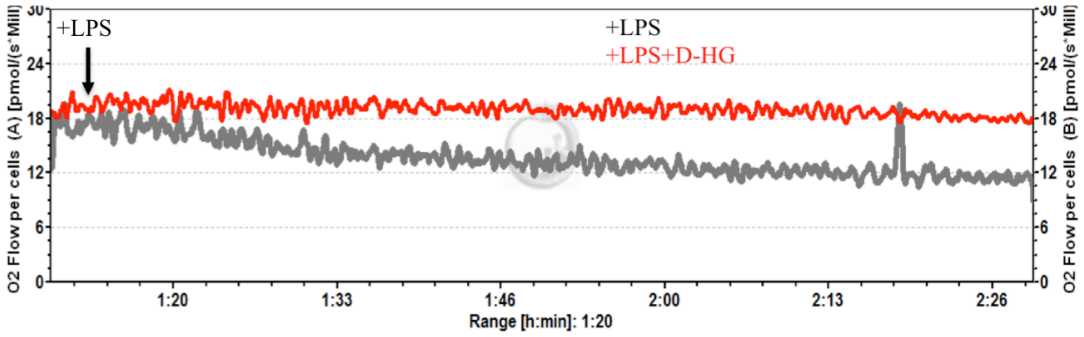

Figure 4.19. Oxygen consumption of DCs in the presence of D-HG. Monocyte-derived iDCs were placed in oxygraph chambers ($1x10^6$/ml) in culture medium. After stabilization of respiration D-HG or medium was added to the chambers and incubated for 10min. Then cells were activated with 100ng/ml LPS and oxygen consumption was monitored for 1hr. One representative experiment of 8 is presented.

LPS stimulation significantly reduced oxygen consumption, which was completely prevented by D-HG (Figure 4.19 and 4.20).

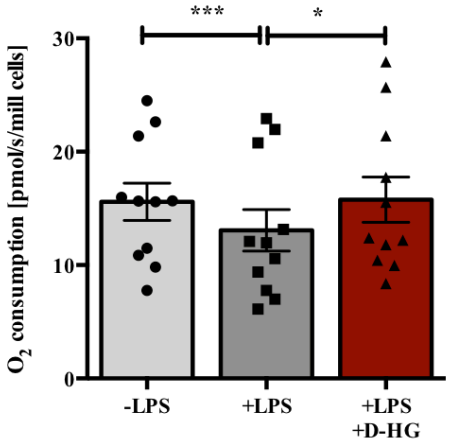

Figure 4.20. Routine respiration of DCs in the presence of D-HG. Oxygraph chamber were filled with 1x10^6/ml monocyte-derived iDCs. After stabilization of respiration 10mM D-HG or medium was added to the chambers and incubated for 10 min. Then cells were activated with 100ng/ml LPS and oxygen consumption was monitored for 1hr. Data represent the mean +/- SEM of 11 independent experiments. Statistical testing was performed with Kruskal-Wallis test. (*p≤0.05, **** p≤0.0001, ns not significant).

ROUTINE respiration reflects the aerobic metabolic activity of the cells in culture medium. As the extent of the LPS induced reduction in ROUTINE respiration varied between the donors, we decided to analyze if the inhibition is related to the levels of IL-12 secreted by DCs. We correlated the percental inhibition of ROUTINE respiration by LPS with IL-12 levels.

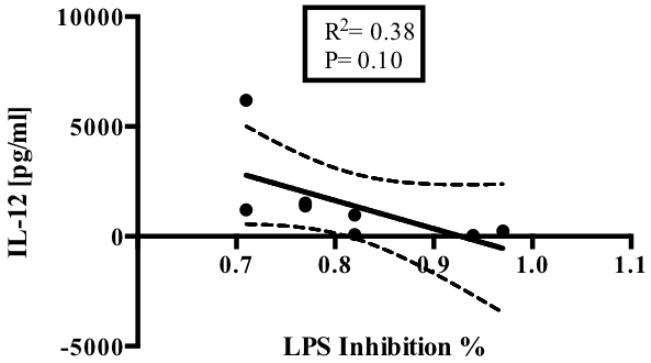

Figure 4.21 Correlation of LPS induced inhibition in ROUTINE respiration with IL-12 secretion by DCs. Percent of LPS inhibition was calculated dividing ROUTINE respiration after 1hr of LPS addition by ROUTINE respiration observed before LPS addition. LPS induced inhibition of respiration was then correlated with IL-12 expression, 1.0 represent no inhibition by LPS. Statistical analysis was tested with linear regression test (*p≤0.05). R^2 = 1 represent that the regression line perfectly fits the data.

The inhibition in basic respiration (ROUTINE) by LPS was not positively correlated with the levels of IL-12 produced.

After 1 hour we investigated respiratory characteristics in more detail by applying oligomycin (ATP synthase inhibitor) to determine LEAK respiration (oxygen consumption to compensate for proton leak) followed by titration of an uncoupler to measure maximum capacity of the electron transfer system. Oxygen consumption not related to the respiratory complexes (residual oxygen consumption, ROX) was determined after rotenone (0,5µM) and myxothiazol (2,5µM) addition. All respiratory parameters were corrected for ROX. Mitochondrial oxygen consumption related to ATP production was calculated as the difference between ROUTINE and LEAK respiration (R-Oligo).

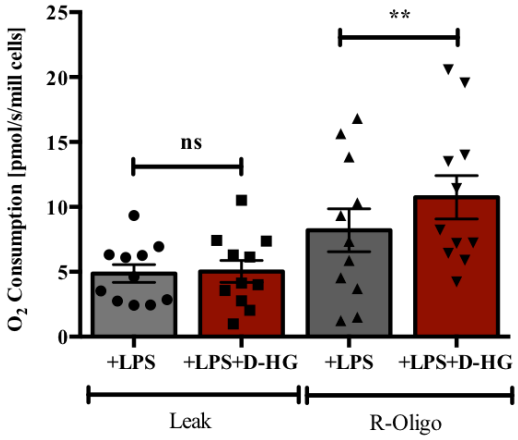

Figure 4.22 Impact of D-HG on Leak and ATP related oxygen consumption in DCs. Oxygraph chambers were filled with $1x10^6$/ml monocyte-derived iDCs, after stabilization of respiration, 10mM D-HG or medium was added to the chambers and incubated for 10min. Then cells were activated with 100ng/ml LPS and oxygen consumption was monitored for 1hr. Leak respiration was determined after the addition of oligomycin and subtracted from ROUTINE respiration to calculate oxygen consumption related to ATP production. Data represent the mean +/- SEM of 11 independent experiments. Statistical significance was tested by Kruskal-Willis Test. (*p≤0.05, ** p≤0.01, ns not significant).

Leak was not affected by D-HG but oxygen consumption related to ATP production was significantly reduced after LPS addition and this effect was prevented by the addition of D-HG (Figure 4.22). The capacity of the electron transfer system was also higher in D-HG treated cells (Figure 4.23). These data point towards reduced substrate flux into mitochondria upon stimulation with LPS, which was prevented in D-HG treated DCs.

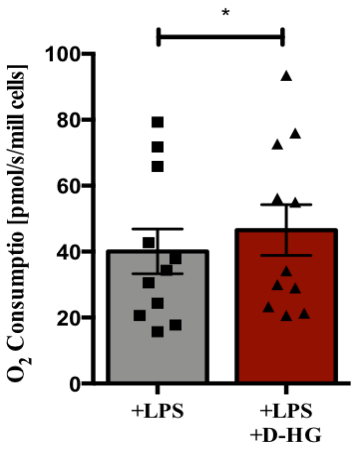

Figure 4.23 Electron Transfer System capacity (ETS) is affected by D-HG in DCs. Oxygraph chambers were filled with 1x10^6/ml monocyte-derived iDCs, After stabilization of respiration D-HG or medium was added to the chambers and incubated for 10 min. Then cells were activated with 100ng/ml LPS and oxygen consumption was monitored for 1hr. After addition of oligomycin, FCCP was titrated up to maximum uncoupled respiration. Data represent the mean +/- SEM of 11 independent experiments. Statistical significance was performed by Wilcoxon Test. (*p≤0.05, ns not significant).

4.1.4.3 The impact of D-HG on the content of Mitochondrial Respiratory Complexes

In order to elucidate whether a change in the complexes of the mitochondrial respiratory system could be associated with the observed LPS effect and the blockade by D-HG, we analyzed respiratory complexes with an antibody mixture detecting all complexes.
Monocytes-derived iDCs were incubated for 1hr with LPS in the presence or absence of D-HG, phospholysates were generated and analyzed by Western blot as previously described in section 3.6.

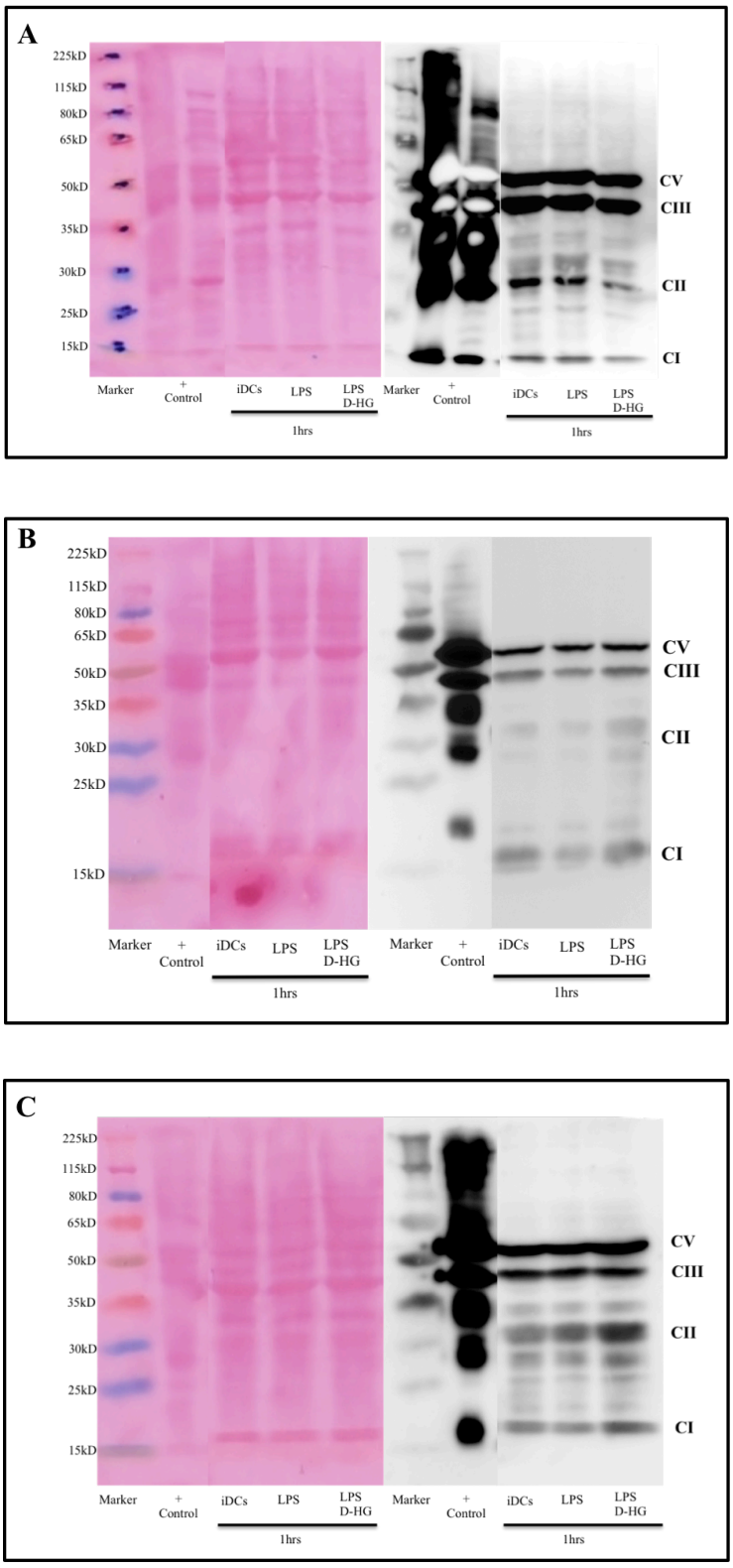

Figure 4.24. Respiratory complexes on DCs treated with D-HG. Monocytes-derived iDCs were seeded ($2.5x10^6$ cells on 4ml) in 6 well plates, incubated for 1hr with LPS and D-HG, phospholysates were prepared and analyzed. Heart mouse lysate was used as positive control. Complex I (CI) with Molecular Weight (MW) of 20KD, Complex II (CII) with MW of 30KD, Complex III (CIII) with MW of 48KD, Complex V (CV) with MW of 55KD.

Complex III and V displayed no changes by the addition of LPS or D-HG. Complex I and II seemed to have a slight increase in protein expression by the addition of D-HG, nevertheless the result was not consistent. In addition we were not able to observe complex IV which should be present at 40KD. Further studies should be performed in order to confirm D-HG effects.

Taken together, we observed a reduction of ROUTINE respiration, mitochondrial capacity and oxygen consumption related to ATP production by LPS which was prevented by D-HG.

Rapid changes in mitochondrial contents do not seem to be an underlying mechanism explaining the effect of LPS on respiration and the prevention by D-HG.

To analyze whether the reduction in mitochondrial respiration is directly linked to IL-12 production we investigated whether mitochondrial inhibition is sufficient to increase IL-12 secretion. Rotenon, a complex I inhibitor was used as well as oligomycin, blocking mitochondrial ATP production.

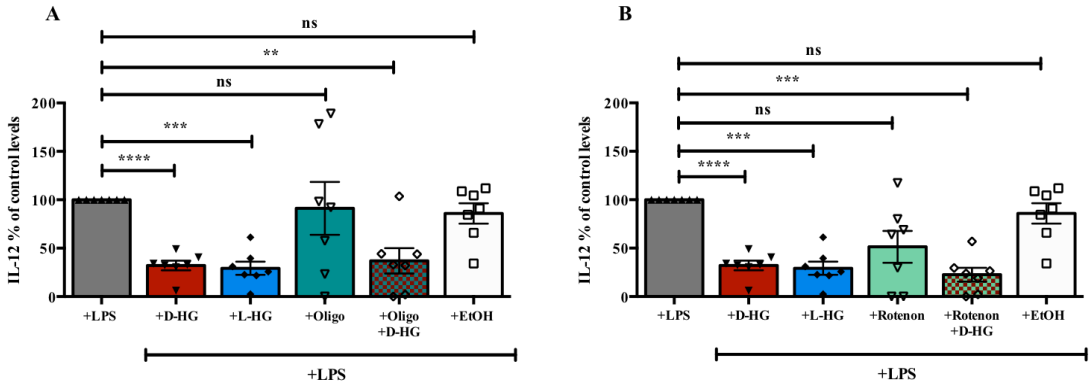

Figure 4.25. Effect of oligomycin and rotenon on IL-12 production by DCs. Monocyte-derived iDCs were plated on 24 well plates ($0.2x10^6$ in 1ml), cells were treated with 100ng/ml LPS, 10mM D-HG/L-HG, 0.5µM oligomycin or 0.1µM rotenon, 0.5µM EtOH served as carrier control. Data represent the mean +/- SEM of 7 independent experiments. Statistical significance was tested by Kruskal Wallis Test. (*p≤0.05, ** p≤0.01, **** p≤0.0001, ns not significant).

Cytokine production of DCs was not negatively affected by the treatment with oligomycin or rotenone. Both compoounds exerted only a slight effect on IL-12 production and this effect was not statistically significant. However, both inhibitors could not rescue the HG

induced reduction in IL-12 secretion, thus inhibition of mitochondrial respiration is not sufficient to increase IL-12 levels.

4.1.4.4 The impact of CsA on IL-12 production

Mitochondria are involved in cellular Ca^{2+} homeostasis. Activation of immune cells results in the release of Ca^{2+} from the endoplasmatic reticulum into the cytosol and subsequently results in the activation of Ca^{2+} influx from the extracellular space. Cyclosporine A (CsA) blocks mitochondrial calcium efflux and allows mitochondria to accumulate a large amount of calcium[123] thereby probably reducing cytosolic calcium which has been shown to reduce IL-12 secretion in myeloid cells [124]. Ca^{2+} accumulation induces dephosporylation of mitochondrial proteins; more Ca^{2+} is related to ahigher respiration.

Taking this in consideration we analyzed whether CsA can modulate the HG induced reduction in IL-12 secretion.

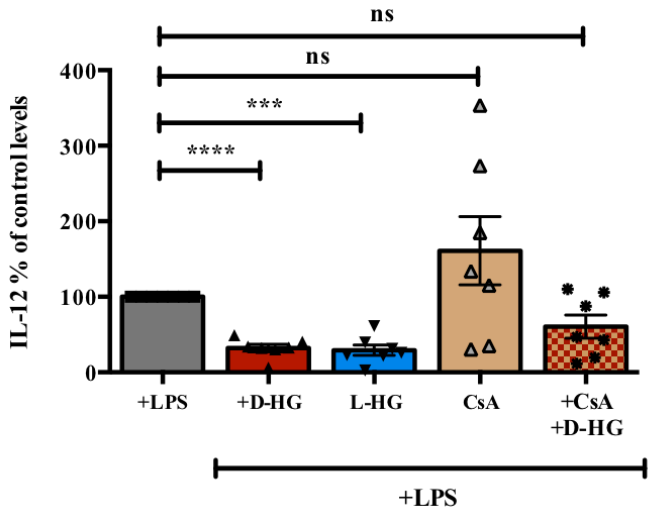

Figure 4.26. Effect of CsA on IL-12 production by dendritic cells. iDCs were activated with 100ng/ml LPS and treated with 10mM D/L-HG, CsA 32pM, and the combination of them. After 24hrs supernatants were collected and IL-12 was measured by ELISA. Data represent the mean +/- SEM of 7 independent experiments. Statistical significance was performed by One Way Anova. *** $p \leq 0.001$,**** $p \leq 0.0001$, ns not significant).

Addition of D-HG or L-HG significantly reduced IL-12 production (Figure 4.26). DCs treated with CsA and LPS displayed a higher IL-12 production compared to LPS alone. Nevertheless this increase was not statistical significant due to donor variation. When CsA was combined with LPS+D-HG, IL-12 production was no longer statistically reduced compared to LPS

In order to analyze if CsA could affect the mitochondrial phenotype we evaluated the impact of CsA in combination with D-HG on Routine respiration.

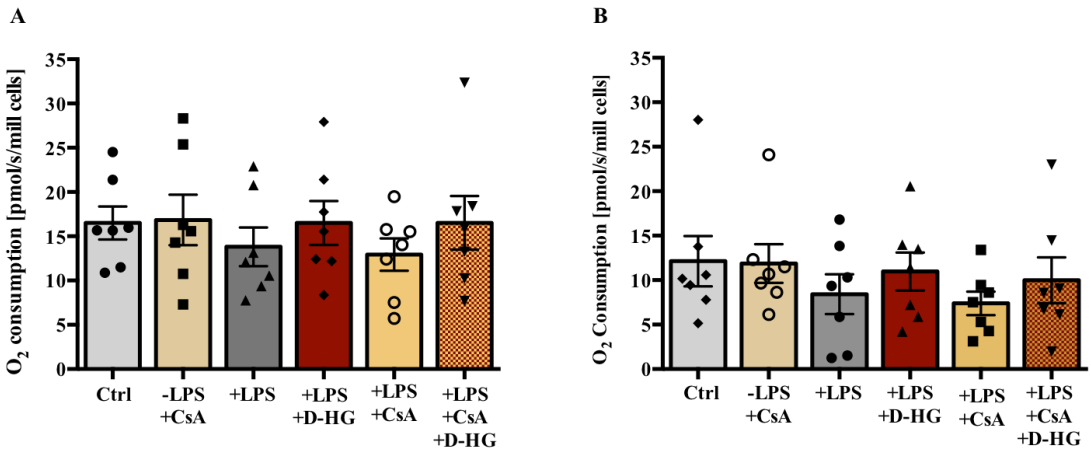

Figure 4.27. Routine respiration and oxygen consumption related to ATP production of DCs in the presence of CsA. Oxygraph chamber was filled with 1x10^6/ml Monocyte-derived iDCs, in 2ml final volume. Cells were activated with 100ng/ml LPS and treated with 10mM D-HG and/or 32pM CsA for 1hr. A) Routine respiration, B) Oxygen consumption related to ATP production. Data represent the mean +/- SEM of 7 independent experiments. Statistical significance was performed by Kruskal-Wallis (ns not significant).

Addition of LPS reduced O_2 consumption even though this effect was not statistically significant in this set of experiments. D-HG addition blocked the effect of LPS. After 1h CsA could not alter the effects of LPS or the combination of LPS and HG. (Figure 4.27 A/B and 4.28).

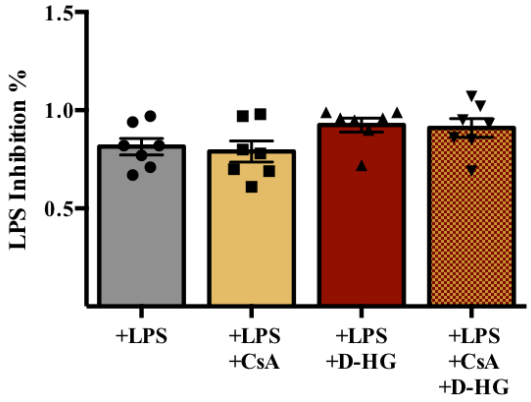

Figure 4.28 Percentual representation of LPS inhibition on DCs treated with CsA and D-HG. Cells were activated with 100ng/ml LPS and treated with 10mM D-HG and/or 32pM CsA for 1hr. Data represent the mean +/- SEM of 7 independent experiments. Statistical significance was performed by Kruskal-Wallis (ns not significant).

Results observed in figures 4.27 and 4.28 investigated the effects after one hour treatment. These results revealed no effect on respiration by LPS+CsA in comparison with DCs+LPS. Nevertheless in two cases we prolonged the measurement for 2 hours and observed a clear effect in the presence of CsA.

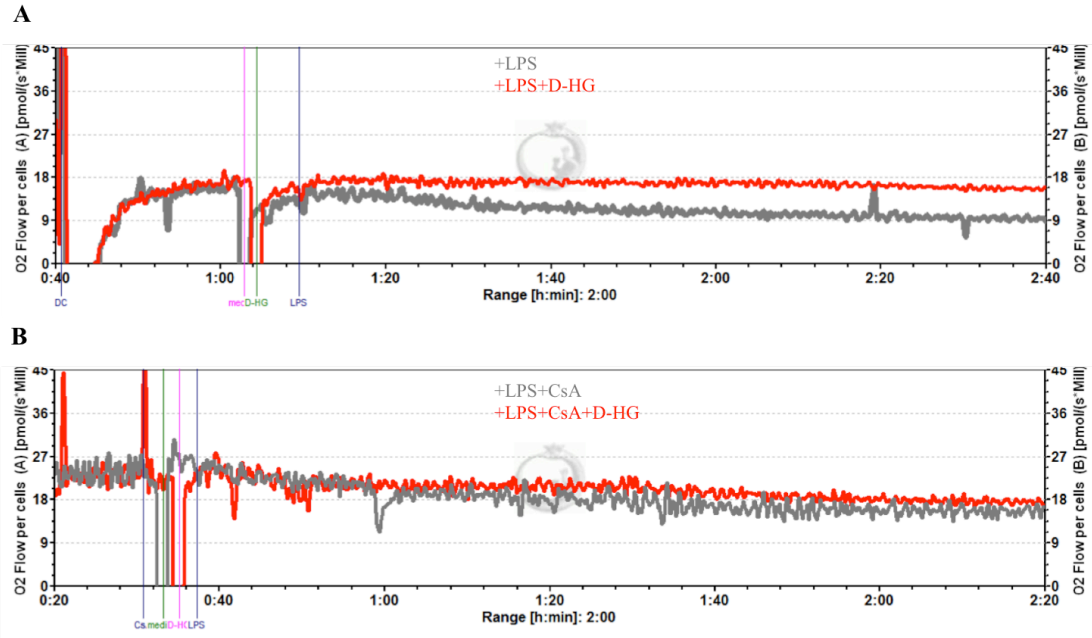

Figure 4.29. Routine respiration of DCs in the presence of CsA after 2hrs. Oxygraph chamber was filled with 1x10^6/ml Monocyte-derived iDCs, in 2ml final volume. Cells were treated with 32pM CsA, after stabilization 10mM D-HG or medium was added and minutes later cells were activated with 100ng/ml LPS, ROUTINE respiration was monitored for 2hr. 1 experiment of 2 is shown.

LPS addition triggered a drop in respiration, which was blocked by D-HG. When D-HG was combined with CsA initially, the drop in respiration was not rescued (Figure 4.27). However, after 2 hours, respiration under CsA + D-HG showed a decline similar to LPS (Figure 4.29). These results point towards an attenuation of the D-HG effect (Figure 4.29). To confirm these results, more experiments should be performed.

4.1.4.5 Impact of D-HG on lactate secretion

Our data point towards a change in substrate flux. As it has been described that activation of myeloid cells increases their glycolytic activity, we analyzed lactate levels in supernatants of LPS stimulated DCs with and without D-HG.

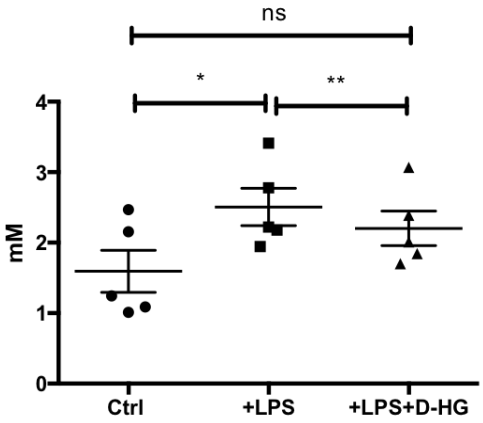

Figure 4.30 Impact of D-HG on lactate secretion in supernatants of activated DCs. iDCs were treated with LPS 100ng/ml and 10mM D-HG for 24 hours, the supernatants were collected and lactate levels were measured enzymatically. Data show the mean +/- SEM of 5 independent experiments. Statistical significance was tested by One Way Anova. (*p≤0.05, ** p≤0.01, ns not significant).

Figure 4.30 shows that iDCs treated with LPS displayed an increased lactate secretion. Under D-HG treatment this increase was less pronounced. Taken together, these results suggest that LPS shifts the metabolism from oxidative phosphorylation to glycolysis. D-HG prevents these metabolic alterations, which might contribute to reduced IL-12 levels.

4.1.5 Gene Expression in DCs treated with D-HG.

Next we investigated whether D-HG could affect gene expression. For this, we took monocytes and differentiated them into DCs. DCs were then exposed to 10mM D-HG for the next 24 hours. We used 10mM α-ketoglutaric acid (Di-keto) as a control as D-HG is structural closely related to ketoglutarate and represents a competitive inhibitor of α-ketoglutarate-dependent dioxygenases [125]. Because of this we wanted to separate possible effects based on this similarity of HG and Di-keto on gene expression from effects which are only induced by HG. Next, we lysed the cells and performed RNAseq analysis (RNAseq analyses was performed by Prof. Dr.Michael Rehli, Depart. of Internal Medicine III).

The mean +/- SEM of 3 independent experiments per treatment were compared for the following conditions: -LPS vs LPS, LPS vs LPS plus D-HG, LPS vs LPS plus Di-Keto.

We only considered genes that were regulated by LPS. Genes that are significantly regulated by LPS and D-HG in comparison to LPS alone are presented in Table 4.1 and 4.2. We excluded genes that are similiarily regulated by HG and Di-Keto in the presence of LPS Genes that showed a Log change ≥ 0.6 for LPS vs LPS plus HG but a Log change <0.6 in the comparison LPS vs LPS plus Di-Keto were considered as upregulated genes. Genes with a Log change <0.6 for LPS vs LPS plus D-HG and no effect of LPS vs LPS plus Di-Keto comparisons were considered downregulated.

4.1.5.1 Genes Upregulated with D-HG

Interestingly the majority of genes (213), were regulated in a similar way by HG and Di-Keto.Table 4.1 shows the 6 genes that were differentially only upregulated by D-HG but not Di-Keto on mRNA level. Among those 6 genes a member of a transmembranal receptor family that couple to G protein (F2RL2) was upregulated by D-HG. Furthermore CXCR5, a cytokine receptor involved in the modulation of B-cell differentiation was also upregulated by D-HG presence.

Table 4.1 Genes Upregulated in DCs by D-HG.

Symbol	Transcript Length	Transcript Type	
BMP6	2780	protein_coding	Bone morphogenetic protein 6;induces cartilage and bone formation
CXCR5	4431	protein_coding	Receptor 5; cytokine receptor that binds to B-lymphocyte chemoattractant (BLC). Involved in B-cell migration into B-cell follicles. May have a regulatory function in Burkitt lymphoma (BL) lymphomagenesis and/or B-cell differentiation
F2RL2	3429	protein_coding	Coagulation factor II (thrombin) receptor-like 2; Receptor for activated thrombin coupled to G proteins that stimulate phosphoinositide hydrolysis
MYO1B	9527	protein_coding	Myosin IB; Motor protein that may participate in process critical to neuronal development and function such as cell migration, neurite outgrowth and vesicular transport
PLAT	6618	protein_coding	Plasminogen activator, tissue; it plays an important role in tissue remodeling and degradation, in cell migration and many other physiopathological events.
SERPINB2	2748	protein_coding	Serpin peptidase inhibitor, clade B (ovalbumin), member 2; Inhibits urokinase-type plasminogen activator.

4.1.5.2 Genes downregulated with D-HG

When we analyzed the genes which were downregulated by D-HG, 191 genes were downregulated in a similar way by HG and Di-keto. Furthermore only 3 genes were reduced by HG but not Di-Keto. HG suppressed expression of IL-18, which is a pro-inflamatory cytokine, resembling the function of IL-12. In a medical thesis[126] and my master thesis the impact of Di-Keto on IL-12 was already investigated and we found no effect excluding the possibility that keto-dependent dioxygenases are involved in the regulation of IL-12.

In addition, we also observed a down regulation in DNAH11, gene involved in ATPase activity, listed in Table 4.2.

Table 4.2 Genes Downregulated in DCs by D-HG.

Symbol ID	Transcript length	Transcript type	
RP11-1D12.1	769	sense_intronic	
C12orf79 (LINC01619)	3642	protein_coding	Long Intergenic Non-Protein Coding RNA 1619.
DNAH11	15998	protein_coding	Dynein, axonemal, heavy chain 11; Dynein has ATPase activity; the force-producing power stroke is thought to occur on release of ADP.
RP11-519G16.3	3886	Antisense	
IL18	2628	protein_coding	Interleukin 18 (interferon-gamma-inducing factor); Augments natural killer cell activity in spleen cells and stimulates interferon gamma production in T-helper type I cells.
RP11-404F10.2	4121	Antisense	

4.1.6 The role of HG on LPS-induced DC maturation

LPS is not only a strong activation stimulus of myeloid cells but can also induce the maturation of immature DCs into mature DCs. During DC maturation, immature DCs loose their high capacity for phagocytosis but gain the ability to present antigens to T cells, which is crucial for the adaptive immune response. Several marker proteins, which are important for antigen presentation, are upregulated by LPS such as CD80 or CD83. In order to further investigate effects of D-HG on DCs, we analyzed the expression of these co-stimulatory molecules that increase during DC activation such as CD80, CD86, CD83, HLA-DR (molecules related to antigen presentation) and CD1a (related to the lipid presentation). DCs were differentiated from monocytes, stimulated with LPS for 24h in the presence or absence of 10mM D-HG.

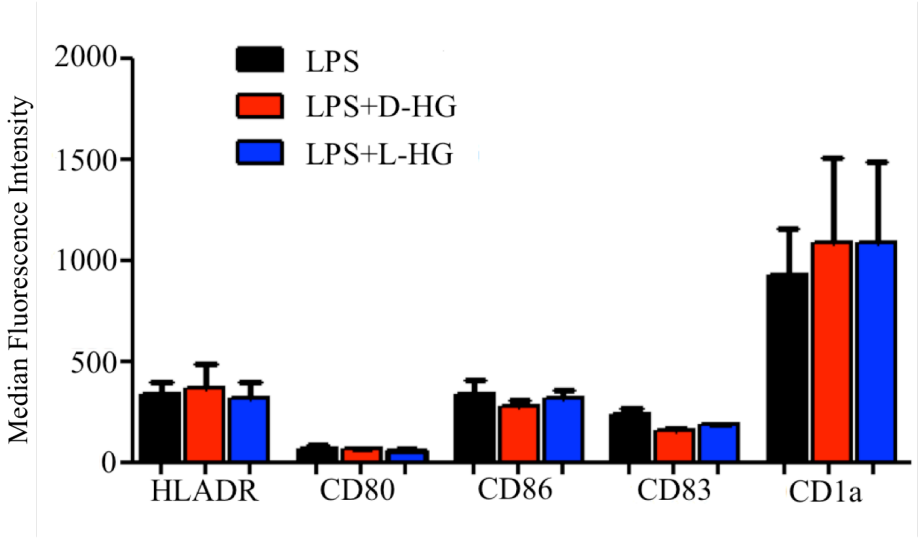

Figure 4.31. Effect of HG on DC maturation. DCs were differentiated from monocytes for 7 days with IL-4 and GM-CSF. After this differentiation process, iDCs were stimulated with LPS (100ng/ml) and 10mM D/L-HG for another 24hrs. Maturation markers were evaluated by flow cytometry.

The presence of HG during the maturation process (day 7 to day 8) did not affect the expression of HLADR, CD80, CD86, CD83 or CD1a (Figure 4.31).

4.1.7 The impact of HG on the differentiation of DCs

Next, we were interested to elucidate whether the presence of HG during the whole differentiation process would inhibit this differentiation process and lead to an even stronger impact on LPS-induced IL-12 secretion. Therefore, DCs were differentiated in 2 different settings: first, monocytes were differentiated for 7 days and stimulated at day 7 with 100ng/ml LPS and D-HG for 24hrs, second, monocytes were differentiated into DCs with D-HG from the beginning of the differentiation process for 7 days and then activated with LPS for last 24 hours. First we analyzed whether IL-12 production is affected in a similar manner as in our previous experiments.

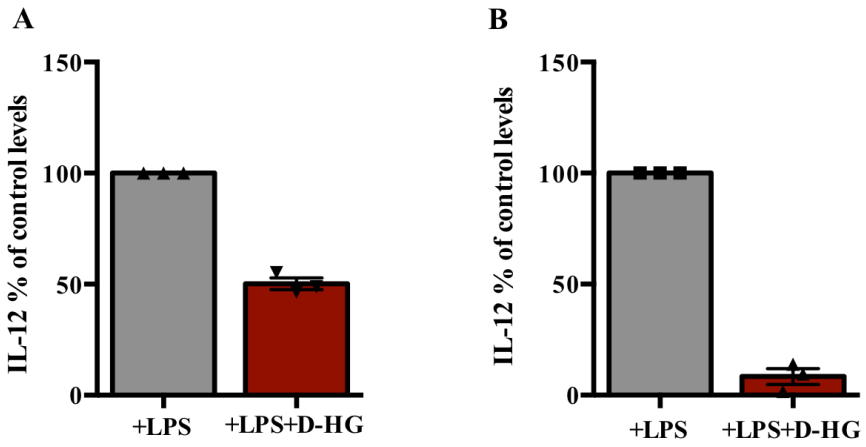

Figure 4.32. Effect of HG on DC IL-12 secretion. Monocytes were differentiated in 2 settings, A) addition of LPS+D-HG during activation process (day 7-8), B) addition of D-HG from day 0 during the whole differentiation process, and at day 7, 100ng/ml LPS was added. Data show the mean +/- SEM of 3 independent experiments. Supernatants were collected after 8 days of culture and ELISA was performed.

The presence of D-HG during the differentiation process affected the capacity of the cells to produce IL-12 much stronger compared to the addition of D-HG only during activation. IL-12 secretion was almost abolished when D-HG was added during differentiation (Figure 4.32).

In order to further investigate effects of D-HG on the differentiation of DCs, surface markers involved in differentiation such as HLA-DR (molecule related with antigen presentation) and CD1a (related to lipid presentation) were stained on DCs differentiated in the presence or absence of 10mM D-HG without LPS stimulation.

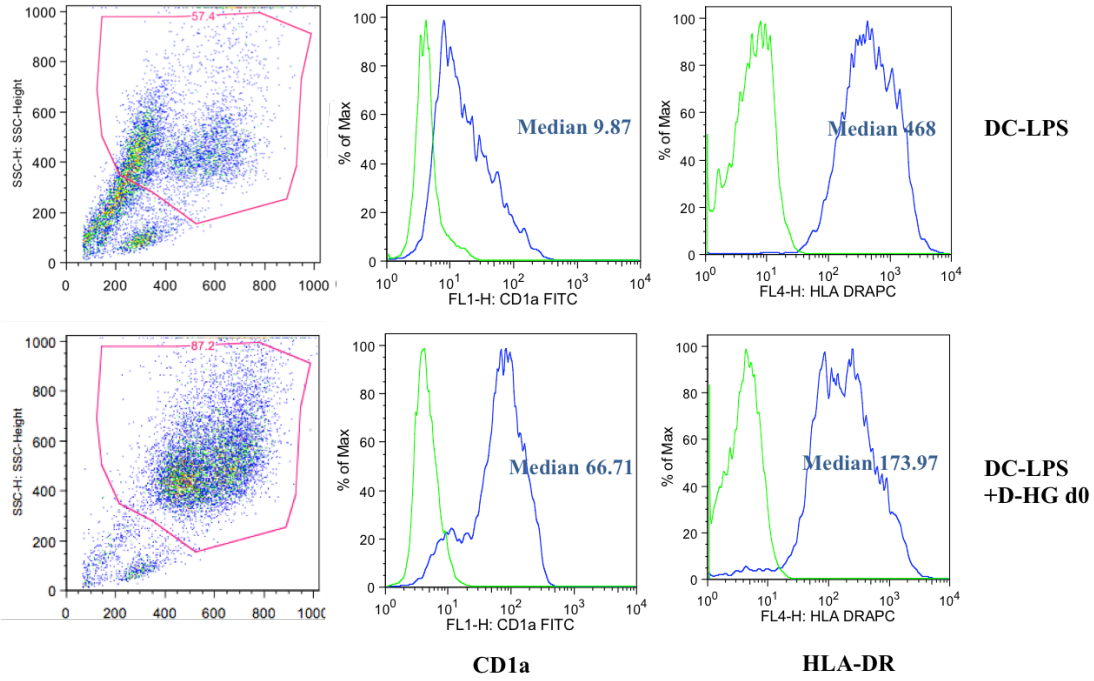

Figure 4.33. Impact of D-HG on the differentiation of monocytes into immature DC. Monocytes were differentiated with IL-4 and GM-CSF for 7 days. The figure represents gating strategy and histogram plots of iDCs (7 days culture) for CD1a and HLA-DR expression in absence (upper panel) or in presence (lower panel) of D-HG during the differentiation process. Expression of differentiation markers were evaluated by flow cytometry. One representative experiment out of three is presented.

iDCs treated with D-HG during the entire differentiation process showed a reduced HLA-DR expression while the contrary holds true for CD1a (Figure 4.33). A 5-fold increase of CD1a expression was observed in D-HG treated cells in comparison to untreated cells (cells without D-HG treatment).

Next we differentiated iDCs under the same settings mentioned on Figure 4.33 but in this case cells were activated for 24hrs with 100ng/ml LPS.

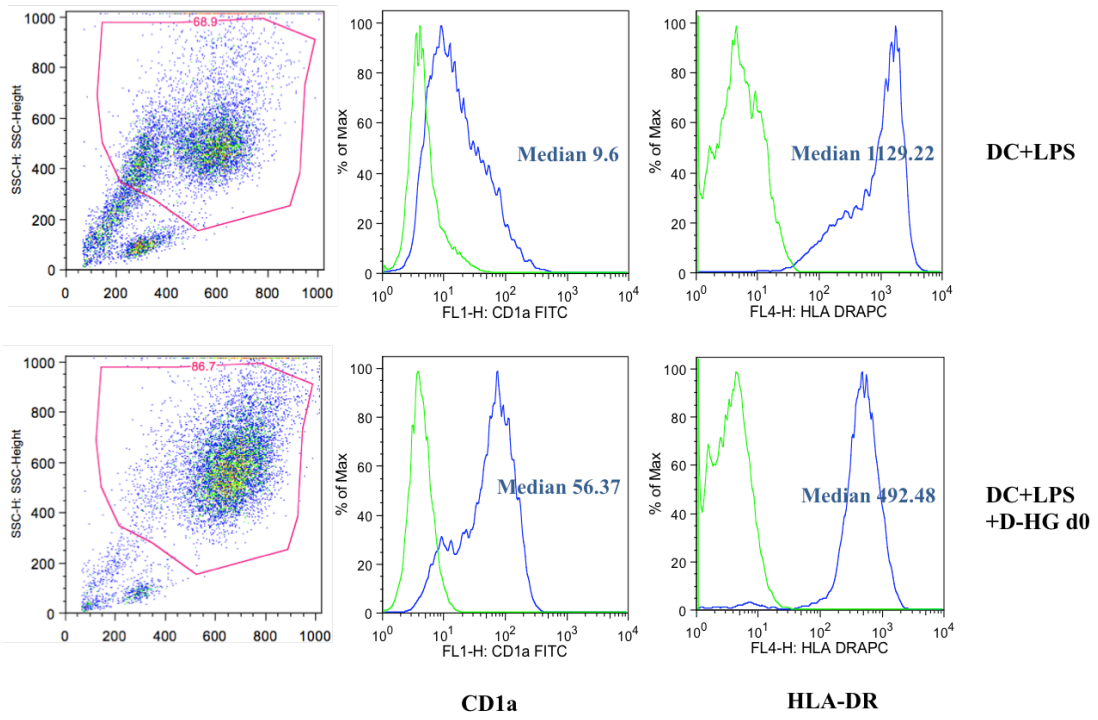

Figure 4.34. Impact of D-HG on DC maturation. Monocytes were differentiated with IL-4 and GM-CSF for 7 days in the absence (upper panel) or presence(lower panel) of 10mM D-HG. On day 7 iDCs were stimulated with LPS for 24hrs. One representative experiment out of three is presented.

The downregulation of HLA-DR and the upregulation of CD1a (Figure 4.34) by HG was still observed after DC maturation with LPS (Figure 4.35, Figure 4.36), (Figure 4.35, 4.36). Therefore, LPS did not overcome the effect of 10mM D-HG.

In summary, long term treatment of DCs with D-HG exerted an even stronger impact on IL-12 levels compared to short -term effects. Furthermore HG changed the surface marker expression.

Further investigations are necessary to elucidate the long-term impact of D-HG on DCs differentiation.

4.2 Glioblastoma cell lines

We found a strong impact of HG on DC metabolism. It has been reported, that IDH mutations and HG have also an impact on the prognosis of patients with glioblastomas. Based on these findings we analyzed whether D-HG has also an impact on mitochondrial respiration of tumor cells. We investigated the impact of D-HG on the respiration of different glioma cell lines.

4.2.1 U87

We started to analyze the U87 cell line, a commonly studied grade IV glioma cell line, which was obtained from a stage four 44 year-old cancer patient and is characterized by epithelial morphology [127].

4.2.1.1 High resolution respirometry of U87

We analyzed the effect of D-HG on glioblastoma cell respiration in detail by high-resolution respirometry using a classical respirometric approach.

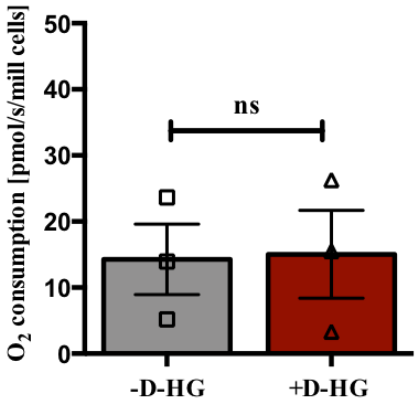

Figure 4.35. Routine respiration of U87 in the presence of D-HG. Oxygraph chambers were filled with $1x10^6$/ml U87 cells in 2ml final volume. After stabilization of respiration D-HG or medium was added to the chambers and oxygen consumption was monitored for 1hr. Data represent the mean +/- SEM of 3 independent experiments. Statistical significance was tested by Wilcoxon Test. (*$p \leq 0.05$, ns not significant).

In figure 4.35 we observed no significant effect on the O_2 consumption by the addition of D-HG. After 1 hour we investigated respiratory characteristics in more detail by applying oligomycin (ATP synthase inhibitor) to determine LEAK respiration followed by titration of an uncoupler to measure maximum capacity of the electron transfer system. All respiratory parameters were corrected for residual oxygen consumption rates, determined after the addition of rotenone and myxothiazol.

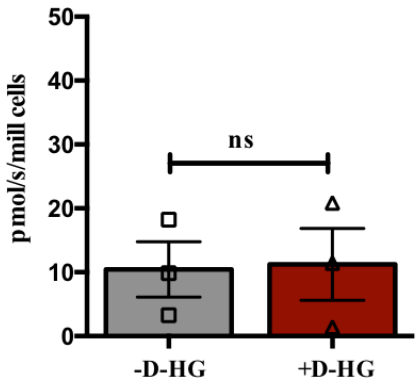

Figure 4.36. Impact of D-HG on ATP related oxygen consumption U87 cells. Oxygraph chambers were filled with $1x10^6$/ml U87 cells in 2ml final volume. After stabilization of respiration D-HG or medium was added to the chambers and oxygen consumption was monitored for 1hr. Leak respiration was determined after the addition of oligomycine and subtracted from ROUTINE respiration to calculate oxygen consumption related to ATP production. Data represent the mean +/- SEM of 3 independent experiments. Statistical significance was tested by Wilcoxon Test. (*p≤0.05, ns not significant).

Oxygen consumption related to ATP production was not affected by the addition of D-HG. These results suggest that D-HG has no immediate effect on U87 respiration (Figure 4.36). However, we cannot exclude an impact after a prolonged incubation time. Further experiments should be performed in order to elucidate long-term effects of D-HG on mitochondrial respiration of U87 cells.

4.2.2 TP365

4.2.2.1 High resolution respirometry of TP365

We then analyzed the effect of D-HG on a second glioblastoma cell line (TP365 under low glucose medium.

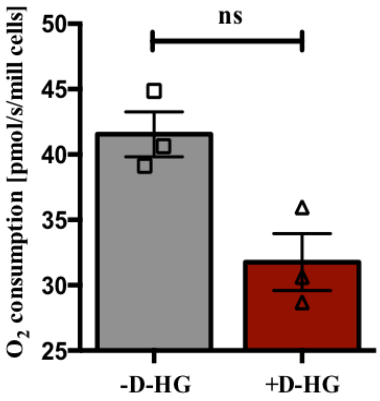

Figure 4.37. Routine respiration of TP365 in the presence of D-HG. Oxygraph chambers were filled with $1x10^6$/ml TP365 cells in 2ml final volume. After stabilization of respiration D-HG or medium was added to the chambers and oxygen consumption was monitored for 1hr. Data represent the mean +/- SEM of 3 independent experiments. Statistical significance was tested by Wilcoxon Test. (*$p \leq 0.05$, ns not significant).

In TP365 we observed a trend for a reduction in O_2 consumption under D-HG treatment although statistical significance was not reached (Figure 4.37). We then analyzed whether D-HG triggers an effect on oxygen consumption related to ATP production.

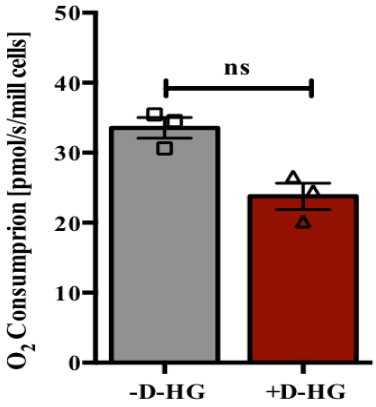

Figure 4.38. Impact of ATP related oxygen consumption in TP365 cells. Oxygraph chambers were filled with $1x10^6$/ml TP365 cells in 2ml final volume. After stabilization of respiration D-HG or medium was added to the chambers and oxygen consumption was monitored for 1hr. Leak respiration was determined after the addition of oligomycine and subtracted from ROUTINE respiration to calculate oxygen consumption related to ATP production. Data represent the mean +/- SEM of 3 independent experiments. Statistical significance was performed by Wilcoxon Test. (*$p \leq 0.05$, ns not significant).

Although not significant, we again found a trend of reduced oxygen consumption related to ATP production in the TP365 cell line in the presence of D-HG.

5. Discussion

Isocitrate dehydrogenases (IDHs) catalyze the oxidative decarboxylation of isocitrate into α-ketoglutarate (α-KG). IDH1 and IDH2 are obligate homodimers and use nicotinamide adenine dinucleotide phosphate (NADP+) as a cofactor whereas IDH3 exists as heterotetramer and uses nicotinamide adenine dinucleotide (NAD)[128]. IDH2 and IDH3 are located in the mitochondria, whereas IDH1 is located in the cytosol. Together with the pentose pathway IDH1 and IDH2 enzymes are the most important source of NADPH. Point mutations in isocitrate dehydrogenase (IDH) 1 and 2 are frequently found in neoplasias including acute myeloid leukemia (AML) and glioma. Data from glioma patients showed a positive correlation between mutated IDH and overall survival [129] whereas the prognostic impact of IDH mutations in AML varies across studies. A retrospective analysis by DiNardo et al. found no impact of IDH mutation status on overall survival in patients with AML [130]. The opposite is observed in a study of more than 800 AML patients [128]. Here IDH mutations constituted a poor prognostic factor in a subgroup of cytogenetically normal AML patients with mutated NPM1 without FLT3-ITD.

IDH mutations were mapped structurally to key residues within the active site, specifically the R132 codon in IDH1, and the R172 and R140 codons in IDH2. All mutations are generally heterozygous, suggesting a gain of function as a possible cancer mechanism. In line it has been shown that mutated IDH gains the neomorphic ability to convert α-KG into the oncometabolite D-2-hydroxyglutaric acid (D-HG). IDH mutations suppress hematopoietic differentiation in leukemia models[131]. However, little is known how HG can affect non-malignant hematopoietic cells.

As a first step to address the impact of HG on non-malignant hematopoietic cells, we investigated whether human primary myeloid cells would take up HG. For this purpose we incubated monocyte-derived DCs with HG and determined intracellular levels of HG by mass spectrometry analysis in the Institute of Functional Genomics in Regensburg.
DCs treated with LPS exhibited low endogenous levels of HG, but incubation with 10mM D-HG resulted in uptake of extracellular D-HG and 100 fold increased levels in intracellular HG. This demonstrated the capacity of DCs to uptake HG. Recently we could show that also primary human T-cells can uptake HG [132]. At physiological pH, HG

exists as hydrophilic dicarboxylate anion and most likely requires specific transport systems to translocate across membranes. Several possible receptors for D-HG and L-HG have been tested in oocytes. From these investigations D-HG and L-HG were substrates of the organic anion transporters OAT1, OAT3, OAT4 and the sodium dicarboxylate cotransporter 3 (NaDC3) [133]. Further studies should address the expression of those transporters in human myeloid and lymphoid cells to clarify whether these transporters are possibly involved in HG transport in primary hematopoietic cells.

5.1 Effect of HG on the short term LPS response of immature DCs

Dendritic cells are the most important link between innate and adaptive immunity. They capture antigens and present them to T cells, which leads to T cell activation and polarization. IL-12 levels secreted by dendritic cells have an important role in the regulation of a T cell response. High levels of IL-12 induce a Th1 response, whereas low IL-12 and high IL-10 secretion leads to Th2 differentiation [134].

We studied the impact of D-HG on the LPS-stimulated cytokine response of human monocyte-derived DCs. IL-12 p70 was significantly decreased in supernatants of stimulated DCs when LPS and HG were added simultaneously. In contrast, other cytokines were not changed or even up regulated (IL-10) in the presence of D-HG. IL-12 protein is a dimer composed of two subunits. Therefore, we analyzed the expression of both subunits by flow cytometry. D-HG did not affect the expression of the p35 subunit whereas p40 was clearly reduced indicating a selective regulation of this gene. In a previous work, the transcriptional regulation of p35 and p40 was analyzed after 4h stimulation with and without D-HG and the data indicate a statistically not significant impact of HG on the transcription of both subunits in DCs [126].

We also tested whether the enantiomer of D-HG, L-HG, would also modulate IL-12 secretion. Interstingly also L-HG inhibited IL-12 secretion by DCs. Most cancer-associated IDH mutations seem to be associated with elevation of the D-enantiomer rather than the L-enantiomer, however in kidney tumors elevations of the L-enantiomer of HG has been described [135]. Accumulation of L-HG is not based on an IDH mutation in renal cell carcinoma, but mediated by reduced expression of L-HG-dehydrogenase, which metabolizes L-HG back to α-KG. Therefore, not only D-HG but also L-HG represents an

oncometabolite even though the underlying mechanisms of elevation are different. What is more, in breast carcinoma it has been shown that independent of an IDH mutation, MYC activation and glutamine metabolism correlates with elevated HG levels and poor prognosis[136]. Hence, different mechanism can lead to elevated HG levels in tumor tissues dependent on the cancer type.

As IL-12 is not only a marker for DC activation but also a marker for successful differentiation of DCs, we hypothesized that D-HG might suppress the immune response by altering the differentiation, activation and antigen presentation of DCs, resulting in reduced T cell activation and the capacity of tumor cells to escape the effects of the immune surveillance.

In a next set of experiments we analyzed the impact of D-HG on the final maturation process of monocyte-derived DCs, which can be induced *in vitro* by incubation of immature DCs with LPS. For this purpose immature DCs were generated starting with human monocytes isolated from peripheral blood. After 7 days of differentiation with GM-CSF and IL-4, cells were incubated for another 24hrs with LPS to induce maturation. When D-HG (10mM) was added during the maturation no change in the expression of maturation markers such as CD80, CD86 or CD83 occurred indicating that the LPS-induced maturation response was not altered by D-HG even though LPS-induced IL-12 secretion was disturbed.

5.2. Long term effects of HG on DC differentiation

Next we investigated the impact of D-HG after long term incubation with D-HG during the 7 day differentiation process from monocytes to DCs. After 7 days we analyzed surface antigens of immature DCs. In parallel, DCs were treated with LPS for another 24hrs and we analyzed surface markers and IL-12 secretion. As analyzed by flow cytometry, immature DCs showed lower surface expression of HLA-class II molecules (HLA-DR) and increased levels of CD1a when HG was present during the differentiation process. Furthermore, suppression of IL-12 secretion was much stronger after long term incubation of DCs with HG and subsequent stimulation with LPS. The downregulation of HLA-class II molecules and the strong reduction of IL-12 secretion may lead to a “tolerogenic” DC phenotype with decreased ability of antigen presentation and T-cell activation.

In conclusion, our results indicate that the oncometabolite D-HG impairs the APC function of DCs by down regulation of HLA-class II, as well as IL-12 secretion, which potentially may contribute to the immune escape of tumor cells in a tumor environment with HG accumulation.

5.3. Impact of HG on TLR signaling

Toll-like receptors (TLRs) are receptors expressed by cells of the innate immune system that are stimulated by bacteria, viruses and fungi. LPS is one of the best studied immunostimulatory components of bacteria and stimulates TLR4. Upon LPS recognition, TLR4 recruits downstream adaptors and triggers signaling pathways which finally lead to the activation of transcription factors [137]. IκB kinase and MAPK (mitogen-activated protein kinase) pathways are activated.

In order to elucidate underlying mechanisms responsible for the effect of D-HG on DCs activity, we analyzed TLR4 signaling pathways, IκB, P-Akt, P-p38, ERK, and HIF by western blot analyses as these pathways are crucial for the regulation of IL-12 production. DCs were treated with D-HG and stimulated with 100ng/ml LPS. First of all we investigated the NF-κB pathway. IκB-phosphorylation leads to the degradation of IκB proteins and subsequent activation of NF-κB. After 1h LPS-stimulation IκB was clearly degraded and D-HG had no effect on its degradation suggesting that the NF-κB pathway is not altered by D-HG.

Furthermore, LPS raises the level of hypoxia-inducible factor-1α (HIF-1α) in macrophages, and HIF-1α promotes the production of inflammatory cytokines, such as IL-6 and IL-12 [138]. Additionally to these reports, high levels of cellular HG have been reported to lead to the hydroxylation of HIF-1α, thereby decreasing HIF expression. In addition to these findings, HG has been reported to competitively inhibit the binding of α-KG to several histone demethylases, including JmjC-domain-containing histone demethylase proteins (JHDM) leading to a widely aberrant histone methylation profile [125]. Likewise, it has been reported that HG acts as an inhibitor of hydroxymethylases like TET methylcytosine dioxygenases (TET) 1 and 2, involved in DNA demethylation [47]. However, in our experiments we were neither able to detect consistent upregulation of HIF after LPS stimulation nor an effect of D-HG. Further analysis elucidating an effect of D-HG effect on the methylation profile of DCs is currently addressed in another PhD thesis.

Extracellular signal-related kinase (ERK) and p38 mitogen-activated protein (MAP) kinases have also been demonstrated to be involved in the regulation of LPS-stimulated IL-12 gene expression. While p38 promotes induction of IL-12 mRNA in macrophages, ERK activation suppresses LPS-mediated IL-12 transcription [139]. Again no effect of D-HG could be found.

Conflicting results have been published regarding the LPS-triggered activation of PI3K/Akt pathway. Fukao et al. reported that it negatively regulates LPS-induced IL-12 production in murine DCs [140] but Utsugi et al. described a positive impact of this pathway on human monocyte-derived cells [141]. In our experiments P-Akt was only slightly upregulated by LPS and D-HG had no impact on the expression level.

In summary all studied pathways triggered by LPS were not significantly changed by D-HG treatment and cannot explain its negative impact on IL-12 production.

5.3.1 Impact of G-Protein-coupled receptors and cAMP on IL-12 production

Unfortunately we were not able to demonstrate that D-HG disrupts or modulates the mentioned signaling pathways; therefore we asked whether the D-HG effect observed on IL-12 levels could be related to its binding/signaling via G-proteins as a group of G protein-coupled receptors (GPCR) serve as hydroxycarboxylic acid receptors [120] and therefore could represent possible receptors for D-HG.

G-proteins have been shown to play a role in the cytokine production of myeloid cells. Especially GPR109A has been reported to be involved in the suppression of IL-12 regulation in macrophages [142]. With this in mind we decided to adress the expression of GPR109A in DCs treated with D-HG. Monocytes were differentiated for 7 days and the impact of HG on GPR109A expression was analyzed in iDCs and LPS matured DCs. We were able to demonstrate that immature DCs already express GPR109A and that mRNA expression is up regulated during the maturation of DCs by LPS. Addition of D-HG modestly reduced GPR109A expression. To elucidate whether a stimulation of GPR109A exerts a similar reduction on IL-12 secretion as HG, we applied niacin. In contrast to previous reports with macrophages [142] we found no effect on IL-12 production by the GPR109A ligand niacin, which excludes that HG signals via GPR109A in human DCs. Therefore macrophages and DCs may have different suceptibilty regarding niacin treatment.

Several reports show a relation between cyclic adenosine monophosphate (cAMP) and DC function [122,143,144]. It has been shown that Forskolin, a cAMP inducing factor, inhibits IL-12 production [122]. Thus we treated DCs with a cAMP analog, and Forskolin in comparison to D-HG, In line with previous observations [122] we found a significant reduction in IL-12 production by the addition of cAMP and forskolin similar to the impact of HG. These results indicated that IL-12 reduction by D-HG could be associated with an increase in cAMP levels. However, we were not able to measure increased cAMP levels in DCs even with Forskolin as positive control stimulus, which indicates that the test system was not reliable. Therefore, these analyses have to be repeated with another method.

5.4 The role of HG on Mitochondrial Respiration and lactate production of Dendritic Cells

cAMP plays an important role in PKA signaling pathway activation, which has been reported to modulate the activation of mitochondrial respiration [145–147]. Moreover, several studies have shown effects of HG on mitochondrial respiration [45,148,149]. Furthermore, metabolic alterations have been implicated in the activation of immune cells. Therefore we wondered whether IL-12 inhibition by HG could be associated with altered metabolism in DCs. A metabolic shift from OXPHOS towards glycolysis is regarded as an important event in the activation process of LPS stimulated macrophages[150] and monocytes[151]. Furthermore DC maturation is linked to a reduction in OXPHOS and increase in glycolysis[152]. In our experiments LPS treatment changed the metabolic profile of DCs in a similar manner. LPS diminished ROUTINE respiration, oxygen consumption related to ATP production and the capacity of the electron transfer system in DCs whereas lactate secretion was increased. HG treatment blocked the reduction in mitochondrial activity and diminished the increase in glycolysis. In line, we recently could show that HG triggers an increase in oxidative phosphorylation and reduces the glycolytic activity of human T cells [132]. Our data are in line with a tolerogenic phenotype of HG-treated DCs as Malinarich stated that tolerogenic DCs are characterized by increased OXPHOS and reduced glycolysis[152]. Moreover, Malinarich and colleagues demonstrated that tolerogenic DCs displayed a poor immunogenic phenotype, with low levels of IFN-γ and IL-12p40 production, and increased levels of IL-10 production. In addition to this, in transcriptomic studies of tolerogenic DCs, Malinarich and colleagues observed an upregulation of

differentially expressed genes involved in OXPHOS, mitochondrial dysfunction, mTOR and HIF signaling. While IL-12 was also suppressed in our HG-DCs, we detected only a slight increase in complex I and II.

An impact of HG on OXPHOS has also been described in tumor cell lines. Here, IDH mutated cells have been shown to display increased OXPHOS activity [153,154]. In our experiments exogenous application of HG to glioblastoma cell lines did not alter mitochondrial activity. Other publication describes even a negative effect on respiration in IDH mutated cells and after addition of exoegenous HG. Chan and colleagues observed that D-HG inhibited mitochondrial cytochrome c oxidase (COX) activity in acute myeloid leukemia cells [155]. Fu et al. reported an inhibition of respiration and ATP synthase in glioblastoma cells [156]. Taken together, HG blocked the LPS induced decrease in mitochondrial respiratory activity and the increase in glycolysis. However, as blocking of mitochondrial respiration was not sufficient to increase IL-12 levels in the presence of HG in DCs, we conclude that additional mechanisms are involved.

Mitochondria play an important role not only for ATP production but also in cellular calcium homeostasis. On the other hand calcium affects mitochondrial activity. To investigate the role of mitochondrial calcium flux on IL-12 production, we added CsA.

Increased cytosolic calcium levels have been shown to reduce IL-12 secretion in macrophages [119]. We speculated that HG leads to increased cytosolic calcium levels, thereby reducing IL-12 production. CsA is capable to increase the calcium storage capacity of mitochondria, thereby probably counter balancing the effect of HG.

Notably, DCs treated with CsA and LPS showed an increase in IL-12 production in comparison to iDCs stimulated with LPS, nevertheless this increase was not statistically significant. CsA attenuated the suppressive effect of D-HG, but did not entirely rescue it. In line, CsA treatment could partially prevent the impact of HG on the LPS induced decline in respiration, although with some time delay.

This delayed effect point towards an attenuation of the D-HG effect as the one observed in IL-12 levels. These results are contradictory to the effect observed by Huang and colleagues, where they demonstrated that CsA treated DCs show a reduced IL-12 production [157].

5.5 Effect of HG on the RNA expression of Dendritic Cells

In order to elucidate a more global effect of D-HG on DCs we performed RNAseq analyses. To our knowledge this is the first global gene expression analysis in DCs treated with D-HG. As a control DCs were incubated with Di-ketoglutarate, which is a structural closely related molecule but had no impact on IL-12 secretion.

Three criteria were applied: First, genes that were significantly different in LPS-stimulated DCs compared to untreated DCs. Second, genes that were significantly different in LPS+D-HG-treated DCs compared to LPS-stimulated DCs. Third, genes that were not significantly affected by Di-Keto treatment. Using these three criteria, only 6 genes were differentially upregulated and 6 genes downregulated by D-HG.

D-HG upregulated F2RL2, a member of a transmembrane receptor family that couple to G proteins[158]. F2RL2 gene encodes the Protease activated receptor 3 (PAR-3). PAR3 directly dimerizes with PAR1 to induce a specific PAR1/Gα13-binding conformation that favors Gα13 activation [159]. As previously mentioned, GPR109A and its ligand niacin were not involved in the reduction of IL-12 in our experiments, but this does not exclude that other G-proteins may be involved. HG-induced related changes in PAR-3 signalling could be involved in suppression of IL-12. Agonist peptides of PAR-1 and PAR-4 but not PAR-3 hav been shown to induce IL-6 release from monocytes whereas IL-12 was not increased [160]. In further experiments the impact of PAR-3 on DCs should be analyzed.

In the present work HG also upregulated the gene , Bone Morphogenetic Protein 6 (BMP6), which has been described to be upregulated by pro-inflammatory cytokines (IL-17 and TNF-α) in rheumatoid arthritis synoviocytes [161]. Also in a previous study by Varas and colleagues, the authors demonstrated that BMP signaling pathway are important for the regulation of CD4+ T-cell proliferation [162]. Interestingly Maurer and colleagues described that BMP 7 inhibited the differentiation of human CD14+ monocytes to osteoclasts [163]. Therefore it would be intersting to study the relation between disturbed DC differentiation by HG and BMP 6 levels during DC differentiation.

Another gene upregulated by D-HG was C-X-C Motif Chemokine Receptor 5 (CXCR5). iDC express different chemokine recptors which regulate their migration in response to CCR5 ligands such as RANTES, MIP-1α and MIP-β. Maturation of DCs by LPS, TNF-α,

or CD40 ligation down-regulates CXCR5 expression[164]. Upregulated expression by HG is another marker for a disturbed DC differentiation.

Another gene upregulated by D-HG was Myosin 1B (MYO1B). MYO1B is involved in neuronal development and function such as cell migration and vesicular transport. Little is known on its role in myeloid cells. However as MYO1B controls the formation of secretory granules it could probably be involved in the secretion of IL-12 in DCs [165].

The plasminogen activator/plasmin system is an enzymatic cascade involved in the control of matrix turnover and thereby can regulate cell invasion and migration of tumor and immune cells.

Plasminogen Activator, Tissue Type (PLAT) gene was also upregulated by D-HG treatment. PLAT gene encodes tissue-type plasminogen activator protein, involved in the breakdown of blood clots, which has been related with the secretion of IL-6 cytokine after a stroke event via NMDA receptors activation and upregulation of endothelin 1 (ET-1) and JNKmitogen-activated protein kinase (MAPK)[166]. In the present work, we found no effect on JNK pathway by the addition of D-HG, results that contradicts the data by Armstead and colleagues[166].

Another gene upregulated by D-HG effect was plasminogen activator inhibitor-2 (SERPINB2), an inhibitor of urokinase plasminogen activator (uPA). Ponnala and collegues demonstrated in gliomas cells, that silencing of the uPA receptor induced a switch from glycolytic metabolism to oxidative phosphorylation (OXPHOS) and generated reactive oxygen species (ROS) predisposing glioma cells to mitochondrial outer membrane permeabilization[167]. These reports could point towards a possible relation between upregulation of OXPHOS by HG through inhibition of uPA.

Next we analyzed genes downregulated after 24hrs of treatment with D-HG. Interestingly, we observed a downregulation of the IL-18 gene. The IL-18 gene encodes Interleukin-18 (IL-18), a pro inflamatory cytokine, which has a similar function as IL-12 [168]. Interleukin-18 is a member of IL-1 superfamily of cytokines. The main function is synergistically with IL-12 to induce Th1 differentiation and interferon-γ secretion. IL-18 downregulation by D-HG could give a hint in direction of an immunosuppressive capacity of D-HG.

Also downregulated was Long non-coding RNA LINC01619, which recently has been reported to regulate miR-27a/FOXO1 and induce endoplasmic reticulum stress-mediated podocyte injury in diabetic nephropathy. In diabetic rats and high glucose cultured

podocytes, LINC01619 triggered oxidative stress [169]. This findings suggest that LINCO1619 downregulation in DCs could be a feedback mechanism to suppress D-HG-induced oxidative stress.

We also demonstrated a downregulation on Dynein heavy chain 11, axonemal (DNAH11). Mutations in the coding region of DNAH11 have been linked to primary ciliary dyskinesia, an autosomal recessive disorder that leads to chronic respiratory disorders [170] and diabetic nephropathy[171]. Furthermore, mutations have been described in a minority of AML patients by Ahn and colleagues. They demonstrated a prevalence of IDH1 and 2 Mutations after transplantation (16.5%), whereas the prevalence of DNAH11 mutations was just 1. 7% [172]. The DNAH11 mutation was only associated with ASXL2 mutations but not with the IDH mutations excluding a link with higher HG levels. It is possible that high HG levels in IDH mutated AML downregulate DNAH11 independent of a mutation which could be analyzed in further investigations.

6. Summary

Tumor development is commonly associated with genetic alterations such as activation of oncogenes or the silencing of tumor suppressor genes. Recently point mutations in genes encoding isocitrate dehydrogenase (IDH) have gained substantial interest in glioma classification. IDH mutations are also frequently found in neoplasias including acute myeloid leukemia (AML). Mutated IDH aquires the function to produce the oncometabolite D-2-hydroxyglutarate (D-HG). D-HG levels in the tissue of glioma patients can reach concentrations up to 35mM. Nevertheless, little is known on the impact of D-HG on non-malignant human immune cells.

In the present work, we compared the effect of both HG enantiomers, D-HG and L-2-Hydroxyglutarate (L-HG) on dendritic cell (DC) maturation and activation, and found similar effects with both enantiomers. We also analyzed the impact of D-HG on the respiration of DCs and two glioblastoma cell lines.

We found that D-HG was taken up by LPS-stimulated DCs. Furthermore, the presence of D-HG during maturation and activation of DCs strongly affected the production of IL-12. Especially when DCs were treated with D-HG during the entire maturation process, the IL-12 production was extremely reduced.

To elucidate the mechanism by which D-HG modulates IL-12 production, we studied the principal components of the Toll-like receptor 4 signaling pathway involved in IL-12 p70 production (NF-κB, HIF-α, PI3-kinase pathway components). However, we found no significant effect of D-HG treatment on any of these pathways after 1hr or 24hrs of incubation. As we found an increase of GPR109A expression after LPS stimulation, we studied a possible involvement of this receptor but found no significant relation between IL-12 production and the reported GPR109A ligand, niacin.

Cyclic adenosine monophosphate (cAMP) has been described to be involved in DC function. We found significant reduction of IL-12 production by the treatment of DCs with cAMP and the cAMP-inducing-factor forskolin. However, due to technical problems, we could not detect cAMP in DCs. As several reports state a possible relation between cAMP signaling pathways and mitochondrial respiration, we analyzed the impact of D-HG on mitochondrial respiration of LPS-stimulated DCs. We observed an inhibition of

routine respiration caused by LPS, whereas pre-treatment with D-HG blocked this LPS effect. As treatment with oligomycin and rotenone (inhibitors of mitochondrial respiration) did not recover IL-12 suppression, the impact of HG on respiration alone is not sufficient to explain the suppressive effect of HG.

To further analyze the effect of D-HG on mitochondrial respiration we utilized an inhibitor of mitochondrial calcium efflux, cyclosporine A (CsA). We noticed an increase of IL-12 levels after CsA treatment compared with DCs activated without CsA treatment. Combination of CsA and D-HG in LPS-stimulated DCs partially rescued IL-12 levels caused by D-HG treatment. During high resolution respirometry studies we observed a delayed reduction of routine respiration 2hrs after CsA treatment. Also, we found a modest increase of respiratory chain complex expression in stimulated DCs treated with D-HG (complex I and II). Moreover, lactate secretion studies showed an increase of lactate levels by LPS. D-HG was able to block this increase. These observations point towards the capacity of D-HG to interfere with the metabolic shift from oxidative phosphorylation into glycolysis promoted by LPS. This could also explain the suppressive effect of D-HG on IL-12 production.
IDH mutations are associated with glioma development and prognosis. Nevertheless the effect of D-HG on mitochondrial respiration of glioma cell lines is poorly documented. In the present work, we found no consistent effect on mitochondrial respiration by D-HG in two glioma cell lines.

Furthermore, we investigated global effects of HG on DCs by RNAseq analyses. Surprisingly most genes were similarily regulated by HG and our control substance di-ketoglutarate most likely due to its close structural similarity. Only 6 genes were upregulated and 3 genes were downregulated by HG. Further investigations have to be performed to investigate the link between the identified genes and DC function.

7. Zusammenfassung

Tumoren werden durch Mutationen in Protoonkogenen und Tumorsurpressorgenen verursacht. Diese Mutationen führen entweder zur Aktivierung von Onkogenen oder zum Stilllegen von Tumorsupressorgenen. Aktuell wurden Punktmutationen im Gen der Isocitrat-Dehydrogenase (IDH) für die Klassifizierung von Gliomen beschrieben. IDH Mutationen werden neben dem Gliom, häufig in der Akuten myeloischen Leukämie gefunden. Durch die Mutation bekommt die IDH die Fähigkeit D-2-hydroxygluterat (D-HG) zu produzieren. D-HG kann im Tumorgewebe von Gliom Patienten eine Konzentration bis zu 35mM erreichen. Der Effekt von D-HG auf humane Immunzellen ist bisher wenig untersucht.

In dieser Arbeit wurde der Einfluss von D-HG auf die Reifung und Aktivierung von dendritischen Zellen (DCs) untersucht und mit der Wirkung des Enantiomers L-HG verglichen. Die Effekte beider Enantiomere waren vergleichbar. Außerdem wurde der Einfluss von D-HG auf die Atmung von DCs und zwei Glioblastom Zelllinien untersucht. Zuerst bestätigten wir das D-HG von LPS aktivierten DCs aufgenommen wird. Des Weiteren sahen wir eine stark reduzierte IL-12 Produktion in DCs, wenn D-HG während der Reifung präsent war.

Um den Mechanismus des Effekts von D-HG auf die IL-12 Produktion zu analysieren, wurden zentrale Proteine des Toll-like Rezeptors (TLR) 4 Signalwegs, die bei der IL-12 p70 Produktion beteiligt sind (NF-κB, HIF-α, PI3-kinase Signalweg), untersucht. Jedoch zeigte D-HG weder nach 1 Stunde noch nach 24h einen signifikanten Effekt auf die Aktivität oder Menge der untersuchten Proteine. Die Aktivierung von DCs mit LPS führte auch zu einer erhöhten Expression des G Protein gekoppelten Rezeptors GPR109A, aber auch hier konnte kein Zusammenhang mit dem IL-12 supprimierenden Effekt von D-HG hergestellt werden, da Niacin, ein GPR109A Ligand keinen Einfluss auf die IL-12 Produktion hatte.

Cyclisches Adenosinmonophosphat (cAMP) ist ein wichtiger sekundärer Botenstoff der als wichtig für die DC Funktion beschrieben wurde. Die Behandlung von DCs mit cAMP und Foskolin, einem cAMP-induzierenden Faktor führte zu einer signifikanten Reduktion der IL-12 Produktion. Einige Arbeitsgruppen beschreiben einen Zusammenhang zwischen cAMP Signalweg und der Atmung, deshalb wurde der des Weiteren der Einfluss von D-HG auf die Atmung von DCs untersucht. LPS reduzierte die basale Atmung, diese

Reduktion konnte durch eine D-HG Vorinkubation blockiert werden. Allerdings kam es durch die Behandlung mit Oligomycin und Rotenon (Inhibitoren der Atmungskette) zu keiner Erhöhung der verminderten IL-12 Produktion.
Um den Einfluss von D-HG auf die Atmung weiter zu charakterisieren wurden DCs mit Cyclosporin A (CsA) behandelt. CsA inhibiert den Transport von Calcium aus dem Mitochondrium. CsA erhöhte die IL-12 Produktion im Vergleich zur IL-12 Produktion nach Aktivierung mit LPS alleine. Auch in Kombination mit D-HG war die IL-12 Produktion höher als nur mit D-HG. CsA führte außerdem zu einer verspäteten Reduktion der basalen Atmung nach 2 Stunden.
Des Weiteren wurde die Expression der Atmungsketten Komplexe mittels Western Blot untersucht. Komplex I und II waren vermehrt in D-HG behandelten DCs messbar. Um den Effekt von D-HG auf den Metabolismus weiter zu untersuchen wurde die Laktatkonzentration im Überstand bestimmt. LPS führte zu einer Erhöhung der Laktatlevel, D-HG war in der Lage diese Erhöhung zu Blockieren. Diese Beobachtung weist darauf hin, dass D-HG fähig war, die durch LPS induzierte metabolische Umstellung von oxidative Phosphorylierung hin zur Glykolyse zu beeinflussen. Dies könnte auch die verminderte IL-12 Produktion erklären, da die metabolische Umstellung für die Aktivierung eine Rolle spielen könnte.
Weiterhin wurde der Effekt von D-HG auf die Atmung von Gliom Zelllinien untersucht. In dieser Arbeit fanden wir keinen konsistenten Effekt von D-HG auf die Atmung von U87 Zellen und TP365,

In weiteren Analysen wurde mittels RNAseq Effekte von HG auf die Genexpression von DCs untersucht. Es zeigte sich, dass HG und di-Ketoglutarat weitestgehend vergleichbare Veränderungen in der Genexpression induzieren. Dies hängt wahrscheinlich damit zusammen, dass diese beiden Substanzen chemisch eng verwandt sind. Allerdings wurden durch HG 6 Gene hochreguliert und 3 Gene supprimiert, die nicht durch Ketoglutarat reguliert waren. In weiteren Untersuchungen muss der Zusammenhang zwischen der DC Funktion und diesen Genen analysiert werden.

8. References

1. Deimling A von. *Gliomas*. Springer; 2009.
2. Bear MF, Connors BW, Paradiso MA. *Neuroscience - Exploring the Brain*. 3rd ed.; 2007.
3. Kandel ER, Schwartz JH, Jessel TM. *Principles of Neural Science*. 4th ed. McGraw-Hill; 2000.
4. Grier JT, Batchelor T. Low-Grade Gliomas in Adults. 2006:681-693.
5. Louis DN, Ohgaki H, Wiestler OD, et al. The 2007 WHO classification of tumours of the central nervous system. *Acta Neuropathol*. 2007;114(2):97-109. doi:10.1007/s00401-007-0243-4.
6. Dolecek TA, Propp JM, Stroup NE, Kruchko C. CBTRUS Statistical Report : Primary Brain and Central Nervous System Tumors Diagnosed in the United States in 2005-2009. *Neuro Oncol*. 2012;14(1):28-36. doi:10.1093/neuonc/nos218.
7. Louis DN, Perry A, Reifenberger G, et al. The 2016 World Health Organization Classification of Tumors of the Central Nervous System : a summary. *Acta Neuropathol*. 2016;131(6):803-820. doi:10.1007/s00401-016-1545-1.
8. Johnson DR, Guerin JB, Giannini C, Morris JM, Eckel LJ, Kaufmann TJ. 2016 Updates to the WHO Brain Tumor Classification System: What the Radiologist Needs to Know. *RadioGraphics*. 2017;37(7):2164-2180. doi:10.1148/rg.2017170037.
9. Ohgaki H, Kleihues P. Genetic profile of astrocytic and oligodendroglial gliomas. 2011:177-183. doi:10.1007/s10014-011-0029-1.
10. Kim Y-H, Nobusawa S, Mittelbronn M, et al. Molecular Classification of Low-Grade Diffuse Gliomas. *Am J Pathol*. 2010;177(6):2708-2714. doi:10.2353/ajpath.2010.100680.
11. Stupp R, Mason WP, van den Bent MJ, et al. Radiotherapy plus Concomitant and Adjuvant Temozolomide for Glioblastoma. *N Engl J Med*. 2005;352(10):987-996. doi:10.1056/NEJMoa043330.
12. Verhaak RGW, Hoadley KA, Purdom E, et al. Integrated genomic analysis identifies clinically relevant subtypes of glioblastoma characterized by

abnormalities in PDGFRA, IDH1, EGFR, and NF1. *Cancer Cell*. 2010;17(1):98-110. doi:10.1016/j.ccr.2009.12.020.

13. Balss J, Meyer J, Mueller W, Korshunov A, Hartmann C, von Deimling A. Analysis of the IDH1 codon 132 mutation in brain tumors. *Acta Neuropathol*. 2008;116(6):597-602. doi:10.1007/s00401-008-0455-2.
14. Nobusawa S, Watanabe T, Kleihues P, Ohgaki H. IDH1 Mutations as Molecular Signature and Predictive Factor of Secondary Glioblastomas. *Clin Cancer Res*. 2009;15(19):6002 LP-6007. http://clincancerres.aacrjournals.org/content/15/19/6002.abstract.
15. Watanabe T, Nobusawa S, Kleihues P, Ohgaki H. IDH1 Mutations Are Early Events in the Development of Astrocytomas and Oligodendrogliomas. *Am J Pathol*. 2009;174(4):1149-1153. doi:10.2353/ajpath.2009.080958.
16. Yan H, Parsons DW, Jin G, et al. IDH1 and IDH2 mutations in gliomas. *N Engl J Med*. 2009;360(8):765-773. doi:10.1056/NEJMoa0808710.
17. Toedt G, Barbus S, Wolter M, et al. Molecular signatures classify astrocytic gliomas by IDH1 mutation status. *Int J cancer*. 2011;128(5):1095-1103. doi:10.1002/ijc.25448.
18. Gravendeel LAM, Kloosterhof NK, Bralten LBC, et al. Segregation of non-p.R132H mutations in IDH1 in distinct molecular subtypes of glioma. *Hum Mutat*. 2010;31(3):E1186-99. doi:10.1002/humu.21201.
19. Wong TZ, Turkington TG, Hawk TC, Coleman RE. PET and Brain Tumor Image Fusion. *Cancer J*. 2004;10(4).
20. Chen W, Cloughesy T, Kamdar N, et al. Imaging proliferation in brain tumors with 18F-FLT PET: comparison with 18F-FDG. *J Nucl Med*. 2005;46(6):945-952.
21. Bergmann R, Pietzsch J, Fuechtner F, et al. 3-O-methyl-6-18F-fluoro-L-dopa, a new tumor imaging agent: investigation of transport mechanism in vitro. *J Nucl Med*. 2004;45(12):2116-2122.
22. Pirotte B, Goldman S, Massager N, et al. Comparison of 18F-FDG and 11C-methionine for PET-guided stereotactic brain biopsy of gliomas. *J Nucl Med*. 2004;45(8):1293-1298.
23. Herholz K, Holzer T, Bauer B, et al. 11C-methionine PET for differential diagnosis of low-grade gliomas. *Neurology*. 1998;50(5):1316-1322.
24. Shields AF, Grierson JR, Dohmen BM, et al. Imaging proliferation in vivo with [F-

18]FLT and positron emission tomography. *Nat Med*. 1998;4(11):1334-1336. doi:10.1038/3337.

25. Miyagawa T, Oku T, Uehara H, et al. “Facilitated” amino acid transport is upregulated in brain tumors. *J Cereb Blood Flow Metab*. 1998;18(5):500-509. doi:10.1097/00004647-199805000-00005.
26. Warburg O, Wind F, Negelein E. THE METABOLISM OF TUMORS IN THE BODY. *J Gen Physiol*. 1927;8(6):519 LP-530. http://jgp.rupress.org/content/8/6/519.abstract.
27. Warburg O. On the Origin of Cancer Cells. *Science (80-)*. 1956;123(3191):309 LP-314. http://science.sciencemag.org/content/123/3191/309.abstract.
28. Stryer L. *Biochemistry*. Fourth. New york: Freeman and Company; 1995.
29. Feron O. Pyruvate into lactate and back: from the Warburg effect to symbiotic energy fuel exchange in cancer cells. *Radiother Oncol*. 2009;92(3):329-333. doi:10.1016/j.radonc.2009.06.025.
30. Dang C V, Semenza GL. Oncogenic alterations of metabolism. 1999;(1):68-72.
31. Vander Heiden MG, Cantley LC, Thompson CB. Understanding the Warburg effect: the metabolic requirements of cell proliferation. *Science*. 2009;324(5930):1029-1033. doi:10.1126/science.1160809.
32. Griguer CE, Oliva CR, Gillespie GY. Glucose metabolism heterogeneity in human and mouse malignant glioma cell lines. *J Neurooncol*. 2005;74(2):123-133. doi:10.1007/s11060-004-6404-6.
33. Fantin VR, St-Pierre J, Leder P. Attenuation of LDH-A expression uncovers a link between glycolysis, mitochondrial physiology, and tumor maintenance. *Cancer Cell*. 2006;9(6):425-434. doi:10.1016/j.ccr.2006.04.023.
34. Lim HY, Ho QS, Low J, Choolani M, Wong KP. Respiratory competent mitochondria in human ovarian and peritoneal cancer. *Mitochondrion*. 2011;11(3):437-443. doi:https://doi.org/10.1016/j.mito.2010.12.015.
35. Scott DA, Richardson AD, Filipp F V, et al. Comparative metabolic flux profiling of melanoma cell lines: beyond the Warburg effect. *J Biol Chem*. 2011;286(49):42626-42634. doi:10.1074/jbc.M111.282046.
36. Dang L, Jin S, Su SM. IDH mutations in glioma and acute myeloid leukemia. *Trends Mol Med*. 2010;16(9):387-397. doi:https://doi.org/10.1016/j.molmed.2010.07.002.

37. Dimitrov L, Hong CS, Yang C, Zhuang Z, Heiss JD. New Developments in the Pathogenesis and Therapeutic Targeting of the IDH1 Mutation in Glioma. 2015;12. doi:10.7150/ijms.11047.

38. Dang L, White DW, Gross S, et al. Cancer-associated IDH1 mutations produce 2-hydroxyglutarate. *Nature*. 2009;462(7274):739-744. http://dx.doi.org/10.1038/nature08617.

39. Ward PS, Patel J, Wise DR, et al. The common feature of leukemia-associated IDH1 and IDH2 mutations is a neomorphic enzyme activity converting alpha-ketoglutarate to 2-hydroxyglutarate. *Cancer Cell*. 2010;17(3):225-234. doi:10.1016/j.ccr.2010.01.020.

40. Mardis ER, Ding L, Dooling DJ, et al. Recurring Mutations Found by Sequencing an Acute Myeloid Leukemia Genome. *N Engl J Med*. 2009;361(11):1058-1066. doi:10.1056/NEJMoa0903840.

41. Rakheja D, Boriack RL, Mitui M. Papillary thyroid carcinoma shows elevated levels of 2-hydroxyglutarate. 2011:325-333. doi:10.1007/s13277-010-0125-6.

42. DiNardo CD, Propert KJ, Loren AW, et al. Serum 2-hydroxyglutarate levels predict isocitrate dehydrogenase mutations and clinical outcome in acute myeloid leukemia. *Blood*. 2013;121(24):4917-4924. doi:10.1182/blood-2013-03-493197.

43. Parsons DW, Jones S, Zhang X, et al. An Integrated Genomic Analysis of Human Glioblastoma Multiforme. *Science*. 2008;321(5897):1807. doi:10.1126/science.1164382.

44. Yang I, Tihan T, Han SJ, et al. CD8+ T-cell infiltrate in newly diagnosed glioblastoma is associated with long-term survival. *J Clin Neurosci Off J Neurosurg Soc Australas*. 2010;17(11):1381-1385. doi:10.1016/j.jocn.2010.03.031.

45. Smolková K, Ježek P. The role of mitochondrial NADPH-dependent isocitrate dehydrogenase in cancer cells. *Int J Cell Biol*. 2012;2012. doi:10.1155/2012/273947.

46. Wise DR, Ward PS, Shay JES, Cross JR, Gruber JJ, Sachdeva UM. Hypoxia promotes isocitrate dehydrogenase- dependent carboxylation of α -ketoglutarate to citrate to support cell growth and viability. 2011:1-7. doi:10.1073/pnas.1117773108.

47. Young RM, Simon MC. Untuning the tumor metabolic machine: HIF-alpha: pro- and antitumorigenic? *Nat Med*. 2012;18(7):1024-1025. doi:10.1038/nm.2865.

48. Gupta R, Webb-Myers R, Flanagan S, Buckland ME. Isocitrate dehydrogenase mutations in diffuse gliomas: clinical and aetiological implications. *J Clin Pathol*. 2011;64(10):835 LP-844.

49. Brooks WH, Markesbery WR, Gupta GD, D P, Roszman TL, D P. Relationship of Lymphocyte Invasion and Survival of Brain Tumor Patients. 1978:219-224.

50. Jacobs JFM, Idema AJ, Bol KF, et al. Prognostic significance and mechanism of Treg infiltration in human brain tumors. *J Neuroimmunol*. 2010;225(1-2):195-199. doi:10.1016/j.jneuroim.2010.05.020.

51. Donson AM, Birks DK, Schittone SA, et al. Increased immune gene expression and immune cell infiltration in high-grade astrocytoma distinguish long-term from short-term survivors. *J Immunol*. 2012;189(4):1920-1927. doi:10.4049/jimmunol.1103373.

52. DiLillo DJ, Yanaba K, Tedder TF. B cells are required for optimal CD4+ and CD8+ T cell tumor immunity: therapeutic B cell depletion enhances B16 melanoma growth in mice. *J Immunol*. 2010;184(7):4006-4016. doi:10.4049/jimmunol.0903009.

53. Halama N, Michel S, Kloor M, et al. Localization and density of immune cells in the invasive margin of human colorectal cancer liver metastases are prognostic for response to chemotherapy. *Cancer Res*. 2011;71(17):5670-5677. doi:10.1158/0008-5472.CAN-11-0268.

54. Ottensmeier CH, Perry KL, Harden EL, et al. Upregulated Glucose Metabolism Correlates Inversely with $CD8^+$ T-cell Infiltration and Survival in Squamous Cell Carcinoma. *Cancer Res*. 2016;76(14):4136 LP-4148.

55. Silzle T, Randolph GJ, Kreutz M, Kunz‐Schughart LA. The fibroblast: Sentinel cell and local immune modulator in tumor tissue. *Int J Cancer*. 2004;108(2):173-180. doi:10.1002/ijc.11542.

56. Dong J, Grunstein J, Tejada M, et al. VEGF-null cells require PDGFR alpha signaling-mediated stromal fibroblast recruitment for tumorigenesis. *EMBO J*. 2004;23(14):2800-2810. doi:10.1038/sj.emboj.7600289.

57. Karnoub AE, Dash AB, Vo AP, et al. Mesenchymal stem cells within tumour stroma promote breast cancer metastasis. *Nature*. 2007;449(7162):557-563. doi:10.1038/nature06188.

58. Mantovani A, Sozzani S, Locati M, Allavena P, Sica A. Macrophage polarization:

tumor-associated macrophages as a paradigm for polarized M2 mononuclear phagocytes. *Trends Immunol*. 2002;23(11):549-555.

59. Condeelis J, Pollard JW. Macrophages: obligate partners for tumor cell migration, invasion, and metastasis. *Cell*. 2006;124(2):263-266. doi:10.1016/j.cell.2006.01.007.
60. Sawaya RE, Yamamoto M, Gokaslan ZL, et al. Expression and localization of 72 kDa type IV collagenase (MMP-2) in human malignant gliomas in vivo. *Clin Exp Metastasis*. 1996;14(1):35-42.
61. Uhm JH, Dooley NP, Villemure JG, Yong VW. Glioma invasion in vitro: regulation by matrix metalloprotease-2 and protein kinase C. *Clin Exp Metastasis*. 1996;14(5):421-433.
62. Beliën ATJ, Paganetti PA, Schwab ME. Membrane-type 1 Matrix Metalloprotease (MT1-MMP) Enables Invasive Migration of Glioma Cells in Central Nervous System White Matter. *J Cell Biol*. 1999;144(2):373-384.
63. Sameshima T, Nabeshima K, Toole BP, et al. Expression of emmprin (CD147), a cell surface inducer of matrix metalloproteinases, in normal human brain and gliomas. *Int J cancer*. 2000;88(1):21-27.
64. Li R, Huang L, Guo H, Toole BP. Basigin (murine EMMPRIN) stimulates matrix metalloproteinase production by fibroblasts. *J Cell Physiol*. 2001;186(3):371-379.
65. Wagner S, Czub S, Greif M, et al. Microglial/macrophage expression of interleukin 10 in human glioblastomas. *Int J cancer*. 1999;82(1):12-16.
66. Huettner C, Czub S, Kerkau S, Roggendorf W, Tonn JC. Interleukin 10 is expressed in human gliomas in vivo and increases glioma cell proliferation and motility in vitro. *Anticancer Res*. 1997;17(5A):3217-3224.
67. Wagner S, Stegen C, Bouterfa H, et al. Expression of matrix metalloproteinases in human glioma cell lines in the presence of IL-10. *J Neurooncol*. 1998;40(2):113-122.
68. Yeung YT, Bryce NS, Adams S, et al. p38 MAPK inhibitors attenuate pro-inflammatory cytokine production and the invasiveness of human U251 glioblastoma cells. *J Neurooncol*. 2012;109(1):35-44. doi:10.1007/s11060-012-0875-7.
69. Parkin J, Cohen B. An overview of the immune system. *Lancet*. 2001;357(9270):1777-1789. doi:10.1016/S0140-6736(00)04904-7.

70. Abbas AK, Lichtman AH, Pillai S. *Cellular and Molecular Immunology*. Philadelphia: Elsevier/Saunders; 2012.

71. Delves PJ, Martin SJ, Burton DR, Roitt IM. *Roitt's Essential Immunology*. 13th ed. WILEY; 2017.

72. Janeway CA, Travers P, Walport M, Shlomchik MJ. *Immunobiology*. 5th ed. New York: Garland Science; 2001.

73. Swanson JA. Shaping cups into phagosomes and macropinosomes. *Nat Rev Mol Cell Biol*. 2008;9(8):639-649. doi:10.1038/nrm2447.

74. Mantegazza AR, Magalhaes JG, Amigorena S, Marks MS. Presentation of phagocytosed antigens by MHC class I and II. *Traffic*. 2013;14(2):135-152. doi:10.1111/tra.12026.

75. Fecci PE, Mitchell DA, Whitesides JF, et al. Increased Regulatory T-Cell Fraction Amidst a Diminished CD4 Compartment Explains Cellular Immune Defects in Patients with Malignant Glioma. *Cancer Res*. 2006;66(6):3294 LP-3302.

76. Gustafson MP, Lin Y, New KC, et al. Systemic immune suppression in glioblastoma: the interplay between CD14+HLA-DRlo/neg monocytes, tumor factors, and dexamethasone. *Neuro Oncol*. 2010;12(7):631-644. doi:10.1093/neuonc/noq001.

77. Rodrigues JC, Gonzalez GC, Zhang L, et al. Normal human monocytes exposed to glioma cells acquire myeloid-derived suppressor cell-like properties. *Neuro Oncol*. 2010;12(4):351-365. doi:10.1093/neuonc/nop023.

78. Schlecker E, Stojanovic A, Eisen C, et al. Tumor-Infiltrating Monocytic Myeloid-Derived Suppressor Cells Mediate CCR5-Dependent Recruitment of Regulatory T Cells Favoring Tumor Growth. *J Immunol*. 2012;189(12):5602-5611. doi:10.4049/jimmunol.1201018.

79. Lowther DE, Hafler DA. Regulatory T cells in the central nervous system. 2012;248:156-169.

80. Mogensen TH. Pathogen Recognition and Inflammatory Signaling in Innate Immune Defenses. *Clin Microbiol Rev*. 2009;22(2):240-273. doi:10.1128/CMR.00046-08.

81. Hargadon KM. Tumor-altered dendritic cell function: implications for anti-tumor immunity. *Front Immunol*. 2013;4:192. doi:10.3389/fimmu.2013.00192.

82. Paul WE. *Fundamental Immunology*. 4th ed. Philadelphia: Lippincott-Raven

83. Banchereau J, Steinman RM. Dendritic cells and the control of immunity. *Nature*. 1998;392(March):245-252. doi:10.1038/32588.

84. Sallusto F, Cella M, Danieli C, Lanzavecchia A. Dendritic cells use macropinocytosis and the mannose receptor to concentrate macromolecules in the major histocompatibility complex class II compartment: downregulation by cytokines and bacterial products. *J Exp Med*. 1995;182(2):389-400.

85. Winzler C, Rovere P, Rescigno M, et al. Maturation stages of mouse dendritic cells in growth factor-dependent long-term cultures. *J Exp Med*. 1997;185(2):317-328.

86. Nijman HW, Kleijmeer MJ, Ossevoort MA, et al. Antigen capture and major histocompatibility class II compartments of freshly isolated and cultured human blood dendritic cells. *J Exp Med*. 1995;182(1):163-174.

87. Pierre P, Turley SJ, Gatti E, et al. Developmental regulation of MHC class II transport in mouse dendritic cells. *Nature*. 1997;388(6644):787-792. doi:10.1038/42039.

88. Cella M, Scheidegger D, Palmer-Lehmann K, Lane P, Lanzavecchia A, Alber G. Ligation of CD40 on dendritic cells triggers production of high levels of interleukin-12 and enhances T cell stimulatory capacity: T-T help via APC activation. *J Exp Med*. 1996;184(2):747-752.

89. Koch F, Stanzl U, Jennewein P, et al. High level IL-12 production by murine dendritic cells: upregulation via MHC class II and CD40 molecules and downregulation by IL-4 and IL-10. *J Exp Med*. 1996;184(2):741-746.

90. Sousa CR e, Hieny S, Scharton-Kersten T, et al. In Vivo Microbial Stimulation Induces Rapid CD40 Ligand–independent Production of Interleukin 12 by Dendritic Cells and their Redistribution to T Cell Areas. *J Exp Med*. 1997;186(11):1819-1829.

91. Albert ML, Jegathesan M, Darnell RB. Dendritic cell maturation is required for the cross-tolerization of CD8+ T cells. *Nat Immunol*. 2001;2(11):1010-1017. doi:10.1038/ni722.

92. Buelens C, Verhasselt V, De Groote D, Thielemans K, Goldman M, Willems F. Human dendritic cell responses to lipopolysaccharide and CD40 ligation are differentially regulated by interleukin-10. *Eur J Immunol*. 1997;27(8):1848-1852. doi:10.1002/eji.1830270805.

93. Chaux P, Moutet M, Faivre J, Martin F, Martin M. Inflammatory cells infiltrating

human colorectal carcinomas express HLA class II but not B7-1 and B7-2 costimulatory molecules of the T-cell activation. *Lab Invest*. 1996;74(5):975-983.

94. Smallie T, Ricchetti G, Horwood NJ, Feldmann M, Clark AR, Williams LM. IL-10 inhibits transcription elongation of the human TNF gene in primary macrophages. *J Exp Med*. 2010;207(10):2081 LP-2088.
95. Banks WA, Kastin AJ, Gutierrez EG. Penetration of interleukin-6 across the murine blood-brain barrier. *Neurosci Lett*. 1994;179(1-2):53-56.
96. Ferguson-Smith AC, Chen YF, Newman MS, May LT, Sehgal PB, Ruddle FH. Regional localization of the interferon-beta 2/B-cell stimulatory factor 2/hepatocyte stimulating factor gene to human chromosome 7p15-p21. *Genomics*. 1988;2(3):203-208.
97. Curiel TJ, Coukos G, Zou L, et al. Specific recruitment of regulatory T cells in ovarian carcinoma fosters immune privilege and predicts reduced survival. *Nat Med*. 2004;10(9):942-949. doi:10.1038/nm1093.
98. Kawai T, Akira S. Toll-like receptors and their crosstalk with other innate receptors in infection and immunity. *Immunity*. 2011;34(5):637-650. doi:10.1016/j.immuni.2011.05.006.
99. Kawai T, Akira S. Pathogen recognition with Toll-like receptors. *Curr Opin Immunol*. 2005;17(4):338-344. doi:10.1016/j.coi.2005.02.007.
100. Manukyan MC, Weil BR, Wang Y, et al. The phosphoinositide-3 kinase survival signaling mechanism in sepsis. *Shock*. 2010;34(5):442-449. doi:10.1097/SHK.0b013e3181e14ea9.
101. Janeway CAJ, Medzhitov R. Innate immune recognition. *Annu Rev Immunol*. 2002;20:197-216. doi:10.1146/annurev.immunol.20.083001.084359.
102. Israël A. The IKK Complex, a Central Regulator of NF-κB Activation. *Cold Spring Harb Perspect Biol*. 2010;2(3):a000158. doi:10.1101/cshperspect.a000158.
103. Hayden MS, West AP, Ghosh S. NF-kappaB and the immune response. *Oncogene*. 2006;25(51):6758-6780. doi:10.1038/sj.onc.1209943.
104. Dong C, Davis RJ, Flavell RA. MAP kinases in the immune response. *Annu Rev Immunol*. 2002;20:55-72. doi:10.1146/annurev.immunol.20.091301.131133.
105. Kim L, Denkers EY. Toxoplasma gondii triggers Gi-dependent PI 3-kinase signaling required for inhibition of host cell apoptosis. *J Cell Sci*. 2006;119(Pt 10):2119-2126. doi:10.1242/jcs.02934.

106. Quan J-H, Chu J-Q, Kwon J, et al. Intracellular Networks of the PI3K/AKT and MAPK Pathways for Regulating Toxoplasma gondii-Induced IL-23 and IL-12 Production in Human THP-1 Cells. *PLoS One*. 2015;10(11):e0141550. doi:10.1371/journal.pone.0141550.

107. la Sala A, Gadina M, Kelsall BL. G(i)-protein-dependent inhibition of IL-12 production is mediated by activation of the phosphatidylinositol 3-kinase-protein 3 kinase B/Akt pathway and JNK. *J Immunol*. 2005;175(5):2994-2999.

108. Orth JHC, Preuss I, Fester I, Schlosser A, Wilson BA, Aktories K. Pasteurella multocida toxin activation of heterotrimeric G proteins by deamidation. *Proc Natl Acad Sci U S A*. 2009;106(17):7179-7184. doi:10.1073/pnas.0900160106.

109. Hildebrand D, Heeg KM, Hildebrand D, et al. Regulation of Toll-like receptor 4-mediated immune responses through Pasteurella multocida toxin-induced G protein ... Regulation of Toll-like receptor 4-mediated immune responses through Pasteurella multocida toxin-induced G protein signalling. 2012;(May 2017). doi:10.1186/1478-811X-10-22.

110. Andreesen R, Picht J, Löhr GW. Primary cultures of human blood-born macrophages grown on hydrophobic teflon membranes. *J Immunol Methods*. 1983;56(3):295-304. doi:http://dx.doi.org/10.1016/S0022-1759(83)80019-2.

111. Inaba K, Swiggard WJ, Steinman RM, Romani N, Schuler G, Brinster C. Isolation of dendritic cells. *Curr Protoc Immunol*. 2009;Chapter 3:Unit 3.7. doi:10.1002/0471142735.im0307s86.

112. Gnaiger E, Steinlechner-Maran R, Mendez G, Eberl T, Margreiter R. Control of mitochondrial and cellular respiration by oxygen. *J Bioenerg Biomembr*. 1995;27(6):583-596.

113. Figueroa ME, Abdel-Wahab O, Lu C, et al. Leukemic IDH1 and IDH2 Mutations Result in a Hypermethylation Phenotype, Disrupt TET2 Function, and Impair Hematopoietic Differentiation. *Cancer Cell*. 2018;18(6):553-567. doi:10.1016/j.ccr.2010.11.015.

114. Hildebrand D, Heeg KM, Hildebrand D, et al. Regulation of Toll-like receptor 4-mediated immune responses through Pasteurella multocida toxin-induced G protein ... Regulation of Toll-like receptor 4-mediated immune responses through Pasteurella multocida toxin-induced G protein signalling. 2012;(August). doi:10.1186/1478-811X-10-22.

115. Jantsch J, Chakravortty D, Turza N, et al. Hypoxia and hypoxia-inducible factor-1 alpha modulate lipopolysaccharide-induced dendritic cell activation and function. *J Immunol*. 2008;180(7):4697-4705.

116. Willam C. HIF meets NF-κB signaling. *Kidney Int*. 2014;85(2):232-234. doi:https://doi.org/10.1038/ki.2013.362.

117. Moroz E, Carlin S, Dyomina K, et al. Real-Time Imaging of HIF-1α Stabilization and Degradation. *PLoS One*. 2009;4(4):e5077. https://doi.org/10.1371/journal.pone.0005077.

118. Henkel T, Machleidt T, Alkalay I, Krönke M, Ben-Neriah Y, Baeuerle PA. Rapid proteolysis of IκB-α is necessary for activation of transcription factor NF-κB. *Nature*. 1993;365:182. http://dx.doi.org/10.1038/365182a0.

119. Son Y, Kim S, Chung H-T, Pae H-O. Chapter Two - Reactive Oxygen Species in the Activation of MAP Kinases. In: Cadenas E, Packer LBT-M in E, eds. *Hydrogen Peroxide and Cell Signaling, Part C*. Vol 528. Academic Press; 2013:27-48. doi:https://doi.org/10.1016/B978-0-12-405881-1.00002-1.

120. Ahmed K, Tunaru S, Offermanns S. GPR109A, GPR109B and GPR81, a family of hydroxy-carboxylic acid receptors. *Trends Pharmacol Sci*. 2009;30(11):557-562. doi:http://dx.doi.org/10.1016/j.tips.2009.09.001.

121. FENG WG, WANG YB, ZHANG JS, WANG XY, LI CL, CHANG ZL. cAMP elevators inhibit LPS-induced IL-12 p40 expression by interfering with phosphorylation of p38 MAPK in Murine Peritoneal Macrophages. *Cell Res*. 2002;12(5-6):331-337. http://dx.doi.org/10.1038/sj.cr.7290135.

122. la Sala A, He J, Laricchia-Robbio L, et al. Cholera toxin inhibits IL-12 production and CD8alpha+ dendritic cell differentiation by cAMP-mediated inhibition of IRF8 function. *J Exp Med*. 2009;206(6):1227-1235. doi:10.1084/jem.20080912.

123. Fournier N, Ducet G, Crevat A. Action of cyclosporine on mitochondrial calcium fluxes. *J Bioenerg Biomembr*. 1987;19(3):297-303.

124. Sutterwala FS, Noel GJ, Clynes R, Mosser DM. Selective suppression of interleukin-12 induction after macrophage receptor ligation. *J Exp Med*. 1997;185(11):1977-1985. doi:10.1084/jem.185.11.1977.

125. Xu W, Yang H, Liu Y, et al. Oncometabolite 2-Hydroxyglutarate Is a Competitive Inhibitor of α-Ketoglutarate-Dependent Dioxygenases. *Cancer Cell*. 2011;19(1):17-30. doi:https://doi.org/10.1016/j.ccr.2010.12.014.

126. Ugele IM. Effekte von 2-Hydroxyglutarat auf humane Immunzellen. 2017. https://epub.uni-regensburg.de/35461/.

127. Clark MJ, Homer N, Connor BDO, et al. U87MG Decoded : The Genomic Sequence of a Cytogenetically Aberrant Human Cancer Cell Line. 2010;6(1). doi:10.1371/journal.pgen.1000832.

128. Paschka P, Schlenk RF, Gaidzik VI, et al. IDH1 and IDH2 Mutations Are Frequent Genetic Alterations in Acute Myeloid Leukemia and Confer Adverse Prognosis in Cytogenetically Normal Acute Myeloid Leukemia With NPM1 Mutation Without FLT3 Internal Tandem Duplication. *J Clin Oncol*. 2010;28(22):3636-3643. doi:10.1200/JCO.2010.28.3762.

129. Sun H, Yin L, Li S, et al. Prognostic significance of IDH mutation in adult low-grade gliomas: a meta-analysis. *J Neurooncol*. 2013;113(2):277-284. doi:10.1007/s11060-013-1107-5.

130. DiNardo CD, Ravandi F, Agresta S, et al. Characteristics, clinical outcome, and prognostic significance of IDH mutations in AML. *Am J Hematol*. 2015;90(8):732-736. doi:10.1002/ajh.24072.

131. Chen C, Liu Y, Lu C, et al. Cancer-associated IDH2 mutants drive an acute myeloid leukemia that is susceptible to Brd4 inhibition. *Genes Dev* . 2013;27(18):1974-1985. doi:10.1101/gad.226613.113.

132. Böttcher M, Renner K, Berger R, et al. D-2-hydroxyglutarate interferes with HIF-1α stability skewing T-cell metabolism towards oxidative phosphorylation and impairing Th17 polarization. *Oncoimmunology*. March 2018:1-26. doi:10.1080/2162402X.2018.1445454.

133. Hagos Y, Krick W, Braulke T, Mühlhausen C, Burckhardt G, Burckhardt BC. Organic anion transporters OAT1 and OAT4 mediate the high affinity transport of glutarate derivatives accumulating in patients with glutaric acidurias. *Pflügers Arch - Eur J Physiol*. 2008;457(1):223-231. doi:10.1007/s00424-008-0489-2.

134. Liu KQ, Bunnell SC, Gurniak CB, Berg LJ. T cell receptor-initiated calcium release is uncoupled from capacitative calcium entry in Itk-deficient T cells. *J Exp Med*. 1998;187(10):1721-1727.

135. Shim E-H, Livi CB, Rakheja D, et al. L-2-Hydroxyglutarate: An Epigenetic Modifier and Putative Oncometabolite in Renal Cancer. *Cancer Discov*. 2014;4(11):1290 LP-1298.

http://cancerdiscovery.aacrjournals.org/content/4/11/1290.abstract.

136. Terunuma A, Putluri N, Mishra P, et al. MYC-driven accumulation of 2-hydroxyglutarate is associated with breast cancer prognosis. *J Clin Invest*. 2014;124(1):398-412. doi:10.1172/JCI71180.

137. Lu Y-C, Yeh W-C, Ohashi PS. LPS/TLR4 signal transduction pathway. *Cytokine*. 2008;42(2):145-151. doi:10.1016/j.cyto.2008.01.006.

138. Peyssonnaux C, Cejudo-Martin P, Doedens A, Zinkernagel AS, Johnson RS, Nizet V. Cutting edge: Essential role of hypoxia inducible factor-1alpha in development of lipopolysaccharide-induced sepsis. *J Immunol*. 2007;178(12):7516-7519.

139. Feng G-J, Goodridge HS, Harnett MM, et al. Extracellular Signal-Related Kinase (ERK) and p38 Mitogen-Activated Protein (MAP) Kinases Differentially Regulate the Lipopolysaccharide-Mediated Induction of Inducible Nitric Oxide Synthase and IL-12 in Macrophages: Leishmania Phosph. *J Immunol*. 1999;163(12):6403 LP-6412. http://www.jimmunol.org/content/163/12/6403.abstract.

140. Fukao T, Tanabe M, Terauchi Y, et al. PI3K-mediated negative feedback regulation of IL-12 production in DCs. *Nat Immunol*. 2002;3(9):875-881. doi:10.1038/ni825.

141. Utsugi M, Dobashi K, Ono A, et al. PI3K p110beta positively regulates lipopolysaccharide-induced IL-12 production in human macrophages and dendritic cells and JNK1 plays a novel role. *J Immunol*. 2009;182(9):5225-5231. doi:10.4049/jimmunol.0801352.

142. Zandi-Nejad K, Takakura A, Jurewicz M, et al. The role of HCA2 (GPR109A) in regulating macrophage function. *FASEB J Off Publ Fed Am Soc Exp Biol*. 2013;27(11):4366-4374. doi:10.1096/fj.12-223933.

143. Braun MC, Kelsall BL. Regulation of interleukin-12 production by G-protein-coupled receptors. *Microbes Infect*. 2001;3(2):99-107.

144. Vandenbroeck K, Alloza I, Gadina M, Matthys P. Inhibiting cytokines of the interleukin-12 family: recent advances and novel challenges. *J Pharm Pharmacol*. 2004;56(2):145-160. doi:10.1211/0022357022962.

145. Papa S, Rasmo D De, Technikova-Dobrova Z, et al. Respiratory chain complex I, a main regulatory target of the cAMP/PKA pathway is defective in different human diseases. *FEBS Lett*. 2012;586(5):568-577. doi:10.1016/j.febslet.2011.09.019.

146. Leadsham JE, Gourlay CW. CAMP/PKA signaling balances respiratory activity with mitochondria dependent apoptosis via transcriptional regulation. *BMC Cell Biol*. 2010;11. doi:10.1186/1471-2121-11-92.

147. Tasken K, Aandahl EM. Localized effects of cAMP mediated by distinct routes of protein kinase A. *Physiol Rev*. 2004;84(1):137-167. doi:10.1152/physrev.00021.2003.

148. Xu W, Yang H, Liu Y, et al. Oncometabolite 2-hydroxyglutarate is a competitive inhibitor of alpha-ketoglutarate-dependent dioxygenases. *Cancer Cell*. 2011;19(1):17-30. doi:10.1016/j.ccr.2010.12.014.

149. Wise DR, Ward PS, Shay JES, et al. Hypoxia promotes isocitrate dehydrogenase-dependent carboxylation of alpha-ketoglutarate to citrate to support cell growth and viability. *Proc Natl Acad Sci U S A*. 2011;108(49):19611-19616. doi:10.1073/pnas.1117773108.

150. Kelly B, O'Neill LAJ. Metabolic reprogramming in macrophages and dendritic cells in innate immunity. *Cell Res*. 2015;25(7):771-784. doi:10.1038/cr.2015.68.

151. Dietl K, Renner K, Dettmer K, et al. Lactic acid and acidification inhibit TNF secretion and glycolysis of human monocytes. *J Immunol*. 2010;184(3):1200-1209. doi:10.4049/jimmunol.0902584.

152. Malinarich F, Duan K, Hamid RA, et al. High Mitochondrial Respiration and Glycolytic Capacity Represent a Metabolic Phenotype of Human Tolerogenic Dendritic Cells. *J Immunol*. 2015;194(11):5174 LP-5186. http://www.jimmunol.org/content/194/11/5174.abstract.

153. Grassian AR, Parker SJ, Davidson SM, et al. IDH1 mutations alter citric acid cycle metabolism and increase dependence on oxidative mitochondrial metabolism. *Cancer Res*. 2014;74(12):3317-3331. doi:10.1158/0008-5472.CAN-14-0772-T.

154. Navis AC, Niclou SP, Fack F, et al. Increased mitochondrial activity in a novel IDH1-R132H mutant human oligodendroglioma xenograft model: in situ detection of 2-HG and α-KG. *Acta Neuropathol Commun*. 2013;1(1):18. doi:10.1186/2051-5960-1-18.

155. Chan SM, Thomas D, Corces-Zimmerman MR, et al. Isocitrate dehydrogenase 1 and 2 mutations induce BCL-2 dependence in acute myeloid leukemia. *Nat Med*. 2015;21(2):178-184. doi:10.1038/nm.3788.

156. Fu X, Chin RM, Vergnes L, et al. 2-Hydroxyglutarate Inhibits ATP Synthase and

mTOR Signaling. *Cell Metab*. 2015;22(3):508-515. doi:10.1016/j.cmet.2015.06.009.

157. Huang E, Showalter L, Xu S, Czernliecki BJ, Koski GK. Calcium mobilizing treatment acts as a co-signal for TLR-mediated induction of Interleukin-12 (IL-12p70) secretion by murine bone marrow-derived dendritic cells. *Cell Immunol*. 2017;314:26-35. doi:10.1016/j.cellimm.2017.01.010.
158. Pruitt KD, Tatusova T, Maglott DR. NCBI reference sequences (RefSeq): a curated non-redundant sequence database of genomes, transcripts and proteins. *Nucleic Acids Res*. 2007;35(Database issue):D61-5. doi:10.1093/nar/gkl842.
159. McLaughlin JN, Patterson MM, Malik AB. Protease-activated receptor-3 (PAR3) regulates PAR1 signaling by receptor dimerization. *Proc Natl Acad Sci*. 2007;104(13):5662 LP-5667. http://www.pnas.org/content/104/13/5662.abstract.
160. Li T, Wang H, He S. Induction of interleukin-6 release from monocytes by serine proteinases and its potential mechanisms. *Scand J Immunol*. 2006;64(1):10-16. doi:10.1111/j.1365-3083.2006.01772.x.
161. Varas A, Valencia J, Lavocat F, et al. Blockade of bone morphogenetic protein signaling potentiates the pro-inflammatory phenotype induced by interleukin-17 and tumor necrosis factor-α combination in rheumatoid synoviocytes. *Arthritis Res Ther*. 2015;17(1):192. doi:10.1186/s13075-015-0710-6.
162. Varas A, Martinez VG, Hernandez-Lopez C, Hidalgo L, Entrena A, Valencia J. Role of BMP signalling in peripheral CD4+ T cell proliferation. *Inmunología*. 2009;28. doi:10.1016/S0213-9626(09)70035-6.
163. Maurer T, Zimmermann G, Maurer S, Stegmaier S, Wagner C, Hansch GM. Inhibition of osteoclast generation: a novel function of the bone morphogenetic protein 7/osteogenic protein 1. *Mediators Inflamm*. 2012;2012:171209. doi:10.1155/2012/171209.
164. Hwang SL, Chung NP-Y, Chan JK-Y, Lin C-LS. Indoleamine 2, 3-dioxygenase (IDO) is essential for dendritic cell activation and chemotactic responsiveness to chemokines. *Cell Res*. 2005;15(3):167-175. doi:10.1038/sj.cr.7290282.
165. Delestre-Delacour C, Carmon O, Laguerre F, et al. Myosin 1b and F-actin are involved in the control of secretory granule biogenesis. *Sci Rep*. 2017;7(1):5172. doi:10.1038/s41598-017-05617-1.
166. Armstead WM, Hekierski H, Pastor P, Yarovoi S, Higazi AA-R, Cines DB.

Release of IL-6 After Stroke Contributes to Impaired Cerebral Autoregulation and Hippocampal Neuronal Necrosis Through NMDA Receptor Activation and Upregulation of ET-1 and JNK. *Transl Stroke Res*. February 2018. doi:10.1007/s12975-018-0617-z.

167. Ponnala S, Chetty C, Veeravalli KK, Dinh DH, Klopfenstein JD, Rao JS. Metabolic remodeling precedes mitochondrial outer membrane permeabilization in human glioma xenograft cells. *Int J Oncol*. 2012;40(2):509-518. doi:10.3892/ijo.2011.1255.
168. Dembic Z. Chapter 6 - Cytokines of the Immune System: Interleukins BT - The Cytokines of the Immune System. In: Amsterdam: Academic Press; 2015:143-239. doi:https://doi.org/10.1016/B978-0-12-419998-9.00006-7.
169. Bai X, Geng J, Li X, et al. Long Noncoding RNA LINC01619 Regulates MicroRNA-27a/Forkhead Box Protein O1 and Endoplasmic Reticulum Stress-Mediated Podocyte Injury in Diabetic Nephropathy. *Antioxid Redox Signal*. January 2018. doi:10.1089/ars.2017.7278.
170. Bartoloni L, Blouin J-L, Pan Y, et al. Mutations in the DNAH11 (axonemal heavy chain dynein type 11) gene cause one form of situs inversus totalis and most likely primary ciliary dyskinesia. *Proc Natl Acad Sci U S A*. 2002;99(16):10282-10286. doi:10.1073/pnas.152337699.
171. Saeed M. Locus and gene-based GWAS meta-analysis identifies new diabetic nephropathy genes. *Immunogenetics*. November 2017. doi:10.1007/s00251-017-1044-0.
172. Ahn J-S, Kim H-J, Kim Y-K, et al. DNMT3A R882 Mutation with FLT3-ITD Positivity Is an Extremely Poor Prognostic Factor in Patients with Normal-Karyotype Acute Myeloid Leukemia after Allogeneic Hematopoietic Cell Transplantation. *Biol Blood Marrow Transplant*. 2016;22(1):61-70. doi:https://doi.org/10.1016/j.bbmt.2015.07.030.

9. Index

9.1 Effect of D-HG and α-Ketoglutarate on the RNA expression of Dendritic Cells

In order to elucidate the possible competitive effect of α-Ketoglutarate (Di-Keto) and D-HG on gene expression, we differentiated dendritic cells from monocytes, and treated them with 100ng/ml LPS, 10mM D-HG or 10mM Di-Keto. Genes shown in the following tables satisfied 2 criteria. First, genes were significantly different in LPS-stimulated DCs compared to untreated DCs. Second, genes were significantly different in LPS-stimulated DCs compared to DCs treated either with D-HG or Di-Keto.

Table 9.1 Top 30 genes up regulated by the effect of D-HG and Di-Keto.

		DCs RNA Seq			
	Up-Regulated with D-HG	**P Value**	**FDR**	**transcript type**	**foldchange/ pvalue**
1	MMP1	3.59E-40	4.50E-36	protein_coding	1
2	MYO1B	1.99E-26	1.25E-22	protein_coding	1
3	SLC39A14	1.61E-25	6.74E-22	protein_coding	1
4	AKR1B1	5.44E-25	1.71E-21	protein_coding	1
5	ALDH1A2	5.92E-22	1.48E-18	protein_coding	1
6	SERPINE1	1.02E-19	1.83E-16	protein_coding	1
7	CRISPLD2	6.59E-19	1.03E-15	protein_coding	1
8	SERPINB2	5.30E-16	6.64E-13	protein_coding	1
9	FLT1	6.00E-16	6.84E-13	protein_coding	1
10	HBEGF	6.60E-15	6.89E-12	protein_coding	1
11	MRPS6	6.20E-14	5.97E-11	protein_coding	1
12	MICAL2	1.09E-13	9.09E-11	protein_coding	1
13	IL17RB	2.08E-13	1.63E-10	protein_coding	1
14	SLC5A3	2.84E-13	2.10E-10	protein_coding	1
15	BMP6	3.14E-13	2.14E-10	protein_coding	1
16	SNORD3A	3.59E-12	2.05E-09	snoRNA	1
17	TM4SF1	5.90E-12	3.22E-09	protein_coding	1
18	PTGES	7.52E-12	3.93E-09	protein_coding	1
19	EGLN3	1.55E-11	7.49E-09	protein_coding	1
20	TMEM132A	2.31E-11	1.07E-08	protein_coding	1
21	PLAT	2.72E-11	1.22E-08	protein_coding	1
22	IL23A	4.01E-11	1.73E-08	protein_coding	1
23	VDR	5.47E-11	2.19E-08	snoRNA	1
24	SSTR2	5.59E-11	2.19E-08	protein_coding	1
25	SNORD3C	5.31E-11	2.19E-08	protein_coding	1
26	TGM2	6.48E-11	2.46E-08	protein_coding	1

27	LHFP	8.88E-11	3.27E-08	protein_coding	1
28	FERMT2	9.74E-11	3.49E-08	protein_coding	1
29	NKX3-1	1.05E-10	3.66E-08	protein_coding	1
30	PTGS2	1.22E-10	4.14E-08	protein_coding	1

More than 200 genes were upregulated by the effect of D-HG and Di-Keto, whereas only 6 genes were significantly affected by the specifically effect of D-HG. Which could represent a co-activity between α-Ketoglutarate and D-HG. Next we analyzed genes downregulated by the effect of D-HG/Di-Keto.

Table 9.2 Top 30 genes downregulated by the effect of D-HG and Di-Keto.

	DCs RNA Seq			
Down Regulated with D-HG	**P Value**	**FDR**	**transcript type**	**foldchange/ pvalue**
CXCL13	6.29E-21	1.31E-17	protein_coding	-1
RP11-107E5.3	7.33E-17	1.02E-13	TEC	-1
TNNT2	7.81E-14	6.99E-11	protein_coding	-1
CXCL11	3.25E-13	2.14E-10	protein_coding	-1
RP3-368A4.6	1.01E-12	6.27E-10	protein_coding	-1
ANKRD36C	1.05E-12	6.27E-10	sense_intronic	-1
ADTRP	1.40E-11	7.00E-09	protein_coding	-1
MT1JP	3.90E-10	1.16E-07	transcribed_unprocessed_pseudogene	-1
MARCO	1.04E-09	2.90E-07	protein_coding	-1
SEMA3A	1.42E-09	3.78E-07	protein_coding	-1
RP11-625I7.1	2.26E-09	5.56E-07	lincRNA	-1
IDO2	2.20E-09	5.56E-07	protein_coding	-1
DST	3.87E-09	9.15E-07	protein_coding	-1
RP11-81H14.1	4.90E-09	1.12E-06	lincRNA	-1
C12orf79	6.06E-09	1.36E-06	protein_coding	-1
TTN-AS1	7.15E-09	1.55E-06	antisense	-1
ODC1	1.04E-08	2.16E-06	protein_coding	-1
MALAT1	1.26E-08	2.58E-06	protein_coding	-1
CCL23	1.54E-08	3.11E-06	protein_coding	-1
DNAH11	1.87E-08	3.67E-06	protein_coding	-1
CD163	1.87E-08	3.67E-06	protein_coding	-1
TRAF5	3.95E-08	7.49E-06	protein_coding	-1
RP11-519G16.3	6.95E-08	1.26E-05	antisense	-1
CEMIP	1.17E-07	1.99E-05	protein_coding	-1
LINC01539	1.37E-07	2.30E-05	lincRNA	-1
VPS13A	1.54E-07	2.48E-05	protein_coding	-1
IL18	2.17E-07	3.24E-05	protein_coding	-1
ZNF260	2.25E-07	3.32E-05	protein_coding	-1
PSMD6-AS2	2.33E-07	3.39E-05	antisense	-1
ZNF844	3.64E-07	4.86E-05	protein_coding	-1

More than 190 genes were downregulated by the effect of D-HG and Di-Keto, whereas only 6 genes were significantly affected by the specifically effect of D-HG.

More experiments to confirm these results should be performed, and a new classification criteria could be useful to analize the specific effects of Di-Keto and D-HG in gene expression.

Acknowledgements

First of all, I would like to thank **Prof.Dr.Marina Kreutz** for all the support, continous guidance and boundless patience.

I would also like to thank **Dr.Kathrin Renner** for the exceptional supervision, valuable corrections and patience.

I would like to thank **Dr.Katrin Singer** for kindly taking the time to correct this thesis and her continual encouragement.

Thanks also go to **Prof.Dr.Müller Klieser and Prof.Dr.Wolfram Gronwald** for their valuable feedback during yearly-reports presentations.

To **Monika Wehrstein,** I will always be grateful for the outstanding assistance, endless encouragement, but more importantly for your friendship. I will going to miss you so much!!

To **Stefannie Färber**, I would like to thank you for all the help and assistance during mitochondrial studies.

To **Alice Peuker,** I would like to thank you for the help and technical assistance.

To **Prof.Dr.Pukrop and Research Group** for kindly provide the facilities, materials and experience in WB-OXPHOS studies.

To **Dr. Sven Lang**, for the contribution on HIF and ERK WB studies.

To **Institute of Functional Genomics,** for the contribution in mass spectrometry analysis.

To **Prof.Dr.Michael Rehli** and his research group for the assistance provide on RNAseq studies.

To all my friends in Kreutz´s and Rehli´s Lab, thank you for the extraordinary work environment.

To **MSc. Kathrin Hammon**, Thank you for your kindly contribution in summary correction and translation, but most importantly thank you for always be there and honored me with your friendship.

Frau **Dr. Sakhila Ghimire**, Thank you for kindly taking the time and provide with valuable thesis corrections, thank you also for your outstanding RT-PCR experience and friendship.

Frau **Dr. Carina Matos**, Thank you for always being eager to help and for the relentless motivational words, but most importantly thank you for your friendship.

Frau **Dr. Ines Ugele** for the continuous hard work and assistance in TLR4 studies, but more importantly for your friendship.

This work was economically supported by

Country-related cooperation programme with Mexico: CONACYT • DAAD
Program 50017046 (Personenkennziffer: 91549861)

German Academic Exchange Service's project "STIBET Doctoral Candidates"
Universitat Regensburg

Dedicatoria

A mi Familia
Gracias por el apoyo incondicional, por las constantes palabras de aliento y toda su paciencia. Soy consciente de todos los eventos en los que me he ausentado en estos ultimos años, pero tengan la seguridad que cada paso que doy es gracias al camino que ustedes forjaron.

A mis amigos en México.
Gracias por demostrarme que la distancia no importa cuando el amor existe. No tengo palabras para agradecerles todo su apoyo y confianza.

A mis amigas mexicanas en Alemania. Gracias por convertirse en mi segunda familia, por estar siempre dispuestas a apoyarme y motivarme.

A Lorena Diana Camelo, Gracias por toda la motivación, la ayuda incondicional, por otorgarme tu mano en los momentos más dificiles, por recordarme cuales son mis metas y mis sueños. Gracias por darme el privilegio de considerarme tu amiga.

To my friends in Germany and around the world, I would like to thank you all for always been there when I needed you most, for your motivating words, patience, and love.

To Gela Fisher, I would like to thank you for all your support, kind words and relentless encouragement.